

2014

Poroelastic Inhomogeneities: Applications in Reservoir Geomechanics

Houman Bedayat

Louisiana State University and Agricultural and Mechanical College

Follow this and additional works at: https://digitalcommons.lsu.edu/gradschool_dissertations



Part of the [Petroleum Engineering Commons](#)

Recommended Citation

Bedayat, Houman, "Poroelastic Inhomogeneities: Applications in Reservoir Geomechanics" (2014). *LSU Doctoral Dissertations*. 1803.

https://digitalcommons.lsu.edu/gradschool_dissertations/1803

This Dissertation is brought to you for free and open access by the Graduate School at LSU Digital Commons. It has been accepted for inclusion in LSU Doctoral Dissertations by an authorized graduate school editor of LSU Digital Commons. For more information, please contact gradetd@lsu.edu.

POROELASTIC INHOMOGENEITIES:
APPLICATIONS IN RESERVOIR GEOMECHANICS

A Dissertation

Submitted to the Graduate Faculty of the
Louisiana State University and
Agricultural and Mechanical College
in partial fulfillment of the
requirements for the degree of
Doctor of Philosophy

in

Craft & Hawkins Department of Petroleum Engineering

by

Houman Bedayat

B.S., Sharif University of Technology, 2007

M.S., Sharif University of Technology, 2010

December 2014

©Copyright by Houman Bedayat, 2014
All Rights Reserved

To my parents Ziba and Mahmoud

To my brothers Babak and Arash

&

To my forever love Paria

Acknowledgments

This dissertation could not have been completed without the great support that I have received from so many people over the years. I wish to offer my most genuine thanks to the following people.

To my advisor, Dr. Arash Dahi Taleghani. I would like to express my deepest gratitude to you. The door to your office was always open whenever I had a question about my research. I am indebted for your constant assistance, encouragement and guidance throughout my doctoral studies. Besides being my advisor, you are a good friend and I hope to have the opportunity to work with you in the future again.

To Dr. Yuri A. Antipov. For your help and support and invaluable guidance throughout the research.

To Dr. George Z. Voyiadjis. For your invaluable support. Your great personality is cherished by me as well as all your other students. Thank you for accepting to be in my committee.

To Dr. Karsten E. Thompson. For your comments and feedbacks and for being supportive as the chairman of the department. You will constantly remind me one of the greatest teachers throughout my life.

To Dr. Michael J. Martin and Dr. Shahab Mehraeen. For being in my committee and your time and kind helps.

To the great faculty and friendly staff of PETE department at LSU, Dr. John Rogers Smith, Dr. Richard Hughes, Dr. Mayank Tyagi, Dr. Christopher White, Dr. Dandina Rao,

Andi Donmyer, Janet Dugas, Fenelon Nunes, and George Ohrberg. Special thanks to Dr. Hughes Family for their very memorable thanksgiving dinner parties!

To my favorite authors, Dr. Emmanuel Detournay, Dr. Alexander H.-D. Cheng and Dr. John Rudnicki. I learned a lot from your publications.

To American Association of Drilling Engineers (AADE), GDL Foundation, Petroleum Engineering Department at LSU for your financial supports.

To my officemates. Through the years I was blessed with the greatest officemates, Wei Wang, Siyamak Rostami, Denis Klimenko, Ping Puyang, Miguel Gonzalez-Chavez, Milad Ahmadi, Chennv Fan, Negar Dahi, Juan Felipe Bautista, Mohammad Riyami, Louise M. Smith, Abiola Olabode, Doguhan Yilmaz, Amir Shojaei, Mustafa Hakan Ozyurtkan, and Mohamed Abdelrahim.

To my colleagues in PETE department. Thank you all for being a great friends. Ali Takbiri, Amin Gharabati, Masoud Safari, Reza Rahmani, Azadeh Kafili, Ali Reza Edrisi, Alireza Roostapour, Koray Kinic, Paulina Mwangi, Lawrence Dickerson, Atheer Al Attar, Foad Haeri, Darko Kupresan, Amin Mirsaeidi, Esmaeil Ansari and Kahila Mokhtari.

To my friends in Baton Rouge. Life in Baton Rouge would have been unbearable without you whom I will revere forever. My friends; Ashkan, Azadeh, Nima, Fatemeh, Ali, Kasra, Raysan, Navid, Amirhossein, Sima, Yahya, Roghayeh, Hamidreza, Mohammad, Ehsan, Afshin, Jafar, Arian, Navid, Mohammad, Ali, Saman, Mahan, Samira, Parvaneh, Mahzad, Misagh, Bruce, Debby, Vahid, Sareh, Sara, Fariborz, Maryam, Ava, Ata, Kristen, Pouya, Saaed, Houman. To my roommates; Ali, Amenda, and Tracy. To the members of Iranian Association at LSU; especially Somayeh, Mohsen, Naim and Parichehr.

To my lovely Mother. You mean the world to me, but I don't tell you enough. This one is for you ! مامان جان

To my Father. You sacrificed your life for my brothers and myself and provided unconditional love and care. I would not have made it this far without you. Thank you ! بابا جان

To my brothers, Babak & Arash. You are the people who I trust the most in my life. To their family arinaz, Layli & Ario. Thank you for your kindness.

To Uncle Mahmoud, Aunt Farideh, Haley, Mehrak, Alireza, Amir, Shaliz & their lovely kids. Thank you for all your support.

To my fiancée, Paria. I am lucky to have you in my life. I love you, and look forward to our lifelong journey.

To many great people and places in Baton Rouge. Dr. Aghazadeh, CEBA, Union, Starbucks, Perkin's Rowe, Kona Grill, Hamid Agha, Almazze, Agha Mehdi, Agha Nader, Marguerite Prince Acosta, Acha Bakery, Quad, Health center, Lady of the Lake, Embassy Apartments, and Louisiana fire ants!.

To anyone that may I have forgotten. I apologize. Thank you as well.

Table of Contents

Acknowledgments	iv
List of Tables	x
List of Figures	xi
Abstract	xv
1 Overview	1
1.1 Introduction	1
1.2 Outline	3
1.3 References	5
2 Interacting Double Poroelastic Inclusions	7
2.1 Introduction	7
2.2 Single Inclusion	11
2.2.1 Elastic inclusions	11
2.2.2 Poroelastic inclusions	12
2.3 Two Inclusions	14
2.4 Results and Discussions	18
2.5 Summary	21
2.6 Polynomial Eigenstrains	24
2.7 References	27
3 On the Inhomogeneous Anisotropic Poroelastic Inclusions	31
3.1 Introduction	31
3.2 Anisotropic poroelastic constitutive equations	36
3.3 Eshelby's solution	37
3.4 Poroelastic Inclusions	40
3.5 Results and Discussions	41
3.6 Conclusion	47
3.7 Calculating D_{ijkl}	48
3.8 Results for Ellipsoidal Isotropic Poroelastic Inclusion	49
3.9 A Discussion on the Effective Material Properties of the Medium	50
3.10 References	54
4 Eshelby Solution for Double Ellipsoidal Inhomogeneities: Applications in Geoscience	66

4.1	Introduction	66
4.2	Theory	68
4.2.1	Single inclusion	68
4.2.2	Single inhomogeneity	69
4.2.3	Double interacting inclusions	70
4.3	Formulation	71
4.4	Description of the Mathematica code	74
4.5	Verification and Numerical results	75
4.6	Conclusion	80
4.7	Supplementary data	80
4.8	Double inhomogeneity problem	80
4.9	Detailed formulation of Eshelby tensor D	83
4.10	References	87
5	Drainage of Poroelastic Fractures and Its Implications on the Performance of Naturally Fractured Reservoirs	91
5.1	Introduction	92
5.2	Statement of the Problem & Assumptions	97
5.3	Governing Equations	98
5.3.1	Mode decomposition	100
5.3.2	Fundamental solutions	102
5.4	Results and Discussions	104
5.4.1	Numerical results	105
5.5	Conclusion	110
5.6	References	110
6	Pressurized Poroelastic Inclusions: Short-term and Long-term Asymptotic Solutions	115
6.1	Introduction	116
6.2	Solution Methods	118
6.2.1	General approach	118
6.2.2	Governing equations of poroelastic medium	119
6.2.3	Poroelastic inclusions	121
6.3	Asymptotic Analysis	122
6.3.1	Mode (1) loading	122
6.3.2	Mode (2) loading	125
6.4	Numerical Results	126
6.5	Summary and Conclusion	127
6.6	Diffusion equation solution on an ellipsoidal surface	130
6.7	Duhamel's theorem	132
6.8	References	133
7	Summary and Future Works	135
7.1	Summary	135
7.2	Recommendations for Future Works	138

Appendix: Letters of Permission to Use Published Material	139
Vita.....	142

List of Tables

5.1	Different example descriptions for numerical analysis	105
5.2	Input parameters	106
6.1	The analogy between heat conduction and fluid diffusion equations	130
6.2	Dimensionless conduction shape factors and blending coefficients for different geometries (from Yovanovich et al. (1995))	132

List of Figures

2.1	A single inclusion embedded in an infinite medium. Ω_1 and C^1 are indicating inclusion domain and its elastic moduli tensor, respectively. Ω_0 and C^0 are representing the surrounding matrix and its elasticity moduli tensor, respectively.	11
2.2	Two inclusions embedded in an infinite medium.	15
2.3	This is a schematic picture of a double-inhomogeneity in an infinite poroelastic medium, subjected to a uniaxial stress, σ_{33}^0 . The a_i and \bar{a}_i are the principal half axes and Δ_3 is the distance of the centers of inhomogeneities from each other along x_3 axis.	19
2.4	σ_{33} -stress distribution along the x_3 axis of two co-axial spherical elastic inhomogeneities ($a_1 = \bar{a}_1 = a_2 = \bar{a}_2 = 1, a_3 = \bar{a}_3 = 0.5, \Delta_3 = 4$) under uniaxial tension ($\sigma_{33} = 1, p_1 = p_2 = 0; tension > 0$); for $\nu = 0.3$ and different values of $\gamma = \frac{G^1}{G^0} = \frac{G^2}{G^0}$. Part (a) of the figure shows the results from Moschovidis and Mura (1975) for the same problem.	19
2.5	The above graphs show σ_{33} -stress along the x_1 axis of two co-axial spherical elastic inhomogeneities ($a_1 = \bar{a}_1 = a_2 = \bar{a}_2 = 1, a_3 = \bar{a}_3 = 0.5, \Delta_3 = 4$) in uniaxial tension ($\sigma_{33} = 1, p_1 = p_2 = 0; tension > 0$); for $\nu = 0.3$ and different values of $\gamma = \frac{G^1}{G^0} = \frac{G^2}{G^0}$. Part (a) of the figure shows the results from Moschovidis and Mura (1975) for the same problem.	20
2.6	The above graphs show the effect of spacing between two co-axial spherical poroelastic inhomogeneities, Δ_3 , on σ_{33} and σ_{11} -stresses along the x_3 axis; ($a_1 = \bar{a}_1 = a_2 = \bar{a}_2 = 1, a_3 = \bar{a}_3 = 0.5$). Inclusions are uniformly pressurized and under uniaxial compression ($\sigma_{33} = 1, p_1 = p_2 = 1; Compression > 0$). The plots are generated for $\nu = 0.3$ and different values of $\gamma = \frac{G^1}{G^0} = \frac{G^2}{G^0}$	22
2.7	The above graphs show the effect of size of the two co-axial spherical poroelastic inhomogeneities on σ_{33} and σ_{11} -stresses along the x_3 axis; ($a_1 = \bar{a}_1 = a_2 = \bar{a}_2 = 1, a_3 = 0.5, \bar{a}_3 = 1$). Inclusions are uniformly pressurized and under uniaxial compression ($\sigma_{33} = 1, p_1 = p_2 = 1; Compression > 0$). The plots are generated for $\nu = 0.3$ and different values of $\gamma = \frac{G^1}{G^0} = \frac{G^2}{G^0}$	23

2.8	The above graphs show the effect of different pressure values inside the the two co-axial spherical poroelastic inhomogeneities on σ_{33} and σ_{11} -stresses along the x_3 axis; ($a_1 = \bar{a}_1 = a_2 = \bar{a}_2 = 1, a_3 = \bar{a}_3 = 0.5$). Inclusions are uniformly pressurized and under uniaxial compression ($\sigma_{33} = 1, p_1 = 1, p_2 = 2; Compression > 0$). The plots are generated for $\nu = 0.3$ and different values of $\gamma = \frac{G^1}{G^0} = \frac{G^2}{G^0}$	24
3.1	A single inclusion embedded in an infinite medium. Ω^* and C^* are indicating inclusion domain and its elastic moduli tensor, respectively. Ω and C are representing the surrounding matrix and its elasticity moduli tensor, respectively.	38
3.2	(a) Strain ratio; (b) Stress ratio due to pressure change inside an isotropic poroelastic inhomogeneity. Both graphs are plotted against the inhomogeneity aspect ratio, e . It is assumed g is shear modulus ratio, G^*/G ; $\alpha_{ij} = \delta_{ij}$ (isotropic case); and $\nu^0 = \nu^* = 0.2$. However, the dependence of the solution on ν^0 is weak. These graphs are in exact agreement with Figs. 4 and 7 in Rudnicki (2002a).	41
3.3	A schematic figure of transversely isotropic material. Planes parrel to $x - y$ are the planes of isotropy.	42
3.4	Stress ratio against inhomogeneity aspect ratio, e , for various shear modulus ratio ($g = G^*/G^0$) and Poisson's ratio. The solid lines indicate vertical stress ratio σ_{33}/p , whereas the dotted lines indicate lateral stress ratio σ_{11}/p	45
3.5	Stress ratio for different α_{33} values. $g = \frac{G^*}{G^0}; \nu^0 = \nu^* = 0.2; a_1 = a_2 = a_3 = 1$. (a) σ_{33}/p if $\alpha_{33} = 0.1$; (b) σ_{33}/p if $\alpha_{33} = 1$; (c) σ_{33}^d/p , difference of part (a) and (b); (d) σ_{11}/p if $\alpha_{33} = 0.1$; (e) σ_{11}/p if $\alpha_{33} = 1$; (f) σ_{11}^d/p , difference of part (d) and (e).	46
3.6	Vertical stress ratio σ_{33}/p versus (a) horizontal (b) vertical distance from the inhomogeneity center due to pressure change inside the poroelastic inhomogeneity, for different elastic and poroelastic anisotropic cases. Solid lines show transverse isotropic case; dashed lines show isotropic elastic case. For the isotropic case we assumed $\nu^0 = \nu^* = 0.2$, $g = 1$, $a_1 = a_2 = a_3 = 1$; For transverse isotropic case we used the results reported by (Pena, 1998, pp. 33) for saturated sandstone cores from an oil reservoir in Budare, Venezuela ($c_{11} = 3.6$, $c_{33} = 3.32$, $c_{44} = 0.99$, $c_{66} = 1.19$, $c_{12} = 1.29$, $c_{13} = 1.28$).	47
3.7	A medium consisted of pressurized poroelastic unidirectionally aligned inclusions embedded in an elastic matrix	51

3.8	Longitudinal Young's modulus of the medium $(E_{11})_M$ to Young's modulus of the matrix E_m for $\sigma_{11}^0 = 1$ and $p = 1$ and different inhomogeneity aspect ratios R , and volume ratios β for different material properties ratio of the inhomogeneities and the matrix (a) $E_I/E_m = 0.1$ (b) $E_I/E_m = 1.0$ (c) $E_I/E_m = 2.0$; (d) different p/σ_{11}^0 ratios	55
4.1	An ellipsoidal inclusion with principal axis parallel to Cartesian coordinate system (x_1, x_2, x_3)	69
4.2	Two ellipsoidal inhomogeneities	71
4.3	(a, b) σ_{11} and σ_{33} vs x_1 , for a single void inhomogeneity for various values of a_3/a_2 , compare with Meng et al. (2012) and Healy (2009); (c) σ_{33} vs a_2/a_1 for an ellipsoidal inhomogeneity for various values of $g = \frac{G^*}{G^0}$, compare with Mura (1987).	76
4.4	Stress vs x_3 for two interacting ellipsoidal cavities with uniform unit internal pressure, compare with Moschovidis (1975).	77
4.5	(a) Schematic of an ellipsoidal inhomogeneity which models pore pressure changes in a reservoir. This model calculates stress distribution inside and outside of the reservoir, due to pore pressure changes inside the reservoirs. (b) Changes in $\sigma_{11} = \sigma_{22}$ vs x_3 (c) changes in σ_{33} vs x_3 due to unit pressure drop inside the reservoir. It is assumed $g_1 = \frac{G^*}{G^0} = 0.5$ and $a_2/a_1 = 1$, $a_1/a_3 = 3$. $x_3 = 0$ is center of the inhomogeneity.	78
4.6	(a) Schematic of two ellipsoidal inhomogeneities which models pore pressure changes in two adjacent reservoirs. This model calculates stress distribution inside and outside of two adjacent reservoir, due to pore pressure changes inside the reservoirs. (b) Changes in $\sigma_{11} = \sigma_{22}$ vs x_3 (c) changes in σ_{33} vs x_3 due to unit pressure drop inside two adjacent reservoirs. It is assumed $g_1 = g_2 = \frac{G^*}{G^0} = 0.5$ and $a_2/a_1 = 1$, $a_1/a_3 = 3$. $x_3 = 0$ and $x_3 = -3$ are centers of the two ellipsoidal inhomogeneities.	79
5.1	Aperture size distribution in Groove Creek and Kinlaw formations follow power-law relations. Micro-fractures occur much more frequently than large size fractures (Gale, 2002).	94
5.2	The schematic picture for a single crack in an infinite poroelastic medium.	98
5.3	Volume changes of a single fracture due to production in a low confining stress versus dimensionless time.	107
5.4	Volume changes of a fracture due to production under large confining stresses versus dimensionless time.	108

5.5	Volume changes of a fracture due to production under large confining stresses versus dimensionless time.	109
5.6	Volume changes of a fracture due to production under large confining stresses versus dimensionless time.	109
6.1	An ellipsoidal poroelastic inclusion with principal axes (a_1, a_2, a_3) along major Cartesian coordinate system axis. The fluid pore pressure inside the inclusion and the matrix are p_I and p_0 , respectively ($p_I > p_0$).	117
6.2	(a) Mode 2 leak-off volume ratio (b) Mode 1 volume change ratio (c) Mode 2 volume change ratio; for different inclusion ratios. The material properties are assumed to be $\nu = 0.2$, $\nu_u = 0.4$, $\alpha = 0.89$ and $B = 0.8$	128
6.3	(a) Mode 2 leak-off volume ratio (b) Mode 1 volume change ratio (c) Mode 2 volume change ratio; assuming $R = 10$, and for different undrained Poisson's ratios . The material properties are assumed to be $\nu = 0.2$, $\alpha = 1$	129

Abstract

The scarce amount of conventional hydrocarbon reservoirs and increase of fuel consumption in the world have made production from unconventional hydrocarbon resources inevitable. Because of the low permeability of unconventional formations, fractures are the main paths for the fluid to flow. Therefore, detailed knowledge of the size, orientation, and permeability of the fracture systems are essential for reservoir engineers. Permeability of the fractures is function of their volume and opening, and stress and fluid pore pressure distribution in the formation. Since reservoir pressure may change over the production life of the reservoir, studying stress redistribution and mechanical behavior of the reservoirs due to the fluid pressure alteration plays a critical role in successfully operating the hydrocarbon fields.

This research investigates the behavior of poroelastic inclusions or inhomogeneities due to the pore pressure change, with applications in reservoir geomechanics. Considering different material properties and different pressure/temperature of hydrocarbon bearing formations in comparison to those of the surrounding geological structures, hydrocarbon reservoirs and subsurface fractures can be considered as inhomogeneities embedded inside an infinite poroelastic medium. Moreover, elliptic fractures are special cases of ellipsoidal inhomogeneities when their elastic moduli are zero, and one of the principal axes of the ellipsoid approaches zero.

This dissertation is concerned with these two topics: the thorough study of poroelastic inclusions and their applications in reservoir geomechanics; and poroelastic fractures and their implications on the performance of hydrocarbon reservoirs. Analytical solutions for

applied stress and strain distribution around single and double inhomogeneous poroelastic inclusions due to pore pressure changes in inclusions are derived, using Eshelby Equivalent Method (EIM) and assuming no hydraulic communication between the inclusion and the surrounding medium. This assumption is reasonable for modeling situations with large discrepancy between the permeability of the inclusion and the matrix. Later, considering hydraulic communication between the inclusion and the matrix, solution for the volume change of ellipsoidal poroelastic inclusions are derived.

Chapter 1

Overview

1.1 Introduction

The scarce amount of conventional hydrocarbon reservoirs and increase of fuel consumption in the world have made production from unconventional hydrocarbon resources inevitable. North America in particular has experienced a considerable increase in share of unconventional resources to the total energy needs in the last two decades (MIT, 2011; OPEC, 2011). Energy demand is projected to increase by 41% between 2012 and 2035, with growth averaging 1.5% per annum. The corresponding rising supply to meet the demand growth will come primarily from unconventional sources, by nonOPEC members, and is expected to increase by 10.8 *MBD*. United States, will provide the largest increments of non-OPEC supply, 3.6 *MBD*, during this period (BP, 2014).

Large volumes of these unconventional hydrocarbon resources are stored in tight naturally fractured reservoirs, such as tight sand, shale gas, shale oil and oil shale reservoirs (Holditch and Ephen, 2006; MIT, 2011). Because of the low permeability of these tight formations, fractures are the main paths for the fluid to flow. In other words, fractures and their distribution determine overall permeability of the reservoir. Fractures are of paramount importance for economic production from naturally fractured reservoirs and in their absence, it is impossible to recover hydrocarbons from these reservoirs (Aguilera, 2008). Therefore, detailed knowledge of the size, orientation, and permeability of the fracture systems are essential for reservoir engineers.

On the other hand, the stress regime acting in a reservoir is one of the most important parameters which controls the permeability of the fractured reservoirs. When depletion or injection occurs, fluid pressure in the reservoir changes, which can lead to stress changes in the formation. Length, aperture, and permeability of the fractures in the reservoir are function of the stress distribution in the formation. Moreover, having the knowledge of stress variations in a reservoir, has significant application in well bore stability and drilling wells in depleted zones. Since reservoir pressure may change frequently over the life of hydrocarbon fields, studying stress distribution and mechanical behavior of the reservoirs due to the fluid pressure alteration plays a critical role in successfully operating the hydrocarbon fields.

This research investigates the behavior of poroelastic inclusions (or inhomogeneities) due to change of the pore pressure, with concentration in the applications in reservoir geomechanics. An inclusion is defined as a finite sub-volume of a medium, which can be classified as inhomogeneities, homogeneous inclusions, or inhomogeneous inclusions. An inhomogeneity is a sub-volume of a medium, which has different material properties from the surrounding medium. Although homogeneous inclusions have the same material properties as their surroundings, they may possess different strain status. Inhomogeneous inclusions are finite sub-volumes of a medium, which are made of different materials and may experience different strain status at the same time.

Considering different material properties and different pressure/temperature of hydrocarbon bearing formations in comparison to those of the surrounding geological structures, hydrocarbon reservoirs and subsurface fractures can be considered as inhomogeneities embedded inside an infinite poroelastic medium. Moreover, elliptic fractures are special cases of ellipsoidal inhomogeneities when their elastic moduli are zero, and one of the principal axes of the ellipsoid approaches zero. The fact that most rocks, to some extent, are fractured makes studying poroelastic inhomogeneities interesting for petroleum engineers.

1.2 Outline

This dissertation is concerned with these two topics: the thorough study of poroelastic inclusions and their applications in reservoir geomechanics; and poroelastic fractures and their implications on the performance of hydrocarbon reservoirs.

In Chapter 2, an analytical solution for applied stress and strain distribution around double inhomogeneous poroelastic inclusions due to pore pressure changes in inclusions is provided. To address the problem, an approximate analytical approach used for elastic inclusions is modified for poroelastic inclusions. An application of this model in analyzing earth stress changes around hydrocarbon reservoirs due to fluid withdrawal/injection is discussed at the end of the chapter. This chapter is a modified text from Bedayat and Dahi Taleghani (2013, 2014).

In Chapter 3, the anisotropic poroelastic properties of the rocks and their impact on the stress changes due to pore pressure variations are studied using the Equivalent Inclusion Method (EIM). EIM is used to solve for stress and strain distributions inside and outside of an anisotropic poroelastic inhomogeneous inclusion. Further, the sensitivity of different elastic and poroelastic parameters are analyzed and discussed.

Chapter 4 explains the numerical calculations used in Chapters 2 and 3. In this chapter, the source code and detailed calculations of inside and outside of two interacting ellipsoidal inhomogeneities with arbitrary orientation are presented. Assuming the same material properties for one of the inclusions and the surrounding matrix, this code can also be used for a single inhomogeneity problem.

In Chapters 2 to 4, it is assumed that there is no hydraulic communication between the inclusion and the surrounding medium. Therefore, the fluid pressure in the surrounding rock will not change due to fluid pressure changes in the inclusion and there will be no fluid leak-off from the inclusion. This assumption is reasonable for modeling situations such as rock compaction-drive, gas expansion-drive hydrocarbon reservoirs, or geological carbon

sequestration (Rudnicki, 2002a,b; Chen, 2011; Soltanzadeh and Hawkes, 2012). The lack of hydraulic communication could be thwarted by cap rock or faults. For example, high permeability sandstone formations could be contained by extremely low permeability shale layers. However, neglecting the hydraulic communication between the inclusion and the matrix in the absence of an extremely low permeability matrix around the inclusion is not a valid assumption. Therefore, Chapters 5 and 6 consider hydraulic communication between the inclusion (or fracture) and the matrix.

Chapter 5 is on poroelastic fractures and their implications on the performance of hydrocarbon reservoirs. This chapter provides poroelastic analysis for a single micro-fracture subject to fluid withdrawal (production) through the fracture assuming plain strain condition. Formation is assumed to be a low permeable poroelastic medium. In this chapter the role of natural fractures and their poroelastic properties to explain discrepancy in the measured formation permeability by using different methods is investigated. To achieve this goal, an analytical solution for fracture volume changes due to fluid withdrawal (production) is derived. The roles of differential in-situ stress and formation pressure in determining the crack volume changes are found to be significant. The results could be used to relate the significant reduction in production from some of the shale gas wells to the closure of microfractures or even larger non-propped fractures. This chapter is a modified text from Bedayat and Dahi Taleghani (2012).

Chapter 6 provides the solution for the volume change of ellipsoidal poroelastic inclusions, assuming hydraulic communication between the inclusion and the matrix. A good example of this problem would be the mechanical behavior of a pressurized stationary fracture in a reservoir.

Finally, Chapter 7 summarizes the main results presented in this dissertation and gives recommendations for future works.

1.3 References

- Aguilera, R., 2008. Role of natural fractures and slot porosity on tight gas sands, in: Proceedings of SPE Unconventional Reservoirs Conference, Society of Petroleum Engineers. pp. 10–12. doi:10.2118/114174-MS.
- Bedayat, H., Dahi Taleghani, A., 2012. Drainage of poroelastic fractures and its implications on the performance of naturally fractured reservoirs, in: 46th US Rock Mechanics/Geomechanics Symposium, Chicago, IL, USA.
- Bedayat, H., Dahi Taleghani, A., 2013. The equivalent inclusion method for poroelasticity problems, in: Poromechanics V, American Society of Civil Engineers, Reston, VA. pp. 1279–1288. doi:10.1061/9780784412992.153.
- Bedayat, H., Dahi Taleghani, A., 2014. Interacting double poroelastic inclusions. *Mechanics of Materials* 69, 204–212. doi:10.1016/j.mechmat.2013.10.006.
- BP, 2014. BP energy outlook 2035. Technical Report January. BP.
- Chen, Z.R., 2011. Poroelastic model for induced stresses and deformations in hydrocarbon and geothermal reservoirs. *Journal of Petroleum Science and Engineering* 80, 41–52. doi:10.1016/j.petrol.2011.10.004.
- Holditch, S., Ephen, 2006. Tight gas sands. *Journal of Petroleum Technology* 58. doi:10.2118/103356-MS.
- MIT, 2011. The future of natural gas: an interdisciplinary MIT study. Technical Report. Massachusetts Institute of Technology.
- OPEC, 2011. World oil outlook. Technical Report. Organization of the Petroleum Exporting Countries.
- Rudnicki, J.W., 2002a. Alteration of regional stress by reservoirs and other inhomogeneities: Stabilizing or destabilizing?, in: Vouille, G., Berest, P. (Eds.), Proc. 9th Int. Congr. Rock Mechanics, Vol. 3, Paris, Aug. 25–29, 1999, Paris, France. pp. 1629–1637.

Rudnicki, J.W., 2002b. Eshelby transformations, pore pressure and fluid mass changes, and subsidence, in: Poromechanics II, Proc. 2nd Biot Conference on Poromechanics, Grenoble, France.

Soltanzadeh, H., Hawkes, C.D., 2012. Evaluation of caprock integrity during pore pressure change using a probabilistic implementation of a closed-form poroelastic model. International Journal of Greenhouse Gas Control 7, 30–38. doi:10.1016/j.ijggc.2011.10.006.

Chapter 2

Interacting Double Poroelastic Inclusions^{1, 2}

In this paper, we provide Eshelby solution for applied stress and strain distribution around double inhomogeneous poroelastic inclusions due to pore pressure changes in inclusions. To address the problem, we modified an approximate analytical approach (Moschovidis and Mura, 1975) for poroelastic inclusions. Inhomogeneous Inclusions are finite sub-volumes of a medium, which are made of different materials and may experience different strain status at the same time. This method could have a wide range of applications from rock mechanics problems to tissue mechanics. An application of this model in analyzing earth stress changes around hydrocarbon reservoirs due to fluid withdrawal/injection is discussed at the end of the paper.

2.1 Introduction

Theory of inclusions (Eshelby, 1957, 1959) includes a broad range of problems in engineering. Micromechanics (Nemat-Nasser and Hori, 1999) and mechanics of composite materials (Richard M. Christensen, 2012), damage mechanics (Voyiadjis and Kattan, 2006), mineralogy (Van der Molen and Van Roermund, 1986), biophysics (Marquez et al., 2005) and

² Bedayat, H., & Dahi Taleghani, A., 2013. The Equivalent Inclusion Method for poroelasticity problems. In *Poromechanics V* (pp. 12791288). Reston, VA: American Society of Civil Engineers. doi:10.1061/9780784412992.153

geomechanics (Rudnicki, 2011) are a few examples of the fields in which this theory is being used.

An inclusion is defined as a finite sub-volume of a medium, which can be classified as inhomogeneities, homogeneous inclusions, and inhomogeneous inclusions. An inhomogeneity is a sub-volume of a medium, which has different material properties from the surrounding medium. However, although homogeneous inclusions have same material properties with their surrounding, they may possess different strain status. Inhomogeneous Inclusions are finite sub-volumes of a medium, which are made of different materials and may experience different strain status at the same time.

Elastic and plastic strains, thermal expansion, pressure difference, phase transformation, initial strains, and misfit strains are different types of strain which could be referred to as eigenstrains (Mura, 1987). Eshelby (1957, 1959) solved for stress distribution in an elastic medium due to the presence of inclusions. Eshelby's solution provides stress and strain field around an inclusion in an infinite elastic medium, which undergoes a uniform strain. Later, this technique has been extended to determine the stress and strain in regions with different elastic properties from those of the surrounding material in presence of remote stress boundary conditions. These solutions have had different applications in the last couple of decades. An extended review of recent works in this subject may be found in Zhou et al. (2013).

In this paper, we study stress and strain distribution around a single and double inhomogeneous poroelastic inclusions due to pore pressure changes in inclusions. This method could have a wide range of applications from soil and rock mechanics problems to tissue mechanics. Here, we are mainly interested in dealing with the application of this problem in analyzing stress changes around hydrocarbon reservoirs due to fluid withdrawal or injection.

Rocks in the subsurface may be considered as uniform media with scattered inhomogeneities, different pore pressures or geological properties from the surrounding rocks. Biot (1941) developed a general theory of three dimensional consolidation by solving coupled dif-

fusion and elasticity equations, and later added temperature effects into his theory (Biot, 1956a,b). Later, Rice and Cleary (1976) developed constitutive equations for linear, isotropic, fluid infiltrated porous media based on Biot's theory

$$2G\varepsilon_{ij} = \sigma_{ij} - \frac{\nu}{1+\nu}\sigma_{kk}\delta_{ij} + \frac{1-2\nu}{1+\nu}\alpha p\delta_{ij}, \quad (2.1a)$$

$$\zeta = \frac{1-\nu}{2G(1+\nu)}\alpha\left(\sigma_{kk} + \frac{p}{B}\right), \quad (2.1b)$$

where, δ_{ij} is the Kronecker delta, ε_{ij} and σ_{ij} are the strain and stress components in the solid matrix and p is the fluid pore pressure. Here, the increment of fluid content ζ is defined as the mass of pore fluid per unit bulk volume ($\zeta = \frac{\delta m_f}{\rho_{f0}}$, where ρ_{f0} is the fluid density in the reference state). It is notable that there are four material constants in the above equations: shear modulus G , drained Poisson's ratio ν , Biot-Willis parameter α , and Skempton's coefficient B . The first equation relates strain (ε_{ij}), stress (σ_{ij}), and pore pressure (p). The second equation relates the changes in the fluid mass per unit volume to the first invariant of stress tensor (σ_{kk}). By inverting the first equation to get the stress components and plugging them into the equilibrium equation (after eliminating p and using the small strains definition), Navier equations for displacements can be derived as

$$G\nabla^2 u_i + \frac{G}{1-2\nu_u} \frac{\partial^2 u_j}{\partial x_i \partial x_j} = BK_u \frac{\partial \zeta}{\partial x_i} - F_i, \quad (2.2)$$

where u is the displacement vector, F is the body force per unit bulk volume. The K_u and ν_u are undrained bulk modulus and Poisson's ratio, respectively. Since a complete mathematical analogy exists between thermoelasticity and poroelasticity (Norris, 1992), solution of either cases may be used to solve the other with a slight difference in the interpretation of symbols and parameters.

Considering the small size of hydrocarbon reservoirs in comparison to the geological structures, one may consider reservoirs as inclusions embedded inside an infinite medium. This assumption is made because reservoirs' pore pressures may change due to production, and they may not have similar lithology as the surrounding rocks. Reservoir subsidence, wellbore stability, closure of natural fractures and seismic activities near the faults are some of the negative consequences of the changes in stress and pore pressures in reservoirs. Each of these issues may affect hydrocarbon production in a different way. Rudnicki (2002) modified Eshelby's method to calculate stresses in poroelastic inclusions with different pore pressures, temperatures or elastic moduli. Soltanzadeh et al. (2007) used Eshelby's method to provide effective stress analysis for reservoir compaction due to hydrocarbon production, and found stress changes induced by a uniform pressure change in an ellipsoidal reservoir embedded in an infinite medium. Chen (2011) solved this problem for a single ellipsoidal poroelastic or thermoelastic inclusion embedded in an infinite elastic body. He also considered double inclusion problem, using Hori and Nemat-Nasser (1993) method, in the case that one inclusion encompasses the other one.

In the present work, the stress distribution in the presence of interacting poroelastic inhomogeneities is studied. To have a better understanding of the presented solution, we first briefly review Eshelby's problem in elasticity, and then we will go through required modifications of this formula for poroelasticity. Problems involving interacting inclusions are mostly studied using superposition of elastic fields. Moschovidis and Mura (1975) studied two ellipsoidal non-intersecting inclusions by approximating equivalent eigenstrain using Taylor's series expansions of Eshelby's tensors. Solutions derived using this method is confirmed by numerical finite element calculations (Fond et al., 2001). Shodja et al. (2003) revised this method to achieve a more computationally efficient one by eliminating unnecessary evaluation of derivatives of Eshelby's tensors. Here, we extend the poroelastic solution for a single inclusion to two interacting inclusions. The methodology used in this paper is a

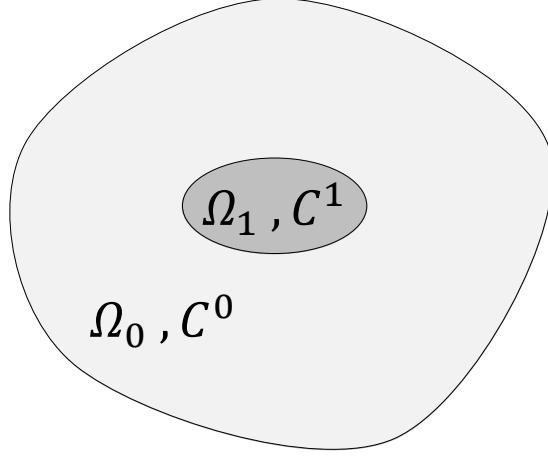


Figure 2.1: A single inclusion embedded in an infinite medium. Ω_1 and C^1 are indicating inclusion domain and its elastic moduli tensor, respectively. Ω_0 and C^0 are representing the surrounding matrix and its elasticity moduli tensor, respectively.

combination of previous results for poroelastic inclusions and Moschovidis and Mura (1975) approach to solve for interactions between poroelastic inclusions.

2.2 Single Inclusion

2.2.1 Elastic inclusions

The problem of an embedded ellipsoidal inclusion ($C_{ijkl}^0 = C_{ijkl}^1 = C_{ijkl}$)³ in an infinite elastic medium, which undergoes a uniform inelastic deformation has been solved by Eshelby (Eshelby, 1957). The contact boundary condition between inclusion and matrix is a welded contact i.e., there is no slippage on the boundary. Figure 3.1 shows a schematic view of the Eshelby's problem. For the case of homogenous ellipsoidal inclusions with uniform eigenstrain, ε^* , Eshelby (1957) solved the stress and displacement fields for both inside and outside of the inclusion through defining a tensor, S_{ijkl} or so-called Eshelby's tensor. Eshelby's tensor is a fourth rank tensor, and in the case of single inclusion problems is a function of geometry and Poisson's ratio of the inclusion (see Mura (1987) for more details about the components of tensor S and its derivation). The main result of the Eshelby's solution can

³For isotropic materials, elastic moduli is given by

$$C_{ijkl} = \frac{2G\nu}{1-2\nu}\delta_{ij}\delta_{kl} + G(\delta_{ik}\delta_{jl} + \delta_{il}\delta_{jk}) .$$

be expressed as

$$\varepsilon_{ij} = S_{ijkl}\varepsilon_{kl}^*, \quad (2.3a)$$

$$\sigma_{ij} = C_{ijkl}^1(\varepsilon_{kl} - \varepsilon_{kl}^*), \quad (2.3b)$$

where ε_{ij} is the actual strain, and ε_{kl}^* is the eigenstrain. To analyze the case of an inhomogeneous inclusions, Eshelby introduced the Equivalent Inclusion Method (EIM). He showed that the inhomogeneous inclusion problem can be reduced to an inclusion problem with equivalent eigenstrains in a homogenous medium, when the eigenstrain is chosen properly. In the case of imposed strain at infinity, ε_{kl}^0 , and given distribution of preliminary eigenstrain ε_{kl}^p , the following consistency equation rises

$$C_{ijkl}^1[\varepsilon_{kl}^0 + \varepsilon_{kl} - \varepsilon_{kl}^p] = C_{ijkl}^0[\varepsilon_{kl}^0 + \varepsilon_{kl} - \varepsilon_{kl}^p - \varepsilon_{kl}^*], \quad (2.4)$$

where

$$\varepsilon_{kl} = S_{ijkl}\varepsilon_{kl}^{**}. \quad (2.5)$$

Here, ε_{kl}^{**} is the equivalent (homogenizing) eigenstrain, $\varepsilon_{kl}^{**} = \varepsilon_{kl}^p + \varepsilon_{kl}^*$. Equation (2.5) can be used to eliminate ε_{kl} from Eq. (2.4) to determine ε_{kl}^{**} . Hence, the total stress field inside the inclusion can be calculated from

$$\sigma_{ij}^T = \sigma_{ij}^0 + \sigma_{ij} = C_{ijkl}^1[\varepsilon_{kl}^0 + \varepsilon_{kl}] = C_{ijkl}^0[\varepsilon_{kl}^0 + S_{klmn}\varepsilon_{mn}^{**} - \varepsilon_{mn}^{**}]. \quad (2.6)$$

2.2.2 Poroelastic inclusions

Now, let's suppose that the inclusion shown in Fig. 3.1 is composed of a poroelastic material rather than an elastic material and is fully saturated with a slightly compressible fluid. Poro-

lastic inclusions may have different elastic or poroelastic properties, and even have different fluid pressure from the surrounding medium. We further assume that there is no hydraulic communication between the inclusion and the surrounding medium; therefore, the fluid pressure in the surrounding rock will not change due to fluid pressure changes in the inclusion. Hence, the surrounding medium may deform in drained conditions. These assumptions are reasonable for modeling situations like rock compaction-drive and gas expansion-drive hydrocarbon reservoirs, or geological carbon sequestration (Rudnicki, 2011; Soltanzadeh and Hawkes, 2012). The lack of hydraulic communication could be provided by a cap rock or faults limiting the formation. For example, high permeability sandstone formations could be contained by extremely low permeability shale layers.

Despite the popularity of Eshelby's equivalent inclusion method in elasticity, this method has not been fully developed for poroelasticity problems except for a few limited cases. Rudnicki (2002) used the Eshelby's equivalent inclusion method to calculate the alteration of local stresses induced by a single inclusion with elastic moduli and pore pressure different from those of the surrounding medium. Using basic linear poroelasticity principles, stress inside the inhomogeneity can be written as (Rice and Cleary, 1976)

$$\sigma_{ij} = \sigma_{ij}^0 + C_{ijkl}^1 \varepsilon_{kl} + \alpha p \delta_{ij}, \quad (2.7)$$

where σ_{ij} are components of stress tensor (positive in compression) and p is the fluid pressure inside the inclusion. Therefore, Eq. (2.6) can be modified for poroelastic medium:

$$\sigma_{ij}^T = \sigma_{ij} + \sigma_{ij}^0 = C_{ijkl}^1 [\varepsilon_{kl} + \varepsilon_{kl}^0] + \alpha p \delta_{ij} = C_{ijkl}^0 [S_{klmn} \varepsilon_{mn}^{**} - \varepsilon_{mn}^{**} + \varepsilon_{kl}^0]. \quad (2.8)$$

Later, Soltanzadeh et al. (2007) considered the inclusion problem for a plain strain elliptical poroelastic inhomogeneity. They showed that poroelastic dilatational eigenstrain can be found from Eq. (2.1a) by assuming $\sigma_{ij} = 0$ from eigenstrain definition. Thus, poroelastic

eigenstrain can be expressed as

$$\varepsilon_{ij}^* = \frac{\alpha(1-2\nu)}{2G(1+\nu)} p \delta_{ij}. \quad (2.9)$$

All previous methods result in uniform stress and strain distribution inside the inclusion, when the medium is subjected to constant far-field stress and the fluid pressure is constant. However, in the double inclusion case, due to interaction of the inhomogeneities, the stress and strain fields inside the inclusions are no longer uniform, which was the main motivation for studying interacting double poroelastic inclusions problem.

2.3 Two Inclusions

In most practical cases, inclusions are generally existing in large quantities. Existence of multiple inclusions and their interactions affect the stress field in the medium. For instance, uniform stress and strain inside the inclusion is no longer valid for multiple inclusions problem (Shodja and Sarvestani, 2001). An easy approach to deal with this problem is superposing elastic solutions for single inclusions; or in other words, ignoring the interaction between inclusions (Nemat-Nasser and Hori, 1999). Although this method could be a good approximation when inclusions are located far enough from each other, their interactions may not be ignored when they are closely located.

In this section, we derive the stress field of two interacting poroelastic inclusions by modifying Moschovidis and Mura (1975) solution for two interacting elastic inclusions.

Consider two inclusions Ω_1 and Ω_2 (see Fig. 2.2), which are under an applied stresses, σ^0 at infinity. The x_i and \bar{x}_i are local coordinate systems taken at the center of Ω_1 and Ω_2 , respectively. These two coordinate systems are related by

$$x_i - c_i = a_{ij} \bar{x}_j, \quad \bar{x}_i = a_{ji} (x_j - c_j), \quad (2.10)$$

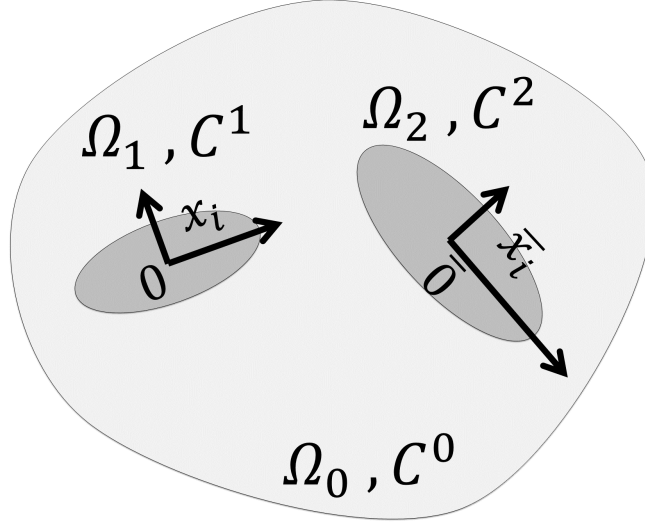


Figure 2.2: Two inclusions embedded in an infinite medium.

where a_{ij} is the direction cosine of a vector connecting center of two inclusions, i.e. between the x_i axis and the \bar{x}_j axis, and c_i is the x_i coordinate of the origin of the coordinate system attached to Ω_2 . To solve this problem, Moschovidis and Mura (1975) used the equivalent inclusion method for each inclusion individually. Then considering the fact that each inclusion may have a different equivalent eigenstrain, they solved the system of consistency equations (Eq. (2.4)) for two elastic inclusions. Following the same approach used for elastic inclusions and considering the pressure related term added to the stress inside the poroelastic medium ($\alpha p \delta_{ij}$), consistency equations for double interacting poroelastic inhomogeneous inclusion system can be modified as

$$C_{ijkl}^1[\varepsilon_{kl}^0 + \varepsilon_{kl}] + \alpha_1 p_1 \delta_{ij} = C_{ijkl}^0[\varepsilon_{kl}^0 + \varepsilon_{kl} - \varepsilon_{kl}^{*1}] \quad \text{in } \Omega_1, \quad (2.11a)$$

$$C_{ijkl}^2[\varepsilon_{kl}^0 + \varepsilon_{kl}] + \alpha_2 p_2 \delta_{ij} = C_{ijkl}^0[\varepsilon_{kl}^0 + \varepsilon_{kl} - \varepsilon_{kl}^{*2}] \quad \text{in } \Omega_2, \quad (2.11b)$$

where superscripts 1 and 2 indicate the corresponding equations for domains Ω_1 and Ω_2 , respectively. Assuming all the strains are given in the form of polynomials with respect

to the local Cartesian coordinate system (see Section 2.6), the applied strain before the disturbance ($\varepsilon_{ij}^0(x)$ and $\bar{\varepsilon}_{ij}^0(x)$) can be written as

$$\varepsilon_{ij}^0(x) = E_{ij} + E_{ijk}x_k + E_{ijkl}x_kx_l + \cdots, \quad (2.12a)$$

$$\bar{\varepsilon}_{ij}^0(x) = \bar{E}_{ij} + \bar{E}_{ijk}\bar{x}_k + \bar{E}_{ijkl}\bar{x}_k\bar{x}_l + \cdots. \quad (2.12b)$$

Here, $E_{ij\dots}$ are constants and the variables with a bar are defined with respect to second inclusion coordination system. Analogously, equivalent eigenstrains ($\varepsilon_{ij}^{*1}(x)$ and $\bar{\varepsilon}_{ij}^{*2}(x)$) can be defined as

$$\varepsilon_{ij}^{*1}(x) = B_{ij}^1 + B_{ijk}^1x_k + B_{ijkl}^1x_kx_l + \cdots, \quad (2.13a)$$

$$\bar{\varepsilon}_{ij}^{*2}(x) = B_{ij}^2 + B_{ijk}^2\bar{x}_k + B_{ijkl}^2\bar{x}_k\bar{x}_l + \cdots, \quad (2.13b)$$

where $B_{ij\dots}$ are constants. Using the concept of higher ranked Eshelby's tensors (see Section 2.6) and Eq. (2.3a), the strains associated with the eigenstrains will be equal to

$$\varepsilon_{ij}^1(x) = D_{ijkl}^1(x)B_{kl}^1 + D_{ijklq}^1(x)B_{klq}^1 + D_{ijklqr}^1(x)B_{klqr}^1 + \cdots, \quad (2.14a)$$

$$\bar{\varepsilon}_{ij}^2(x) = D_{ijkl}^2(\bar{x})B_{kl}^2 + D_{ijklq}^2(\bar{x})B_{klq}^2 + D_{ijklqr}^2(\bar{x})B_{klqr}^2 + \cdots. \quad (2.14b)$$

In the above equations, D represents higher order Eshelby's tensors. For x in Ω_1 , $D^1(x)$ are polynomials of x in Ω_1 , and $D^2(\bar{x})$ are expanded by Taylor series around the origin of the associated local coordinate system. Whereas, for x in Ω_2 , $D^2(\bar{x})$ are polynomials of \bar{x} in Ω_2 , and $D^1(x)$ are approximated by a Taylor expansion of x in Ω_2 . Then the strain, ε_{kl} , in

Eq. (2.11) is the sum of $\varepsilon_{ij}^1(x)$ and $\varepsilon_{ij}^2(x)$

$$\varepsilon_{ij}(x) = \varepsilon_{ij}^1(x) + \varepsilon_{ij}^2(x). \quad (2.15)$$

Using Eqs. (2.12) and (2.14) in the system of Eq. (2.11), values for B^1 and B^2 can be obtained. Finally, it is sufficient to solve the consistency equations in Ω_1 and Ω_2 , to find the constants of polynomial parts of eigenstrain, B . Consequently in Ω_1 we will have

$$\begin{aligned} \Delta C_{stmn}^1 \left\{ \left[D_{mnij}^1(0)B_{ij}^1 + D_{mnijkl}^1(0)B_{ijkl}^1 + \dots \right] \right. \\ \left. + a_{mc}a_{nh} \left[D_{chij}^2(0)B_{ij}^2 + D_{chijk}^2(0)B_{ijk}^2 + D_{chijkl}^2(0)B_{ijkl}^2 + \dots \right] \right\} \\ - C_{stmn}^0 B_{mn}^1 = -\Delta C_{stmn}^1 E_{mn} - \alpha_1 p_1 \delta_{st}, \end{aligned}$$

$$\begin{aligned} \Delta C_{stmn}^1 \left\{ \left[\frac{\partial}{\partial x_p} D_{mnijk}^1(0)B_{ijk}^1 + \dots \right] \right. \\ \left. + a_{mc}a_{nh}a_{pf} \left[\frac{\partial}{\partial \bar{x}_f} D_{chij}^2(0)B_{ij}^2 + \frac{\partial}{\partial \bar{x}_f} D_{chijk}^2(0)B_{ijk}^2 + \frac{\partial}{\partial \bar{x}_f} D_{chijkl}^2(0)B_{ijkl}^2 + \dots \right] \right\} \\ - C_{stmn}^0 B_{mnp}^1 = -\Delta C_{stmn}^1 E_{mnp}, \end{aligned}$$

etc.

(2.16)

To solve the above system of equations, the coefficients of the power series in the left and right hand sides of the equations should be equated. Similar system of equations should be solved for the second inclusion, Ω_2

$$\begin{aligned} \Delta C_{stmn}^2 \left\{ \left[D_{mnij}^2(\bar{0})B_{ij}^2 + D_{mnijkl}^2(\bar{0})B_{ijkl}^2 + \dots \right] \right. \\ \left. + a_{cm}a_{hn} \left[D_{chij}^1(\bar{0})B_{ij}^1 + D_{chijk}^1(\bar{0})B_{ijk}^1 + D_{chijkl}^1(\bar{0})B_{ijkl}^1 + \dots \right] \right\} \\ - C_{stmn}^0 B_{mn}^2 = -\Delta C_{stmn}^2 \bar{E}_{mn} - \alpha_2 p_2 \delta_{st}, \end{aligned}$$

$$\begin{aligned}
& \Delta C_{stmn}^2 \left\{ \left[\frac{\partial}{\partial \bar{x}_p} D_{mnijk}^2(\bar{0}) B_{ijk}^2 + \dots \right] \right. \\
& \left. + a_{cm} a_{hn} a_{fp} \left[\frac{\partial}{\partial x_f} D_{chij}^1(\bar{0}) B_{ij}^1 + \frac{\partial}{\partial x_f} D_{chijk}^1(\bar{0}) B_{ijk}^1 + \frac{\partial}{\partial x_f} D_{chijkl}^1(\bar{0}) B_{ijkl}^1 + \dots \right] \right\} \\
& - C_{stmn}^0 B_{mnp}^2 = -\Delta C_{stmn}^2 E_{mnp}, \\
& etc.
\end{aligned} \tag{2.17}$$

Here, $\Delta C_{stmn}^i = C_{stmn}^0 - C_{stmn}^i$, $i = 1, 2$ and $B_{ij\dots}$ are the coefficients of the polynomial expansion of poroelastic eigenstrains. By obtaining B^1 and B^2 , final strains can be calculated by Eqs. (2.14) and (2.15). The accuracy of results depends on the degree of polynomials employed; however, the dependency is only substantial for very strong interaction effects.

2.4 Results and Discussions

We start this section with two verification examples for solutions developed in previous sections. Let's consider two ellipsoidal inhomogeneities embedded in an infinite poroelastic medium with applied stresses σ_{ij}^0 at infinity. For simplification purposes, the principal axes of the inhomogeneities (i.e. x_i and \bar{x}_i axes) are assumed to be aligned with the Cartesian coordinate system. Figure 2.3 shows the configuration of the inhomogeneities, in which Δ_i is the distance between centers of the inhomogeneities along the i -th coordinate axis ($i = 1, 2, 3$). The dimension of ellipsoidal inclusions along the corresponding coordinate axes are denoted by a_i and \bar{a}_i , respectively ($i = 1, 2, 3$). To verify the accuracy of the proposed approach, we first consider the special case in which fluid pressure is kept constant. Hence, the problem is simplified to two elastic inhomogeneities, which are previously solved by Moschovidis and Mura (1975). Figures 2.4(b) and 2.5(b) demonstrates the σ_{33} -stress along the x_3 and x_1 axes (shown in Fig. 2.3) for inclusions under uniform tensile loading at infinity ($\sigma_{33}^0 = 1$) and different shear modulus ratios of inclusion and matrix, γ . These results are verified to be in exact agreement with the results obtained by Moschovidis and Mura (1975),

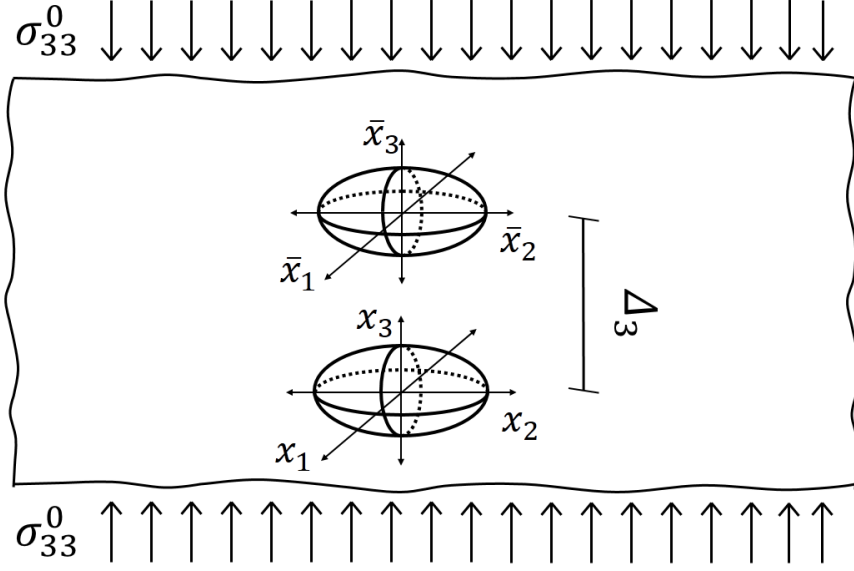


Figure 2.3: This is a schematic picture of a double-inhomogeneity in an infinite poroelastic medium, subjected to a uniaxial stress, σ_{33}^0 . The a_i and \bar{a}_i are the principal half axes and Δ_3 is the distance of the centers of inhomogeneities from each other along x_3 axis.

shown Figs. 2.4(a) and 2.5(a). Here, we applied the equivalent inclusion method for double

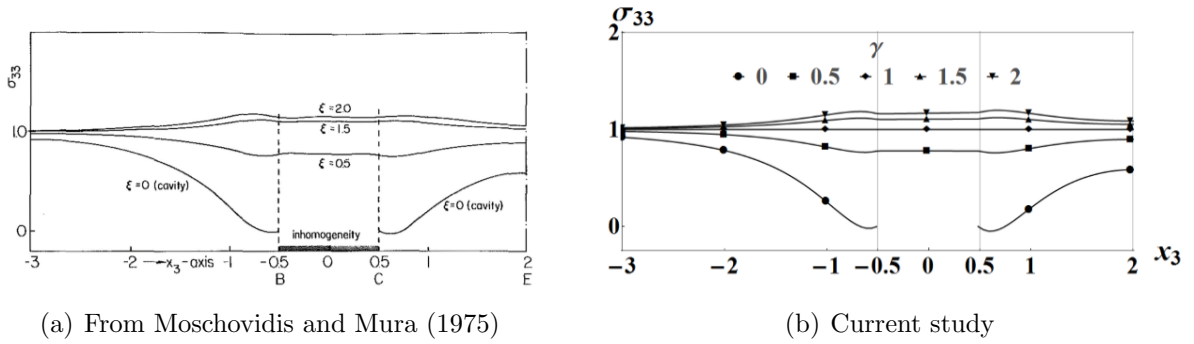
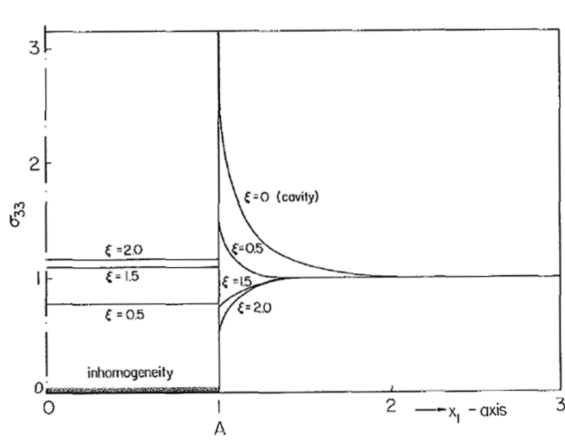


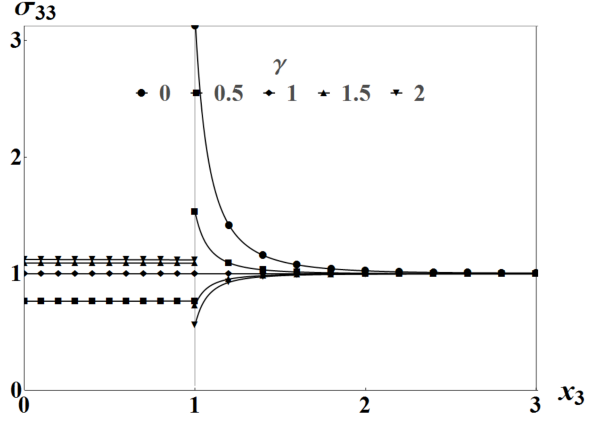
Figure 2.4: σ_{33} -stress distribution along the x_3 axis of two co-axial spherical elastic inhomogeneities ($a_1 = \bar{a}_1 = a_2 = \bar{a}_2 = 1, a_3 = \bar{a}_3 = 0.5, \Delta_3 = 4$) under uniaxial tension ($\sigma_{33} = 1, p_1 = p_2 = 0; tension > 0$); for $\nu = 0.3$ and different values of $\gamma = \frac{G^1}{G^0} = \frac{G^2}{G^0}$. Part (a) of the figure shows the results from Moschovidis and Mura (1975) for the same problem.

poroelastic inclusions problem under several different conditions:

- different spacing between centers of the inhomogeneities.
- different shear modulus ratios of inclusions and matrix.



(a) From Moschovidis and Mura (1975)



(b) Current study

Figure 2.5: The above graphs show σ_{33} -stress along the x_1 axis of two co-axial spherical elastic inhomogeneities ($a_1 = \bar{a}_1 = a_2 = \bar{a}_2 = 1, a_3 = \bar{a}_3 = 0.5, \Delta_3 = 4$) in uniaxial tension ($\sigma_{33} = 1, p_1 = p_2 = 0$; *tension* > 0); for $\nu = 0.3$ and different values of $\gamma = \frac{G^1}{G^0} = \frac{G^2}{G^0}$. Part (a) of the figure shows the results from Moschovidis and Mura (1975) for the same problem.

- different size of the inclusions.
- different pressure value inside the inclusions.

Due to the primary interest of the authors in subsurface problems, compressive stresses are assumed to be positive, hereafter. Figure 2.6 shows the effect of distance between centers of the two co-axial spherical poroelastic inhomogeneities and demonstrates how stress regime changes when inclusions laying closer to each other. As inclusions become closer to each other, they start interacting with each other, so stresses inside the inclusions become non-uniform, especially in stiffer inclusions. Comparison of Figs. 2.4 and 2.6(a) shows more compressive normal stresses near the pressurized inclusions as opposed to elastic inclusions, especially in inclusions with elastic moduli lower than that of the medium. This trend agrees with observations in depleted formations (Sayers et al., 2007). For example, lower mud weights should be used to drill depleted formations to avoid lost circulation; or hydraulic fracture jobs can be done more effective after depletion of a reservoir (Zoback, 2007). As a reservoir depletes due to production, the total horizontal stress in the reservoir rock decreases.

Consequently, fracture gradient decreases inside the reservoir as reservoir tends to shrink but confined by surrounding rocks. Reservoir shrinkage causes the horizontal stresses to redistribute and become more compressive above and below the reservoir (Segall, 1989). These changes in the stress field may cause faulting or seismic activities inside and outside of the reservoir.

Here, we assumed that depletion or pore pressure variations in the reservoir will not change the pore pressure in the surrounding rocks as low permeability cap rock hinders any hydraulic communication between the reservoir and the surrounding rocks. It is notable that since the size of reservoirs are assumed to be much less than the surrounding rocks, hence pore pressure in the surrounding rocks is mainly a hydrostatic pressure. Therefore, we may consider the surrounding rock in the effective stress mode or simply as an elastic medium.

In Fig. 2.7, we showed how the size of inclusions affects the stress distribution around the inclusion. Figures 2.7(a) and 2.7(c) show that normal compressive stresses will be higher in larger inclusions with greater shear modulus ratio, γ . Furthermore for stiff inclusions, compressive stresses near the larger inclusion is greater than that of the smaller one. However, for softer inclusions, the minimum compressive stress in the medium occurs in the vicinity of the larger inclusion.

Finally, Fig. 2.8 shows stress distribution around inclusions with different pore pressures and different sizes. It can be seen that for an unequal pressurized double inclusion system, compressive stresses inside the softer inclusion is larger than that of the stiffer inclusion.

Considering Figs. 2.6 to 2.8, the distance between the inclusions, elasticity modulus ratio, initial stresses and pore pressure conditions are the major factors that may affect the final stress distribution around two inclusions.

2.5 Summary

In this article, an analytical approach originally developed by Moschovidis and Mura (1975) for determining stress distribution around two interacting elastic inhomogeneities, was adopted

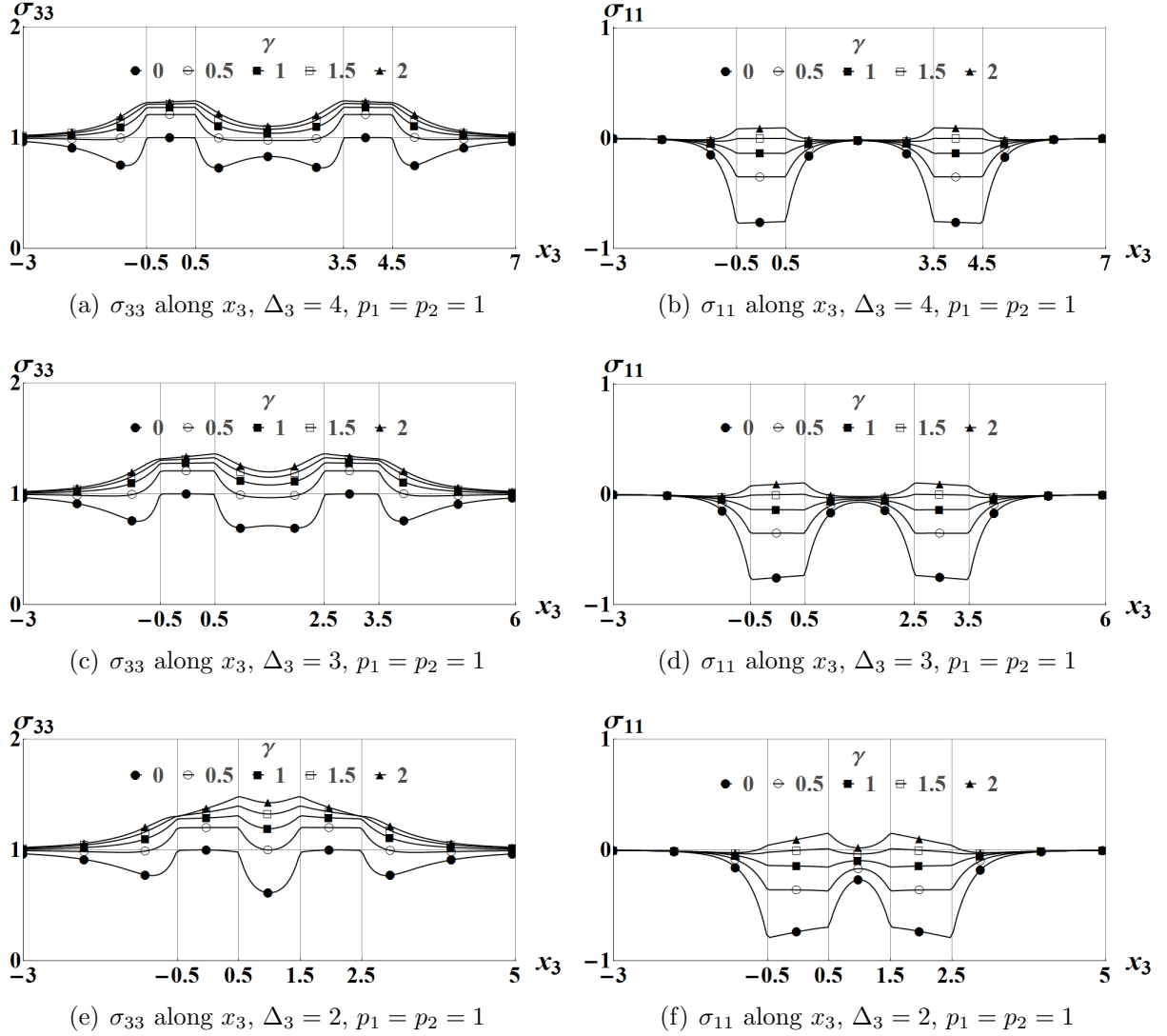


Figure 2.6: The above graphs show the effect of spacing between two co-axial spherical poroelastic inhomogeneities, Δ_3 , on σ_{33} and σ_{11} -stresses along the x_3 axis; ($a_1 = \bar{a}_1 = a_2 = \bar{a}_2 = 1, a_3 = \bar{a}_3 = 0.5$). Inclusions are uniformly pressurized and under uniaxial compression ($\sigma_{33} = 1, p_1 = p_2 = 1$; *Compression* > 0). The plots are generated for $\nu = 0.3$ and different values of $\gamma = \frac{G^1}{G^0} = \frac{G^2}{G^0}$.

for double poroelastic interacting inhomogeneous inclusions. These inclusions are assumed to be embedded in an infinite elastic medium and under nonuniform far-field loading. This method is applicable to three-dimensional problems, and inclusions may be oriented arbitrarily with respect to each other. Using the Equivalent Inclusion Method (EIM) and polynomial expansion of strain fields in the local coordinate systems, we solved for two ellip-

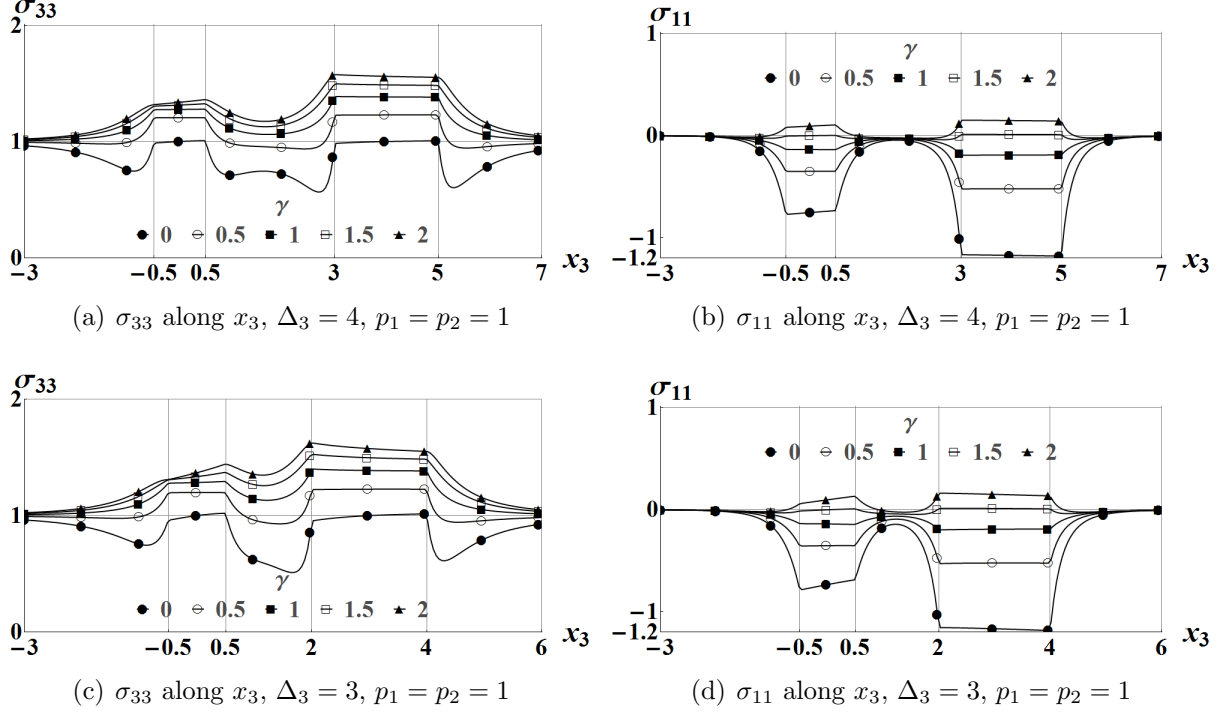


Figure 2.7: The above graphs show the effect of size of the two co-axial spherical poroelastic inhomogeneities on σ_{33} and σ_{11} -stresses along the x_3 axis; ($a_1 = \bar{a}_1 = a_2 = \bar{a}_2 = 1, a_3 = 0.5, \bar{a}_3 = 1$). Inclusions are uniformly pressurized and under uniaxial compression ($\sigma_{33} = 1, p_1 = p_2 = 1; Compression > 0$). The plots are generated for $\nu = 0.3$ and different values of $\gamma = \frac{G^1}{G^0} = \frac{G^2}{G^0}$.

soidal poroelastic inhomogeneities. To solve this problem eigenstrains were expanded, and higher order Eshelby's tensors and their derivatives were calculated at the center of each inhomogeneity. To get more accurate results, it is necessary to use more polynomial terms for eigenstrains and higher rank Eshelby's tensors, especially when dealing with very close inclusions. The results show that the distance of centers of the inhomogeneities and their relative stiffness to the medium affect the associated stress field. Considering same distance for inhomogeneities, the interaction effect is more significant on stiffer inclusions. Poroelastic inclusions could have a wide range of applications from rock mechanics problems to tissue mechanics. Here, we utilized this solution to investigate earth stress changes around depleted hydrocarbon reservoirs.

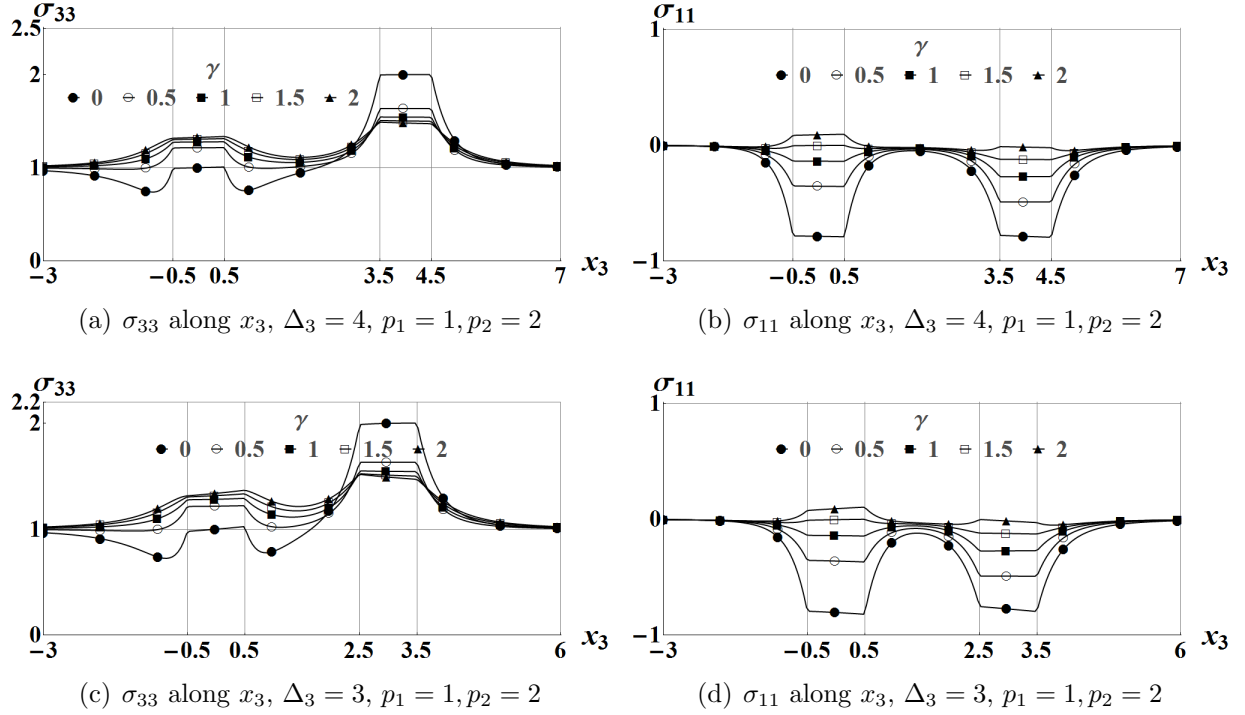


Figure 2.8: The above graphs show the effect of different pressure values inside the two co-axial spherical poroelastic inhomogeneities on σ_{33} and σ_{11} -stresses along the x_3 axis; ($a_1 = \bar{a}_1 = a_2 = \bar{a}_2 = 1, a_3 = \bar{a}_3 = 0.5$). Inclusions are uniformly pressurized and under uniaxial compression ($\sigma_{33} = 1, p_1 = 1, p_2 = 2$; *Compression* > 0). The plots are generated for $\nu = 0.3$ and different values of $\gamma = \frac{G^1}{G^0} = \frac{G^2}{G^0}$.

2.6 Polynomial Eigenstrains

The strain field can be expressed by a polynomial function of coordinates. Here, a short derivation is presented. For Complete derivation and more details, the reader may check Sendekyj (1967), Moschovidis (1975), Moschovidis and Mura (1975), and Mura (1987). Eshelby (1957), showed that the elastic field in the existence of an inclusion can be written as

$$u_i(x) = - \int_{\Omega} C_{jkmn} \epsilon_{mn}^*(x') G_{ij,k}(x - x') dx', \quad (2.18)$$

where for an isotropic material, the Green function $G_{ij}(x - x')$ (Love, 1944) and elastic moduli C_{ijkl} are given as

$$G_{ij}(x - x') = \frac{1}{4\pi\mu} \frac{\delta_{ij}}{|x - x'|} - \frac{1}{16\pi\mu(1 - \nu)} \frac{\partial^2}{\partial x_i \partial x_j} |x - x'|, \quad (2.19)$$

and

$$C_{ijkl} = \frac{2\mu\nu}{1 - 2\nu} \delta_{ij} \delta_{kl} + \mu(\delta_{ik} \delta_{jl} + \delta_{il} \delta_{jk}). \quad (2.20)$$

Substituting Eqs. (2.19) and (2.20) in Eq. (2.18) gives

$$u_i(x) = \frac{1}{8\pi(1 - \nu)} \left[\Psi_{jl,jli} - 2\nu\Phi_{mm,i} - 4(1 - \nu)\Phi_{il,l} \right], \quad (2.21)$$

where

$$\Psi_{ij}(x) = \int_{\Omega} |x - x'| \epsilon_{ij}^*(x') dx', \quad (2.22)$$

and

$$\Phi_{ij}(x) = \int_{\Omega} \frac{\epsilon_{ij}^*(x')}{|x - x'|} dx'. \quad (2.23)$$

Now considering strain definition

$$\epsilon_{ij}(x) = \frac{1}{2} \left(\frac{\partial u_i}{\partial x_j} + \frac{\partial u_j}{\partial x_i} \right), \quad (2.24)$$

the strain field can be written as

$$\epsilon_{ij}(x) = \frac{1}{8\pi(1 - \nu)} [\Psi_{kl,kl ij} - 2\nu\Phi_{kk,ij} - 2(1 - \nu)(\Phi_{ik,kj} + \Phi_{jk,ki})]. \quad (2.25)$$

Assuming that the eigenstrain, $\epsilon_{ij}^*(x)$, consists of polynomial of positions, it can be written as

$$\epsilon_{ij}^*(x) = B_{ij} + B_{ijk}x_k + B_{ijkl}x_kx_l + \cdots, \quad (2.26)$$

where $B_{ij\dots}$ are constant coefficients, Moschovidis and Mura (1975) showed Ψ_{ij} and Φ_{ij} can be expanded in the terms of polynomials as

$$\Psi_{ij}(x) = B_{ijk}\psi_k + B_{ijkl}\psi_{kl} + \cdots, \quad (2.27)$$

$$\Phi_{ij}(x) = B_{ijk}\phi_k + B_{ijkl}\phi_{kl} + \cdots, \quad (2.28)$$

where

$$\psi_{ij\dots k}(x) = \int_{\Omega} x'_i x_j \cdots x'_k |x - x'| dx', \quad (2.29)$$

$$\phi_{ij\dots k}(x) = \int_{\Omega} \frac{x'_i x_j \cdots x'_k}{|x - x'|} dx'. \quad (2.30)$$

Finally, substituting Eqs. (2.27) and (2.28) in Eq. (2.25) gives

$$\epsilon_{ij}(x) = D_{ijkl}(x)B_{kl} + D_{ijklq}(x)B_{klq} + D_{ijklqr}(x)B_{klqr} + \cdots, \quad (2.31)$$

where different orders of tensor D are

$$D_{ijkl}(x) = \frac{1}{8\pi(1-\nu)} \left\{ \psi_{,kl ij} - 2\nu \delta_{kl} \phi_{,ij} - (1-\nu) [\phi_{,kj} \delta_{il} + \phi_{,ki} \delta_{jl} + \phi_{,lj} \delta_{ik} + \phi_{,li} \delta_{jk}] \right\}, \quad (2.32)$$

$$D_{ijklq}(x) = \frac{1}{8\pi(1-\nu)} \left\{ \psi_{q,kl ij} - 2\nu\delta_{kl}\phi_{q,ij} - (1-\nu)[\phi_{q,kj}\delta_{il} + \phi_{q,ki}\delta_{jl} + \phi_{q,lj}\delta_{ik} + \phi_{q,li}\delta_{jk}] \right\}, \quad (2.33)$$

etc.

Higher ranks of tensor D can be calculated by replacing higher rank ψ and ϕ in Eq. (2.33). Eshelby showed that for the interior of an ellipsoidal inclusion, $D_{ijkl}(x)$ is a constant. Later, it has been shown (Eshelby, 1961; Asaro and Barnett, 1975) for any ellipsoidal inclusion with an eigenstrain given in the form of homogeneous polynomial in x_i of degree n , the strain inside the inclusion is an inhomogeneous polynomial in x_i , with the terms of degree $n, (n-2), (n-4), \dots$. Therefore for $x \in \Omega$, we will have

$$D_{ijklq}(x) = D_{ijklq,m}(0)x_m, \quad (2.34)$$

$$D_{ijklqr}(x) = D_{ijklqr}(0) + \frac{1}{2}D_{ijklqr,mn}(0)x_mx_n, \quad (2.35)$$

etc.

2.7 References

- Asaro, R.J., Barnett, D.M., 1975. The non-uniform transformation strain problem for an anisotropic ellipsoidal inclusion. *Journal of the Mechanics and Physics of Solids* 23, 77–83. doi:10.1016/0022-5096(75)90012-5.
- Biot, M.A., 1941. General theory of three-dimensional consolidation. *Journal of Applied Physics* 12, 155. doi:10.1063/1.1712886.
- Biot, M.A., 1956a. General solutions of the equations of elasticity and consolidation for a porous material. *Journal of Applied Mechanics* 78, 91–96.

- Biot, M.A., 1956b. Theory of deformation of a porous viscoelastic anisotropic solid. *Journal of Applied Physics* 27, 459. doi:10.1063/1.1722402.
- Chen, Z.R., 2011. Poroelastic model for induced stresses and deformations in hydrocarbon and geothermal reservoirs. *Journal of Petroleum Science and Engineering* 80, 41–52. doi:10.1016/j.petrol.2011.10.004.
- Eshelby, J.D., 1957. The determination of the elastic field of an ellipsoidal inclusion, and related problems. *Proceedings of the Royal Society A: Mathematical, Physical and Engineering Sciences* 241, 376–396. doi:10.1098/rspa.1957.0133.
- Eshelby, J.D., 1959. The elastic field outside an ellipsoidal inclusion, in: *Proceedings of the Royal Society of London. Series A, Mathematical and Physical*, pp. 561–569.
- Eshelby, J.D., 1961. Elastic inclusions and inhomogeneities, in: Sneddon, I.N., Hill, R. (Eds.), *Progress in Solid Mechanics*, Vol.2. North-Holland, Amsterdam, pp. 89–140.
- Fond, C., Riccardi, A., Schirrer, R., Montheillet, F., 2001. Mechanical interaction between spherical inhomogeneities: an assessment of a method based on the equivalent inclusion. *European Journal of Mechanics - A/Solids* 20, 59–75. doi:10.1016/S0997-7538(00)01118-9.
- Hori, M., Nemat-Nasser, S., 1993. Double-inclusion model and overall moduli of multi-phase composites. *Mechanics of Materials* 14, 189–206. doi:10.1016/0167-6636(93)90066-Z.
- Love, A.E.H., 1944. *A treatise on the mathematical theory of elasticity*. Dover Publications, New York.
- Marquez, J.P., Genin, G.M., Zahalak, G.I., Elson, E.L., 2005. Thin bio-artificial tissues in plane stress: the relationship between cell and tissue strain, and an improved constitutive model. *Biophysical journal* 88, 765–77. doi:10.1529/biophysj.104.040808.
- Moschovidis, Z.A., 1975. Two ellipsoidal inhomogeneities and related problems treated by the equivalent inclusion method. Ph.D. thesis. Northwestern University, Evanston.
- Moschovidis, Z.A., Mura, T., 1975. Two-ellipsoidal inhomogeneities by the Equivalent Inclusion Method. *Journal of Applied Mechanics* 42, 847. doi:10.1115/1.3423718.

- Mura, T., 1987. Micromechanics of defects in solids. Martinus Nijhoff Publishers.
- Nemat-Nasser, S., Hori, M., 1999. Micromechanics: overall properties of heterogeneous materials. Elsevier, Amsterdam.
- Norris, A., 1992. On the correspondence between poroelasticity and thermoelasticity. *Journal of Applied Physics* 71, 1138. doi:10.1063/1.351278.
- Rice, J.R., Cleary, M.P., 1976. Some basic stress diffusion solutions for fluid-saturated elastic porous media with compressible constituents. *Reviews of Geophysics* 14, 227. doi:10.1029/RG014i002p00227.
- Richard M. Christensen, 2012. Mechanics of composite materials. Courier Dover Publications.
- Rudnicki, J.W., 2002. Alteration of regional stress by reservoirs and other inhomogeneities: Stabilizing or destabilizing?, in: Vouille, G., Berest, P. (Eds.), *Proc. 9th Int. Congr. Rock Mechanics*, Vol. 3, Paris, Aug. 25-29, 1999, Paris, France. pp. 1629–1637.
- Rudnicki, J.W., 2011. Eshelbys technique for analyzing inhomogeneities in geomechanics, in: Leroy, Y.M., Lehner, F.K. (Eds.), *Mechanics of Crustal Rocks*. Springer Vienna, pp. 43–72. doi:10.1007/978-3-7091-0939-7.
- Sayers, C., Kisra, S., Tagbor, K., Adachi, J.I., Dahi Taleghani, A., 2007. Calibrating the mechanical properties and in-situ stresses using acoustic radial profiles, in: *Proceedings of SPE Annual Technical Conference and Exhibition*, Society of Petroleum Engineers. pp. 1–8. doi:10.2118/110089-MS.
- Segall, P., 1989. Earthquakes triggered by fluid extraction. *Geology* 17, 942–946. doi:10.1130/0091-7613(1989)017\%3C0942:ETBFE\%3E2.3.CO;2BFE>2.3.CO;2.
- Sendeckyj, G., 1967. Ellipsoidal inhomogeneity problem. Ph.D. thesis. North Western University, Evanston.
- Shodja, H.M., Rad, I., Soheilifard, R., 2003. Interacting cracks and ellipsoidal inhomogeneities by the equivalent inclusion method. *Journal of the Mechanics and Physics of Solids* 51, 945–960. doi:10.1016/S0022-5096(02)00106-0.

- Shodja, H.M., Sarvestani, a.S., 2001. Elastic fields in double inhomogeneity by the Equivalent Inclusion Method. *Journal of Applied Mechanics* 68, 3. doi:10.1115/1.1346680.
- Soltanzadeh, H., Hawkes, C.D., 2012. Evaluation of caprock integrity during pore pressure change using a probabilistic implementation of a closed-form poroelastic model. *International Journal of Greenhouse Gas Control* 7, 30–38. doi:10.1016/j.ijggc.2011.10.006.
- Soltanzadeh, H., Hawkes, C.D., Sharma, J.S., 2007. poroelastic model for production- and injection-induced stresses in reservoirs with elastic properties different from the surrounding rock. *International Journal of Geomechanics* 7, 353–361. doi:10.1061/(ASCE)1532-3641(2007)7:5(353).
- Van der Molen, I., Van Roermund, H., 1986. The pressure path of solid inclusions in minerals: the retention of coesite inclusions during uplift. *Lithos* 19, 317–324. doi:10.1016/0024-4937(86)90030-7.
- Voyiadjis, G.Z., Kattan, P.I., 2006. Advances in damage mechanics: metals and metal matrix composites with an introduction to fabric tensors, 2nd Edition, in: *Advances in Damage Mechanics: Metals and Metal Matrix Composites With an Introduction to Fabric Tensors*, 2nd Edition. second edi ed.. Elsevier Science Ltd, Oxford, p. 740.
- Zhou, K., Hoh, H.J., Wang, X., Keer, L.M., Pang, J.H., Song, B., Wang, Q.J., 2013. A review of recent works on inclusions. *Mechanics of Materials* 60, 144–158. doi:10.1016/j.mechmat.2013.01.005.
- Zoback, M.D., 2007. *Reservoir geomechanics*. Cambridge University Press, New York.

Chapter 3

On the Inhomogeneous Anisotropic Poroelastic Inclusions

Anisotropy in elastic properties has been studied extensively in the last century; however, anisotropy in poroelastic properties, despite its potential importance in different engineering problems, has not been explored thoroughly. In this paper, we provide the Eshelby solution for stress and strain inside and outside of an anisotropic poroelastic inhomogeneity due to pore pressure changes inside the inhomogeneity. Here, the term *anisotropic inhomogeneity*, refers to an inhomogeneity with anisotropic poroelastic constants. To tackle this problem, we use the Equivalent Inclusion Method (EIM). Due to the authors' primary interest in geomechanical problems, discussions and examples are chosen for applications in fluid withdrawal/injection into hydrocarbon reservoirs with transverse isotropic properties. However, the results may have applications in other type of anisotropic poroelastic materials, for instance biological tissues. These analytical results could be used a benchmark to examine different numerical solutions obtained by discretization of governing partial differential equations.

3.1 Introduction

Inclusions are defined as finite sub-volumes of the medium, which may possess different strain status from that of the surrounding environment. On the other hand, an inhomogeneity is a sub-volume of a medium that has different material properties from those of its surrounding.

If the inhomogeneity experiences different loading status at the same time, it is considered as inhomogeneous inclusion. Eshelby (1957, 1959, 1961) solved for stress distribution induced by an ellipsoidal inhomogeneity embedded in an infinite isotropic elastic medium, that undergoes a uniform strain. Later, Eshelby's method has been used to solve more complex problems like inclusions in finite media (Li et al., 2007), interacting inclusions (Shodja et al., 2003; Zhou et al., 2012), or non-ellipsoidal inclusions (Zou et al., 2010). Eshelby's solution has played a vital role in development of many micromechanical models in mechanics of composites, fractures, dislocations, and phase transformations (Voyiadjis and Kattan, 2006; Shodja and Ojaghnezhad, 2007; Li and Wang, 2008). Mura (1987) and Nemat-Nasser and Hori (1999) are two references for more detailed information about the classic problems in the subject. For a review of recent works on inclusions and inhomogeneities see Zhou et al. (2013). Application of Eshelby solution is also recently extended to fluid saturated porous materials.

Presence of pore fluid in the elastic solid porous materials and its coupling with material deformations leads to different class of material behaviors known as the theory of poroelasticity. Poroelasticity assumed the continuum media are consisted of elastic solid matrix and interconnected fluid saturated pores. Poroelastic materials present in a wide range of applications in geomechanics and biomechanics (Berryman, 1997; Wang, 2000; Levin and Alvarez-Tostado, 2003; Dormieux et al., 2006). Rocks, soils, biological tissues, bones, foams, spongy metal alloys, and ceramics are few examples of poroelastic materials. Considering different material properties and different pressure/temperature of hydrocarbon bearing formations in comparison to those of the surrounding geological structures, hydrocarbon reservoirs can be considered as inhomogeneities embedded inside an infinite medium. Rudnicki (2002a,b); Soltanzadeh et al. (2007); Chen (2011); Soltanzadeh and Hawkes (2012); Bedayat and Dahi Taleghani (2013, 2014) used the concept of poroelastic inhomogeneities to model stress alterations in the subsurface due to pore fluid pressure changes. Similarly, biological tissues and bones can also be modeled as poroelastic composites consisted of complicated inhomogeneities. Eshelby theorem has been used widely in biomechanics to model

biomaterials disregarding poroelastic parameters of the medium (Ferrari, 2000; Hellmich and Ulm, 2002; Marquez et al., 2005; Khoshgofta et al., 2007; Malekmotiei et al., 2013);

The theory of linear poroelasticity is originally developed to analyze geomechanical problems (Biot, 1941, 1955). Land subsidence, determination of stresses and displacements associated to fluid withdrawal or fluid injection (Teklu et al., 2012), or determining the rock in-situ stresses (Wang et al., 2007), wellbore stability (Abousleiman and Ekbote, 2005; Mehrabian and Abousleiman, 2013), carbon geological sequestration (Rutqvist et al., 2002), naturally fractured reservoirs (Zhou and Ghassemi, 2011; Bedayat and Dahi Taleghani, 2012; Dahi Taleghani et al., 2014), hydraulic fracturing (Detournay and Cheng, 1991), and geothermal reservoirs (Rawal and Ghassemi, 2014). Meanwhile, the theory of linear poroelasticity is used in biomechanics (Cederbaum et al., 2000) to model different organic materials ranging from human skulls (Nowinski and Davis, 1970; Cowin, 1999) to soft tissues like cartilage (Wu et al., 1999; Li et al., 2003).

Under undrained conditions that excessive pore pressure is not allowed to dissipate, the mechanical response of porous solid-fluid system is dominated by two mechanisms: (i) an increase of pore pressure causes dilation of the solid matrix, and (ii) as the solid part compresses, pore pressure increases. However, under drained conditions, extra pore pressure induced by compression of the solid phase dissipates and secondary deformation of the solid phase takes place. These two mechanisms were formulated by Biot (Biot, 1941) through coupling of fluid diffusion and elasticity equations (see Verruijt (2014) for the earlier history and recent progresses in the theory of linear poroelasticity). Later on, Rice and Cleary (1976) reformulated Biot's constitutive equations for isotropic poroelastic materials as

$$\varepsilon_{ij} = \frac{1}{2G} \left[\sigma_{ij} - \left(\frac{3K - 2G}{9K} \right) \sigma_{kk} \delta_{ij} + \frac{2G}{3K} \alpha p \delta_{ij} \right], \quad (3.1)$$

$$\zeta \frac{\alpha}{K} \left(\frac{\sigma_{kk}}{3} + \frac{p}{B} \right), \quad (3.2)$$

where δ_{ij} is the Kronecker delta ($\delta_{ij} = 1$ for $i = j$, and $\delta_{ij} = 0$ for $i \neq j$), ε_{ij} and σ_{ij} are the components of strain and stress tensor in the solid matrix, respectively; and p is the pore fluid pressure. The increment of fluid content, ζ , is defined as the mass of pore fluid δm_f , per unit bulk volume

$$\zeta = \frac{\delta m_f}{\rho_{f0}}, \quad (3.3)$$

where ρ_{f0} is the pore fluid density in the reference state. There are four material constants in the above equations (compared to two for isotropic elastic materials; B is the Skempton's coefficient).

The Biot coefficient, α , represents the influence of pore fluid pressure on the elastic solid matrix and is a function of solid constituent properties or more specifically pore geometries. The Biot coefficient for isotropic materials is defined as

$$\alpha = 1 - \frac{K}{K_s}, \quad (3.4)$$

where K_s is bulk modulus of the solid material. It can be shown that the range of variation for Biot coefficient is $\phi < \alpha < 1$ (Berryman, 1992), where ϕ is the material porosity.

Similar to the elasticity, most fundamental studies of poroelastic materials assumes isotropic conditions for the medium. The material properties are considered to be isotropic, if their values at a certain point are the same in all directions. In biomechanics, most organic tissues are anisotropic due to their microstructures. For example, bones considered to be anisotropic due to the lamella structure (Turner et al., 1995; Cowin and Doty, 2007). Similarly, anisotropic properties may occur in rocks due to the microstructure geometries (Hudson, 1981; Ghabezloo and Hemmati, 2011; Levasseur et al., 2013; He et al., 2013; Ahmadi et al., 2014a) of the material, sedimentologic layering of rock or damage induced isotropy in an initially isotropic material (Litewka, 2003; Shao et al., 2006; Ahmadi et al., 2014b). Rock anisotropy occurs in different scales ranging from grain-size scale to the large

scale rock masses would show its consequences in engineering problems like drilling vertical or horizontal wells (Aadnoy, 1988).

Poroelastic anisotropy is also utilized to study material behavior in other type of materials as well (Bruschke and Advani, 1990; Shao, 1998; Kanj et al., 2003; Berryman, 2011) too. There are some studies on assessing the impact of anisotropy on fluid flow in geological structures that show neglecting the effect of rock anisotropy may cause unexpected and unrealistic results in failure analysis of geomaterials (Cui et al., 1996; Cheng et al., 1996). Borehole stability analysis (Aoki et al., 1993), effective medium theory in seismology (Schoenberg and Sayers, 1995; Sayers, 2005), hydraulic fracturing (Dahi Taleghani and Olson, 2011; Khan et al., 2012; Shojaei et al., 2014), formation evaluation (Moran and Gianzero, 1979; Bang et al., 2001), and fluid flow in porous media (Rickman, 2009) are some other examples that considering rock anisotropy would have a significant role on the reliability of engineering analyses.

For a poroelastic material, anisotropy could appear in mechanical properties like elastic moduli and Poisson's ratio, and hydraulic properties like permeability and relative permeability, or poroelastic properties like Biot coefficient. In rock mechanics, pre-existing faults and joints (Crampin, 1994; Mueller, 1991), microcracks (Hudson, 1981; Crampin, 1994), differential stresses (Nur and Simmons, 1969), or even failure and damage in isotropic materials may cause anisotropic behavior in the rock masses (Hu et al., 2013). For instance, in sedimentary formations different physical and chemical processes during transportation, deposition, compaction and cementation procedures (Amadei, 1996; Pollard and Fletcher, 2005), or geologically driven phenomena like deposition and compaction may lead to anisotropic properties. Laminated structure of Shales results in directional dependency of rock properties. Thus, major differences in mechanical and poroelastic properties along the direction parallel and perpendicular to the deposition layers may be observed (Sayers, 1994; Khan et al., 2011).

In this paper, we provide an Eshelby solution for stress and strain values inside and outside of an anisotropic poroelastic inhomogeneity due to a pore pressure change inside the inhomogeneity. To tackle the problem, we used Equivalent Inclusion Method (EIM). Here, the term *anisotropic inhomogeneity*, means an inhomogeneous inclusion with anisotropic poroelastic constants.

The outline of this paper is as follows: Sections 3.2 and 4.2.2 review anisotropic poroelastic constitutive equations and Eshelby's solution for elastic materials. Then in Section 6.2.3, we describe our approach to solve the stress and strain in anisotropic poroelastic media. Finally, some numerical examples for stress variations inside and outside of a an anisotropic poroelastic inhomogeneity are provided and discussed in Section 3.5.

3.2 Anisotropic poroelastic constitutive equations

Similar to the isotropic condition, the stress σ_{ij} , the strain ε_{ij} , the fluid pore pressure p , and the variation of fluid content ζ can be defined for anisotropic poroelastic medium. The constitutive equations for anisotropic poroelastic medium are given as (Cheng, 1997)

$$\sigma_{ij} = C_{ijkl}\varepsilon_{kl} - \alpha_{ij}p, \quad (3.5)$$

$$p = M(\zeta - \alpha_{ij}\varepsilon_{ij}), \quad (3.6)$$

where C_{ijkl} is the drained elastic moduli; M is the combined fluid/solid compressibility (Biot modulus); and α_{ij} is the Biot tensorial coefficient. Equations (3.5) and (3.6) contain 28 independent poroelastic constitutive constants: 21 drained elastic moduli, C_{ijkl} ; one Biot modulus, M ; and six Biot coefficients, α_{ij} . The Biot coefficient is given by

$$\alpha_{ij} = \delta_{ij} - C_{ijkl}L_{klmn}^s, \quad (3.7)$$

where L_{klmn}^s is the compliance tensor of the grains or solid phase constituents. Tan and Konietzky (2014) investigated the variation of the Biot coefficient in porous and cracked rocks by a coupled numerical analysis. Their study shows that the distribution of fractures are the most dominant factor in determining the Biot coefficient. In the case of parallel ellipsoidal fractures, the direction of the lowest Biot coefficient is parallel to the fracture's direction. Therefore, in case of high differential stress $\sigma_{33} \gg \sigma_{11}$ and σ_{22} , we expect lower α_{33} than α_{11} and α_{22} .

3.3 Eshelby's solution

Let's consider an ellipsoidal inclusion, which is embedded in a uniform infinite elastic solid. The inclusion undergoes a change in size and shape that could be described by a uniform transformation strain (eigenstrain) ε_{ij}^T , in the absence of the surrounding material; i.e., the eigenstrain is a stress-free transformation strain. Elastic and plastic strains, thermal expansion, pressure difference, phase transformation, initial strains, and misfit strains are different types of strains which could be referred to as eigenstrains (Mura, 1987). Eshelby (1957, 1959) showed that in the presence of the constrained circumference, the actual strain and stress inside the inclusion are uniform and given by

$$\varepsilon_{ij} = S_{ijkl} \varepsilon_{kl}^T, \quad (3.8)$$

$$\sigma_{ij} = C_{ijkl} [\varepsilon_{kl} - \varepsilon_{kl}^T], \quad (3.9)$$

where S is the Eshelby tensor. The Eshelby tensor is a fourth rank tensor which is a function of geometry and Poisson's ratio for an ellipsoidal inclusion. The expanded formula of the Eshelby tensor for different shapes may be found in Mura (1987).

Later, Eshelby's method has been extended to determine the stress and strain in inhomogeneous inclusions. Eshelby introduced the equivalent inclusion method (EIM) to sim-

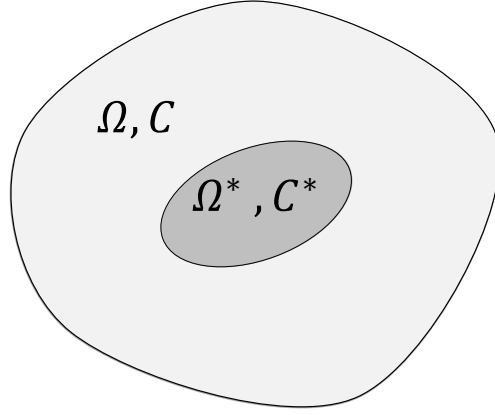


Figure 3.1: A single inclusion embedded in an infinite medium. Ω^* and C^* are indicating inclusion domain and its elastic moduli tensor, respectively. Ω and C are representing the surrounding matrix and its elasticity moduli tensor, respectively.

ulate the regions with different elastic properties from those of the surrounding material (see Fig. 3.1) by modeling a homogenous inclusion with an eigenstrain ε^T , plus a fictitious uniform homogenizing eigenstrain ε^* ; and solved the following equation:

$$C_{ijkl}^0[\varepsilon_{kl} - \varepsilon_{kl}^T - \varepsilon_{kl}^*] = C_{ijkl}^*[\varepsilon_{kl} - \varepsilon_{kl}^T], \quad (3.10)$$

where C_{ijkl}^* and C_{ijkl}^0 are elastic moduli of the inhomogeneity and surrounding material, respectively (hereafter, the superscripts $*$ indicates values for the inhomogeneity and 0 indicates values for the surrounding matrix.) The right hand side of Eq. (3.10), similar to Eq. (6.14), provides the stress inside the inhomogeneity using the inhomogeneity moduli. However, the left hand side of Eq. (6.14) provides the amount of stress interior the inclusion assuming the fictitious eigenstrain. Since both ε^T and ε^* are assumed to be uniform, the equivalent eigenstrain can be defined as

$$\varepsilon^{**} = \varepsilon^T + \varepsilon^*, \quad (3.11)$$

where for the interior points

$$\varepsilon_{ij} = S_{ijkl}\varepsilon_{kl}^{**}, \quad (3.12)$$

$$\sigma_{ij} = C_{ijkl}^*[\varepsilon_{kl} - \varepsilon_{kl}^T]. \quad (3.13)$$

By substituting Eq. (4.4) into Eq. (3.10), ε^{**} can be determined from the following relationship

$$C_{ijkl}^0[S_{klmn}\varepsilon_{mn}^{**} - \varepsilon_{kl}^{**}] = C_{ijkl}^*[S_{klmn}\varepsilon_{mn}^{**} - \varepsilon_{kl}^T]. \quad (3.14)$$

Note that Eq. (4.6) consists of 6 linear equations containing six unknowns (ε^{**}). Solving for ε^{**} in Eq. (4.6), the stress and strain inside the inclusion can be calculated by Eqs. (4.4) and (4.5). This method is valid for both isotropic and anisotropic inhomogeneous inclusions embedded in an isotropic medium. Assuming anisotropic inhomogeneous inclusion, elastic moduli C_{ijkl}^* , C_{ijkl}^0 and S_{ijkl} in Eq. (4.6) are taken for the isotropic material (Mura, 1987).

Similar to Eq. (6.13), stress and strain for the exterior points can be calculated using the fourth rank tensor D_{ijkl}

$$\varepsilon_{ij}(x) = D_{ijkl}(x)\varepsilon_{kl}^*, \quad (3.15)$$

$$\sigma_{ij}(x) = C_{ijkl}\varepsilon_{kl}(x), \quad (3.16)$$

where ε^* is determined from Eq. (3.10), and

$$D_{ijkl}(x) = \frac{1}{8\pi(1-\nu)} \left\{ \psi_{,kl;ij} - 2\nu\delta_{kl}\phi_{,ij} - (1-\nu)[\phi_{,kj}\delta_{il} + \phi_{,ki}\delta_{jl} + \phi_{,lj}\delta_{ik} + \phi_{,li}\delta_{jk}] \right\}. \quad (3.17)$$

$D_{ijkl}(x)$ is similar to the Eshelby's tensor, but for the exterior points (Mura, 1987). Section 3.9 provides the details of calculation for tensor D , ψ , and ϕ . If $x \in \Omega$, then $D_{ijkl}(x) = S_{ijkl}$.

3.4 Poroelastic Inclusions

Rudnicki (2002a) has solved the problem of an isotropic ellipsoidal poroelastic inhomogeneity embedded in an elastic medium, and presented numerical results to show the effect of geometry and material properties on the stresses caused by a fluid pressure change in the inclusion. Using Eqs. (6.8) and (6.14), he derived the relationship between the stress, strain and pore pressure change inside the inclusion (see more details in Section 3.8). However, this solution does not incorporate the possible anisotropy of poroelastic or elastic properties of the inhomogeneity. Chen (2011) used EIM to model a hydrocarbon reservoir as an inhomogeneous isotropic poroelastic inclusion and investigated the effect of change in pore pressure and elastic properties of the reservoir on redistribution of stresses and deformation within the reservoir.

We use a different approach to derive the stress and strain solution for anisotropic poroelastic inclusions. According to the definition of eigenstrain as stress-free transformation strain, poroelastic transformation strain due to the changes in pore pressure ε^T can be obtained by setting $\sigma_{ij} = 0$ in Eq. (3.5)

$$\varepsilon_{mn}^T = C_{mnij}^{-1} \alpha_{ij} p = L_{mnij} \alpha_{ij} p, \quad (3.18)$$

where L_{mnij} is the tensor of elastic compliances, inverse of C_{mnij} , is defined as the solution of the following equation

$$L_{mnij} C_{ijkl} = \frac{1}{2} (\delta_{mk} \delta_{nl} + \delta_{ml} \delta_{nk}). \quad (3.19)$$

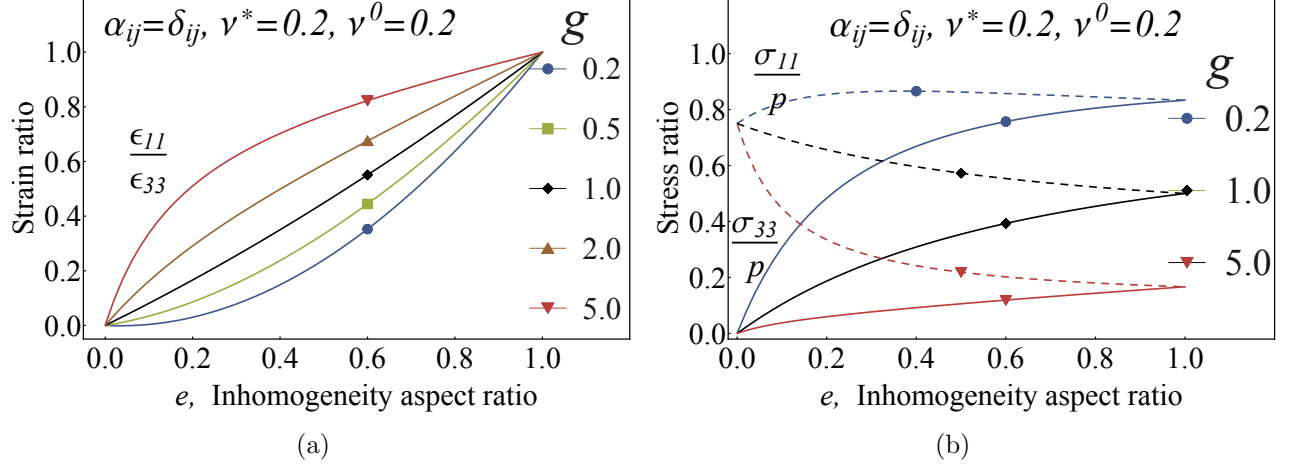


Figure 3.2: (a) Strain ratio; (b) Stress ratio due to pressure change inside an isotropic poroelastic inhomogeneity. Both graphs are plotted against the inhomogeneity aspect ratio, e . It is assumed g is shear modulus ratio, G^*/G ; $\alpha_{ij} = \delta_{ij}$ (isotropic case); and $\nu^0 = \nu^* = 0.2$. However, the dependence of the solution on ν^0 is weak. These graphs are in exact agreement with Figs. 4 and 7 in Rudnicki (2002a).

Now substituting Eq. (6.15) into Eq. (4.6), the equivalent poroelastic eigenstrain ϵ^* can be determined from Eq. (4.6). Consequently, stress and strain for exterior points can be calculated from Eqs. (3.15) and (3.16).

3.5 Results and Discussions

To check the accuracy of the method, we initially verified the solution with the results provided in Rudnicki (2002a) for the isotropic conditions. The ratio of the lateral to the vertical strain $\epsilon_{11}/\epsilon_{33}$ (hereafter, strain ratio), and the change in stress divided by change in pore pressure σ/p (hereafter, stress ratio), against the inclusion aspect ratio e , were in the exact agreement with the solution provided by Rudnicki for a single isotropic poroelastic inhomogeneity (compare Figs. 3.2(a) and 3.2(b) with Figs. 4 and 7 of Rudnicki (2002a)).

Here, we provided the stress and strain values inside the inhomogeneity for different values of elasticity constants G^0, G^*, ν^0 and ν^* ; as well as Biot coefficient α_{ij} ; and inhomogeneity aspect ratio e . To study the anisotropy effect, we start by stress and strain values versus the

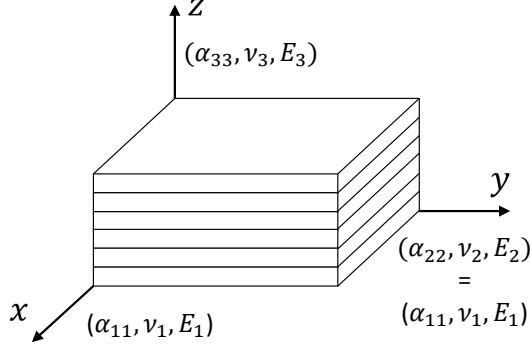


Figure 3.3: A schematic figure of transversely isotropic material. Planes parallel to $x - y$ are the planes of isotropy.

inhomogeneity aspect ratio e , for different α_{ij} , ν^0 , ν^* , and $g = G^*/G^0$. Extrinsic anisotropy in geomaterials is usually results of geologic layering or preferred orientation of the fractures. A common assumption in geophysics is that sedimentary geological formations are transversely isotropic (polar isotropic) (Babuska and Cara, 1991). Here, we assumed this anisotropy condition to demonstrate how the method works, while it can be utilized for different anisotropic conditions without any limitation. One may use the equations of the Backus (1962) to average the elastic properties of layers to represent the material properties by single set of values along along the axis of symmetry. We assumed the axis of symmetry for transversely isotropic inhomogeneity lies along the x_3 axis (i.e. $\alpha_{11} = \alpha_{22} \neq \alpha_{33}$, see Fig. 3.3). Transversely isotropic materials have the same properties in one plane and different properties in the direction normal to that plane (axis of symmetry). This is a realistic assumption for sedimentary geomaterials such as hydrocarbon bearing formations (e.g. Abousleiman and Ekbote (2005)) and some organic tissues like the skeletal muscle (e.g. Morrow et al. (2010)) or the brain tissue (Feng et al., 2013).

The stiffness matrix for transversely isotropic materials can be written using Voigt notation as (Bower, 2011)

$$\mathbf{C} = \begin{bmatrix} c_{11} & c_{12} & c_{13} & 0 & 0 & 0 \\ & c_{11} & c_{13} & 0 & 0 & 0 \\ & & c_{33} & 0 & 0 & 0 \\ & sym & & c_{44} & 0 & 0 \\ & & & & c_{44} & 0 \\ & & & & & (c_{11} - c_{12})/2 \end{bmatrix}, \quad (3.20)$$

where

$$\begin{aligned} c_{11} = c_{22} &= E_p(1 - \nu_{pt}\nu_{tp})\Upsilon, \quad c_{33} = E_t(1 - \nu_p^2)\Upsilon, \quad c_{44} = \frac{E_t}{2(1 + \nu_t)}, \\ c_{12} &= E_p(\nu_p + \nu_{pt}\nu_{tp})\Upsilon, \quad c_{13} = c_{23} = E_p(\nu_{tp} + \nu_p\nu_{tp})\Upsilon = E_t(\nu_{pt} + \nu_p\nu_{pt})\Upsilon, \\ \Upsilon &= \frac{1}{1 - \nu_p^2 - 2\nu_{pt}\nu_{tp} - 2\nu_p\nu_{pt}\nu_{tp}}. \end{aligned} \quad (3.21)$$

Here, we have $E_1 = E_2 = E_p$; $E_3 = E_t$; $\nu_{12} = \nu_{21} = \nu_p$; $\nu_{31} = \nu_{32} = \nu_{tp}$; $\nu_{13} = \nu_{23} = \nu_{pt}$; and the Poisson's ratios should satisfy

$$\frac{\nu_{tp}}{E_t} = \frac{\nu_{pt}}{E_p}. \quad (3.22)$$

The elastic moduli, C_{ijkl} , can be calculated by the replacement of the subscript of c_{pq} according to the following rules for ij (or kl) $\leftrightarrow p$ (or q)

$$11 \leftrightarrow 1, 22 \leftrightarrow 2, 33 \leftrightarrow 3, 23(or32) \leftrightarrow 4, 31(or13) \leftrightarrow 5, 12(or21) \leftrightarrow 6.$$

For this materials Biot coefficient in the symmetry plane are equal, so the Biot coefficient has the form

$$\boldsymbol{\alpha} = \begin{bmatrix} \alpha_{11} & 0 & 0 \\ 0 & \alpha_{11} & 0 \\ 0 & 0 & \alpha_{33} \end{bmatrix}. \quad (3.23)$$

Assuming isotropic elastic and transversely isotropic poroelastic conditions, the stress ratio versus inhomogeneity aspect ratio, for various shear modulus ratios and different Poisson's ratios are plotted in Fig. 3.4. The value of lateral and vertical stress ratio (σ_{11}/p and σ_{33}/p) indicates how changes in pore fluid pressure may affect the total stress magnitude in that direction. In transversely isotropic materials, the variation of the Biot coefficient in the direction of the axis of symmetry α_{33} , affects the vertical stress change more than lateral stresses. Assuming the same values for Poisson's ratio interior and exterior of the inhomogeneity to be $\nu^0 = \nu^* = 0.2$ (Figs. 3.4(a), 3.4(c) and 3.4(e)), the stress ratio in the lateral direction is always higher than the stress ratio in the vertical direction ($\sigma_{11}/p > \sigma_{33}/p$). However, by decreasing the anisotropy degree (as $\alpha_{33} \rightarrow \alpha_{11} = \alpha_{22} = 1$), the stress ratios are approaching the same value for the spherical inhomogeneities (i.e. $e = 1$). Moreover, the stress change ratio is higher in softer inhomogeneities. For example for a depleted aquifer, the reduction in the total horizontal stress is more than reduction in the total vertical stress, especially in softer inclusions.

The effect of Poisson's ratio on the stress ratio is shown in Figs. 3.4(b), 3.4(d) and 3.4(e). These plots show the weak dependency of vertical stress ratio to the Poisson's ratio values, whereas the lateral stress ratio decreases significantly for higher Poisson's ratio values, which is expected by intuition as materials with higher Poisson's ratio are less compressible.

Figure 3.5 shows how anisotropy in the Biot coefficient changes the stress ratio distribution inside and outside of the inclusion. For $\alpha_{33} < 1$, we expect lower stress ratio since lower Biot coefficient means less contribution of the pore pressure changes in the total stress

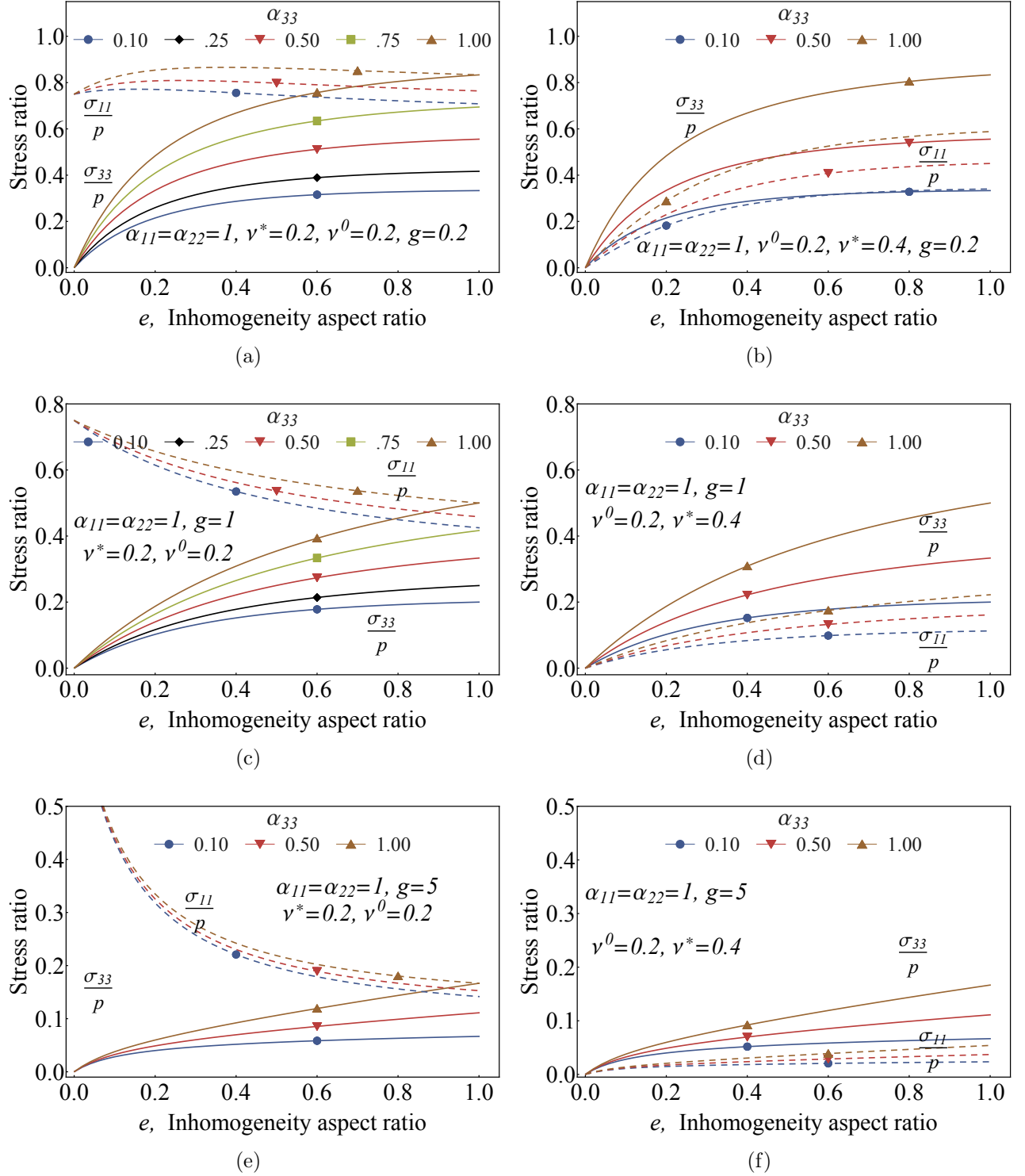


Figure 3.4: Stress ratio against inhomogeneity aspect ratio, e , for various shear modulus ratio ($g = G^*/G^0$) and Poisson's ratio. The solid lines indicate vertical stress ratio σ_{33}/p , whereas the dotted lines indicate lateral stress ratio σ_{11}/p .

(compare Figs. 3.5(a) and 3.5(b) or Figs. 3.5(d) and 3.5(e)). Figures 3.5(c) and 3.5(f) show the difference of stress ratios considering isotropic and anisotropic Biot coefficient. Therefore, we may conclude that in the extreme cases, neglecting the effect of anisotropy leads to a significant error in estimating total stress in the direction of anisotropy (here σ_{33} , see Fig. 3.5(c)); however stress ratio changes are negligible in the other directions (here σ_{11} and σ_{22} , see Fig. 3.5(f)).

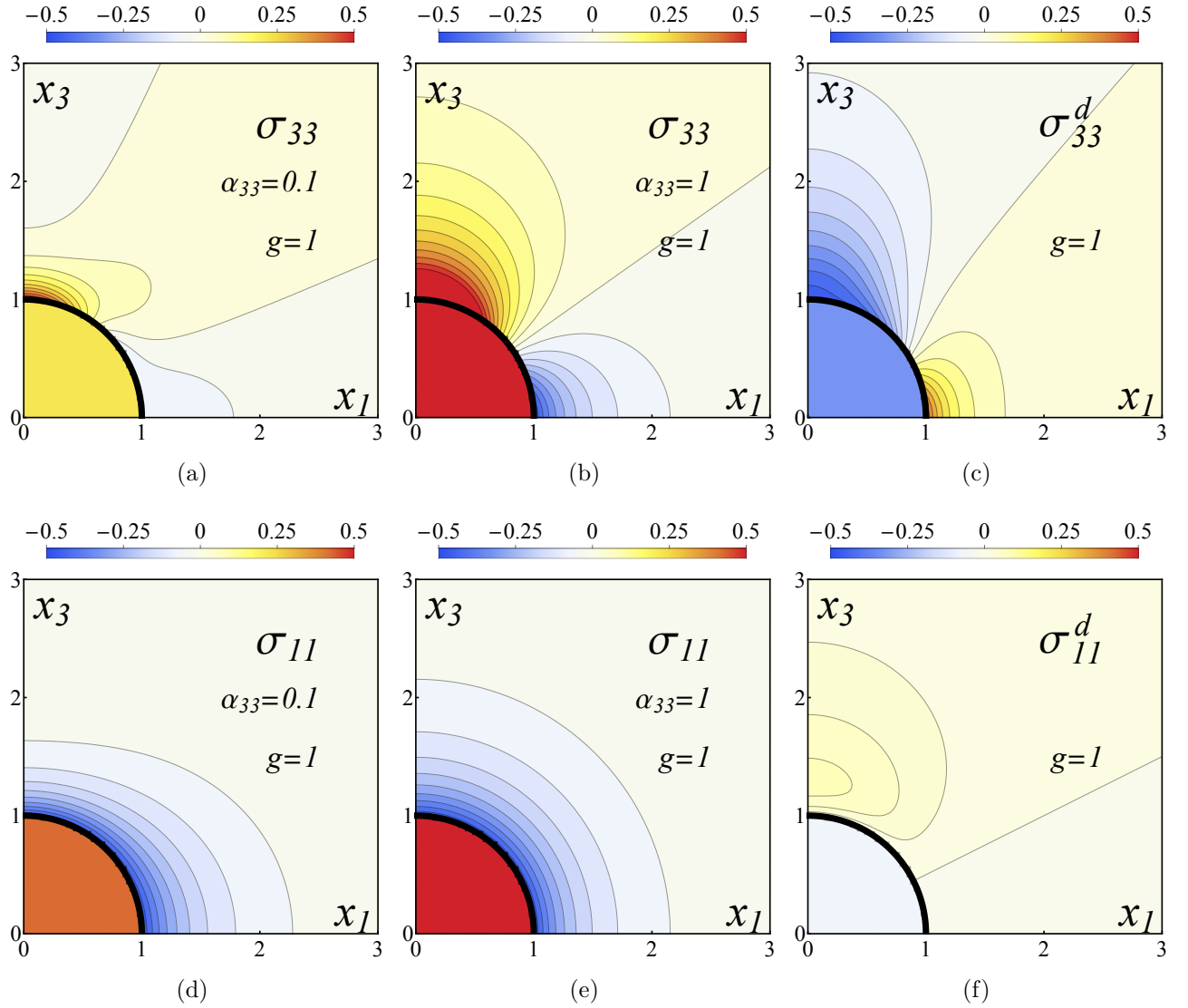


Figure 3.5: Stress ratio for different α_{33} values. $g = \frac{G^*}{G^0}$; $\nu^0 = \nu^* = 0.2$; $a_1 = a_2 = a_3 = 1$. (a) σ_{33}/p if $\alpha_{33} = 0.1$; (b) σ_{33}/p if $\alpha_{33} = 1$; (c) σ_{33}^d/p , difference of part (a) and (b); (d) σ_{11}/p if $\alpha_{33} = 0.1$; (e) σ_{11}/p if $\alpha_{33} = 1$; (f) σ_{11}^d/p , difference of part (d) and (e).

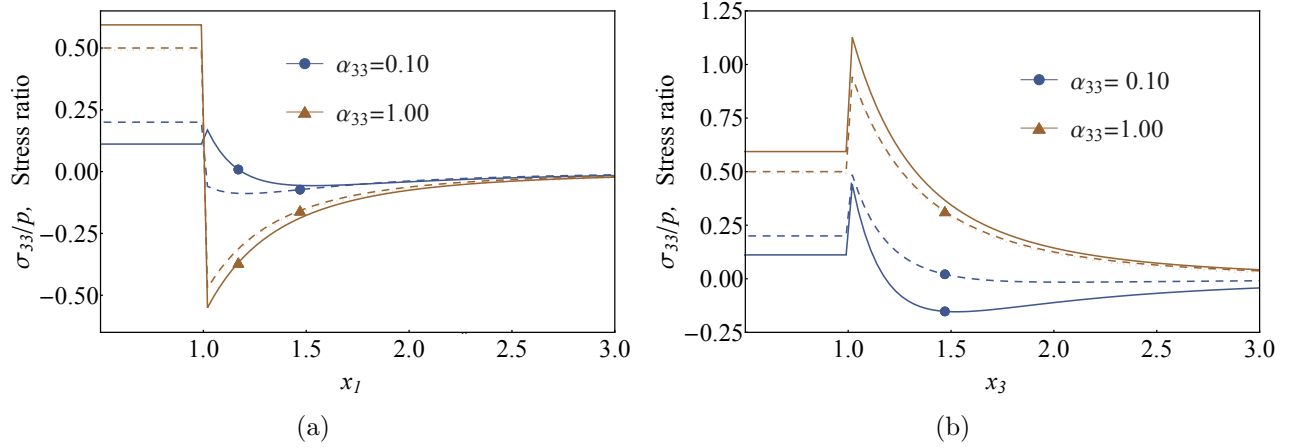


Figure 3.6: Vertical stress ratio σ_{33}/p versus (a) horizontal (b) vertical distance from the inhomogeneity center due to pressure change inside the poroelastic inhomogeneity, for different elastic and poroelastic anisotropic cases. Solid lines show transverse isotropic case; dashed lines show isotropic elastic case. For the isotropic case we assumed $\nu^0 = \nu^* = 0.2$, $g = 1$, $a_1 = a_2 = a_3 = 1$; For transverse isotropic case we used the results reported by (Pena, 1998, pp. 33) for saturated sandstone cores from an oil reservoir in Budare, Venezuela ($c_{11} = 3.6$, $c_{33} = 3.32$, $c_{44} = 0.99$, $c_{66} = 1.19$, $c_{12} = 1.29$, $c_{13} = 1.28$).

Considering anisotropic elastic modulus for the inhomogeneity affects the stress distribution inside and outside the inhomogeneity. Figures 3.6(a) and 3.6(b) show neglecting anisotropic elastic moduli inside the inhomogeneity results in the wrong estimation of stresses, especially when we are dealing with anisotropic Biot coefficient (solid lines show transverse isotropic case; dashed lines show isotropic elastic case).

3.6 Conclusion

In this article, we used Equivalent Inclusion Method (EIM) to solve for stress and strain distribution inside and outside of an anisotropic poroelastic inhomogeneity. Finding the equivalent eigenstrain, we presented graphical results for strain and stress ratio, and further explored the sensitivity of parameters of different elastic and poroelastic parameters on results. We assumed transverse isotropic condition for both poroelastic and elastic parameters of the inhomogeneity. The results show how neglecting the effect of both anisotropic poroelastic and elastic properties may result in large differences in stress calculations. The

stress ratio changes are much larger in the direction parallel to the axis of symmetry than the directions in the plain of symmetry.

3.7 Calculating D_{ijkl}

Suppose we have an ellipsoidal inhomogeneity Ω , with principal half axes a_1, a_2 , and a_3 . The strain and stress field at the point $x = (x_1, x_2, x_3)$, located outside of the inhomogeneity ($x \in D - \Omega$), can be expressed by

$$\varepsilon_{ij}(x) = D_{ijkl}(x)\varepsilon_{kl}^*, \quad (3.24)$$

$$\sigma_{ij}(x) = C_{ijkl}\varepsilon_{kl}(x), \quad (3.25)$$

where

$$D_{ijkl}(x) = \frac{1}{8\pi(1-\nu)} \left\{ \psi_{,kl ij} - 2\nu\delta_{kl}\phi_{,ij} - (1-\nu)[\phi_{,kj}\delta_{il} + \phi_{,ki}\delta_{jl} + \phi_{,lj}\delta_{ik} + \phi_{,li}\delta_{jk}] \right\}, \quad (3.26)$$

and ε^* is homogenizing eigenstrain; C_{ijkl} is elastic moduli of the surrounding medium; and ν is the Poisson's ratio of the inhomogeneity. For the complete derivation and more details check Mura (1987).

In Eq. (3.26)

$$\phi_{,ij} = -\delta_{ij}I_I(\lambda) - x_i I_{I,J}(\lambda) \quad (3.27)$$

$$\begin{aligned}
\psi_{ijkl} = & -\delta_{ij}\delta_{kl}[I_K(\lambda) - a_I^2 I_{IK}(\lambda)] - (\delta_{ik}\delta_{jl} + \delta_{jk}\delta_{il})[I_J(\lambda) - a_I^2 I_{IJ}(\lambda)] \\
& -\delta_{ij}x_k[I_K(\lambda) - a_I^2 I_{IK}(\lambda)]_{,l} - (\delta_{ik}x_j + \delta_{jk}x_i)[I_J(\lambda) - a_I^2 I_{IJ}(\lambda)]_{,l} \\
& -(\delta_{il}x_j + \delta_{jl}x_i)[I_J(\lambda) - a_I^2 I_{IJ}(\lambda)]_{,k} - x_i x_j [I_J(\lambda) - a_I^2 I_{IJ}(\lambda)]_{,kl}
\end{aligned} \tag{3.28}$$

where

$$I_{ij\dots}(\lambda) = 2\pi a_1 a_2 a_3 \int_{\lambda}^{\infty} \frac{ds}{(a_i^2 + s)(a_j^2 + s) \cdots \Delta(s)} \tag{3.29}$$

$$\Delta(s) = \sqrt{(a_1^2 + s)(a_2^2 + s)(a_3^2 + s)} \tag{3.30}$$

and λ is the largest positive root of the equation

$$\frac{x_1^2}{a_1^2 + \lambda} + \frac{x_2^2}{a_2^2 + \lambda} + \frac{x_3^2}{a_3^2 + \lambda} = 1. \tag{3.31}$$

3.8 Results for Ellipsoidal Isotropic Poroelastic Inclusion

According to Rudnicki (2002a), if an isotropic solid is loaded by far field stresses σ^{∞} (or strains, ε^{∞}), the relation between the strains are

$$\varepsilon_{mn}^I + S_{mnkk}\varepsilon_{tt}^I(k - g) + (g - 1)S_{mnkl}\varepsilon_{kl}^I = \varepsilon_{mn}^{\infty} - \frac{1}{3} \frac{\alpha p}{K} S_{mnkk}, \tag{3.32}$$

where $k = K_I/K$ and $g = G_I/G$; and superscripts and subscripts I designates the properties of the inclusion.

In addition, the result for the stress relation can be rewritten by separating the stress components to mean and deviatoric parts ($\sigma_{ij} = (\sigma/3)\delta_{ij} + q_{ij}$) by the following two equations

$$\begin{aligned}
& q_{mn}^I + (g-1) \left\{ S_{mnkl} - \frac{S_{mnkl}[(k-1)S_{mnrr} + \delta_{mn}]}{[3 + S_{rrtt}(k-1)]} \right\} q_{kl}^I \\
& = gq_{mn}^\infty - \frac{2G_I}{3K} \frac{[3S_{mnkk} - S_{rrtt}\delta_{mn}]}{[3 + S_{rrtt}(k-1)]} (\alpha p + k-1),
\end{aligned} \tag{3.33}$$

and

$$\left[1 + \frac{S_{rrtt}}{3}(k-1) \right] + (g-1) \frac{K_I}{2G_I} S_{mmkl} q_{kl} = k\sigma^\infty + \left(1 + \frac{S_{rrtt}}{3}\alpha p \right). \tag{3.34}$$

3.9 A Discussion on the Effective Material Properties of the Medium

Methodology

Let's assume that we have a medium consisted of poroelastic inclusions embedded in an elastic matrix (see Fig. 3.7). Inclusions are assumed to have the same ellipsoidal shape and material properties uniformly distributed in the medium; however, the material properties of the inclusions could be different from that of the matrix. The ratio of the inclusions volume V_I to the total volume of the medium V_M is supposed to be β ($\beta = V_I/V_M$). We used the Eshelby technique (Eshelby, 1957, 1959) and the concept of average stress in the matrix developed by Mori and Tanaka (1973) to determine the effective material properties for this medium. We modified the existing methods available for elastic composites (Tandon and Weng, 1984) and elastic porous materials (Zhao et al., 1989) to analyze the effective material properties by adding the impact of poroelastic stress and strain caused by the pore fluid pressure inside the inclusions.

Suppose that the medium is subjected to far-field stress σ_{ij}^0 and excessive fluid pressure p in the inclusions. The average elastic modulus of the medium (matrix with pressurized inclusions) is represented by \bar{C}_{ijkl} ; whereas C_{ijkl}^0 and C_{ijkl}^1 are the matrix and inclusions

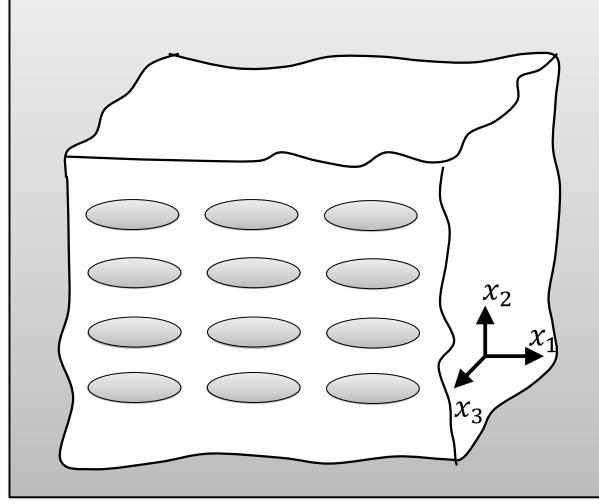


Figure 3.7: A medium consisted of pressurized poroelastic unidirectionally aligned inclusions embedded in an elastic matrix

elastic moduli, respectively. The, stress-strain constitutive equations result in

$$\sigma_{ij}^0 = \bar{C}_{ijkl} \bar{\varepsilon}_{kl}, \quad (3.35)$$

$$\sigma_{ij}^0 = C_{ijkl}^0 \varepsilon_{kl}^0, \quad (3.36)$$

where $\bar{\varepsilon}_{kl}$ is the average strain in the medium; and ε_{kl}^0 is the uniform strain state in the matrix in the absence of the inclusions, i.e. $\bar{C}_{ijkl} = C_{ijkl}^0$. Now considering the impacts of the inclusions in the medium, the average stress in the matrix $(\sigma)_m$, can be written as

$$(\sigma_{ij})_m = \sigma_{ij}^0 + \tilde{\sigma}_{ij} = C_{ijkl}^0 (\varepsilon_{kl}^0 + \tilde{\varepsilon}_{kl}), \quad (3.37)$$

where $\tilde{\varepsilon}_{ij}$ is the additional average perturbed strain from ε_{ij}^0 caused by the presence of the inclusions. Therefore, the corresponding stress $\tilde{\sigma}_{ij}$ can be written as

$$\tilde{\sigma}_{ij} = C_{ijkl}^0 \tilde{\varepsilon}_{kl}. \quad (3.38)$$

On the other hand, the total stress in the inclusions $(\sigma_{ij})_I$, can be calculated by adding σ^{pt} to $(\sigma)_m$, where σ^{pt} is the perturbed stress component induced in the inclusion (by pore pressure and/or dissimilarity between material properties) from the average stress in the matrix $(\sigma)_m$. Based on these definitions, we have

$$(\sigma_{ij})_I = (\sigma_{ij})_m + \sigma_{ij}^{pt} = \sigma_{ij}^0 + \tilde{\sigma}_{ij} + \sigma_{ij}^{pt}. \quad (3.39)$$

Using the equivalent inclusion method (EIM), the perturbed strain and stress components in the inclusion may be calculated as (Eshelby, 1957)

$$\varepsilon_{ij}^{pt} = S_{ijkl} \varepsilon_{kl}^*, \quad (3.40)$$

$$\sigma_{ij}^{pt} = C_{ijkl}^0 [\varepsilon_{kl}^{pt} - \varepsilon_{kl}^*], \quad (3.41)$$

where S_{ijkl} are the components of the Eshelby tensor. Here, ε^* is the fictitious uniform homogenizing eigenstrain and can be determined from solving the below system of equations

$$(\sigma_{ij}^T)_I = C_{ijkl}^1 (\varepsilon_{kl}^0 + \tilde{\varepsilon}_{kl} + \varepsilon_{kl}^{pt} + \varepsilon_{kl}^p) = C_{ijkl}^0 (\varepsilon_{kl}^0 + \tilde{\varepsilon}_{kl} + \varepsilon_{kl}^{pt} - \varepsilon_{kl}^*), \quad (3.42)$$

where ε^p is the poroelastic transformation strain and can be obtained by setting $\sigma_{ij} = 0$ in the poroelastic constitutive equations

$$\varepsilon_{mn}^p = -L_{mnij}^1 \alpha_{ij}^1 p. \quad (3.43)$$

In Eq. (3.43), L_{mnij}^1 is the elastic compliance tensor for the inclusions i.e. inverse of C_{mnij}^1 ; and α_{ij}^1 is the Biot coefficient of the inclusion. Note that $\tilde{\varepsilon}$ and ε_{kl}^* are the only unknown parameters in the system of Eq. (3.42). Considering the fact that the average stress over the matrix and inclusion should be the same as the sum of the farfield stress σ_{ij}^0 and the fluid pore pressure in the inclusions, we have

$$\tilde{\sigma}_{ij} + \beta(\sigma_{ij}^{pt} + \alpha p \delta_{ij}) = 0. \quad (3.44)$$

Substituting Eqs. (3.40), (3.43) and (3.44) into Eq. (3.42), ε^* can be determined from solving the system of linear equations in Eq. (3.42). Finally, the average strain in the medium $\bar{\varepsilon}_{kl}$, can be calculated by volume averaging of the strain values in the inclusion and matrix. Therefore, we have

$$\begin{aligned} \bar{\varepsilon}_{ij} &= (1 - \beta)(\varepsilon_{ij}^0 + \tilde{\varepsilon}_{ij}) + \beta(\varepsilon_{ij}^0 + \tilde{\varepsilon}_{ij} + \varepsilon_{ij}^{pt}) \\ &= \varepsilon_{ij}^0 + \tilde{\varepsilon}_{ij} + \beta \varepsilon_{ij}^{pt}. \end{aligned} \quad (3.45)$$

Using Eqs. (3.36) and (3.45), the average elastic modulus of the medium \bar{C}_{ijkl} can be calculated from Eq. (3.35).

Numerical Results

To calculate the effective material constants of the medium, we applied the appropriate stress at infinity and p inside the inclusions and calculated the corresponding average strains in the medium.

Applying $\sigma_{11}^0 = 1$ at infinity and $p = 1$ inside the inclusions, we calculated the average directional Young modulus \bar{E}_{11} as

$$\sigma_{11}^0 = (E_{11})_M \bar{\varepsilon}_{11}. \quad (3.46)$$

Figure 3.8 shows the longitudinal Young's modulus of the medium $(E_{11})_M$ ratio to Young's modulus of the matrix E_m for different inhomogeneity aspect ratios R , volume ratios β and material properties. Figures 3.8(a) to 3.8(c) are for the case of $\sigma_{11}^0 = p = 1$. Moreover, Fig. 3.8(a) represents a case with softer inhomogeneities than the surrounding matrix, whereas Fig. 3.8(c) represents a case with stiffer inhomogeneities. As we expect in the case of no material properties discrepancy between the inclusions and the matrix, the inhomogeneity aspect ratio will not change the results. Figure 3.8(b) shows that the existence of fluid pressure inside the inclusions causes decrease in longitudinal Young's modulus.

The same approach can be used for determining other material constants for the transverse isotopic poroelastic medium with pressurized inhomogeneities. For example similar to $(E_{11})_M$, the transverse Young's modulus $(E_{22})_M$ can be determined as

$$\sigma_{22}^0 = E_{22} \bar{\varepsilon}_{22}. \quad (3.47)$$

Since the fluid pore pressure impact is the same in all directions, substituting R with $1/R$, we will have $(E_{22})_M|_R = (E_{11})_M|_{1/R}$.

Figure 3.8(d) represents the impact of different fluid pressures in the inhomogeneities (e.g. $p = 0, 0.25, 0.75, 1$ and 2). As shown in this figure, higher pore pressures, i.e. more damage inside the medium, results in lower average stiffness.

3.10 References

Aadnoy, B., 1988. Modeling of the stability of highly inclined boreholes in anisotropic rock formations. SPE Drilling Engineering 3. doi:10.2118/16526-PA.

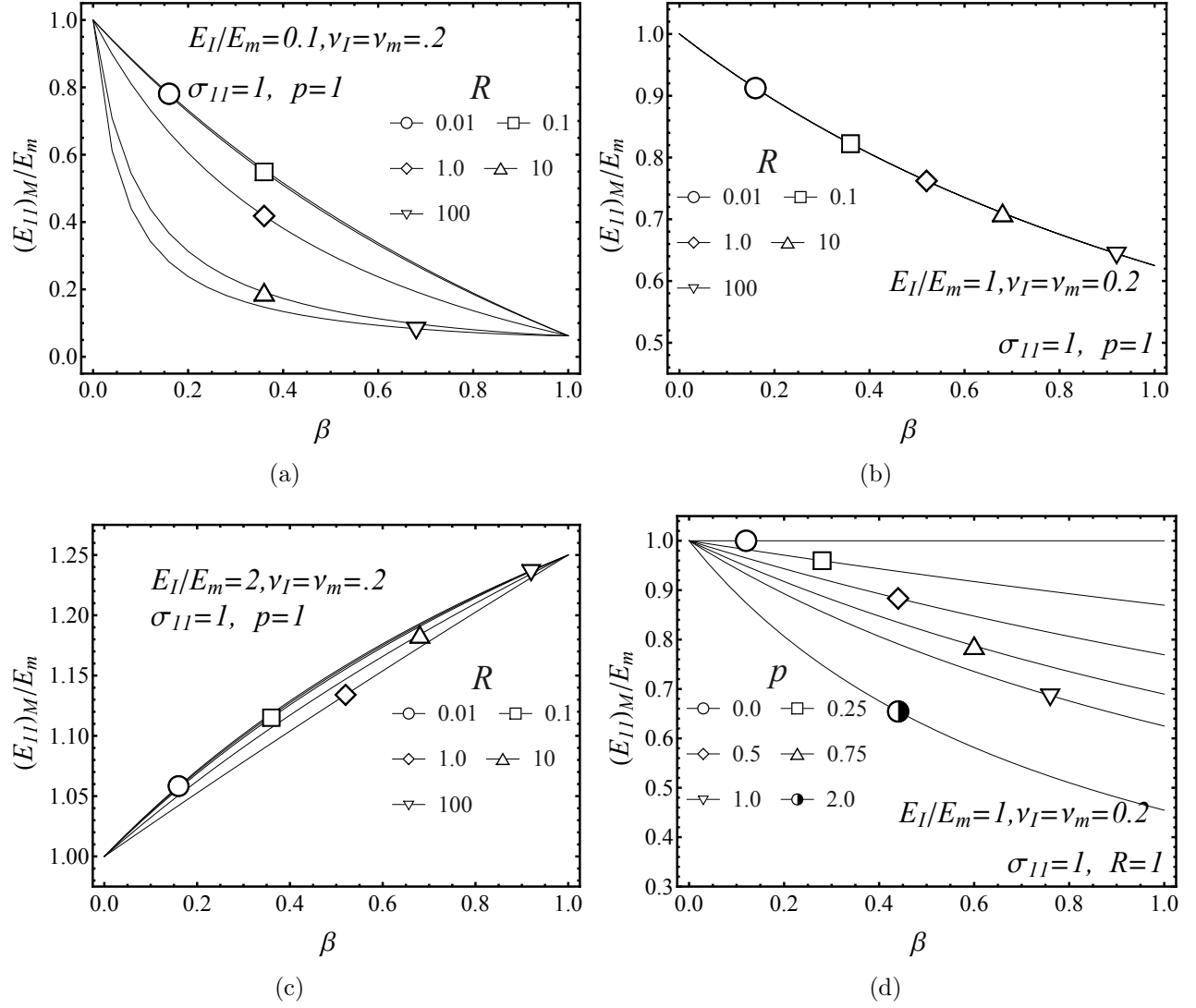


Figure 3.8: Longitudinal Young's modulus of the medium $(E_{11})_M$ to Young's modulus of the matrix E_m for $\sigma_{11}^0 = 1$ and $p = 1$ and different inhomogeneity aspect ratios R , and volume ratios β for different material properties ratio of the inhomogeneities and the matrix (a) $E_I/E_m = 0.1$ (b) $E_I/E_m = 1.0$ (c) $E_I/E_m = 2.0$; (d) different p/σ_{11}^0 ratios

- Abousleiman, Y.N., Ekbote, S., 2005. Solutions for the inclined borehole in a porothermoelastic transversely isotropic medium. *Journal of Applied Mechanics* 72, 102. doi:10.1115/1.1825433.
- Ahmadi, M., Dahi Taleghani, A., Sayers, C.M., 2014a. Direction dependence of fracture compliance induced by slickensides. *GEOPHYSICS* 79, C91–C96. doi:10.1190/geo2013-0227.1.
- Ahmadi, M., Dahi Taleghani, A., Sayers, C.M., 2014b. Direction dependence of fracture compliance ratio induced by slickensides. Accepted for Publication in *Geophysics*.
- Amadei, B., 1996. Importance of anisotropy when estimating and measuring in situ stresses in rock. *International Journal of Rock Mechanics and Mining Sciences & Geomechanics Abstracts* 33, 293–325. doi:10.1016/0148-9062(95)00062-3.
- Aoki, T., Tan, C., Bamford, W., 1993. Effects of deformation and strength anisotropy on borehole failures in saturated shales. *International Journal of Rock Mechanics and Mining Sciences & Geomechanics Abstracts* 30, 1031–1034. doi:10.1016/0148-9062(93)90067-N.
- Babuska, V., Cara, M., 1991. *Seismic anisotropy in the Earth*. Springer.
- Backus, G.E., 1962. Long-wave elastic anisotropy produced by horizontal layering. *Journal of Geophysical Research* 67, 4427–4440. doi:10.1029/JZ067i011p04427.
- Bang, J., Solstad, A., Mjaaland, S., 2001. Formation electrical anisotropy derived from induction-log measurements in a horizontal well. *SPE Reservoir Evaluation & Engineering* 4, 483–488. doi:10.2118/75115-PA.
- Bedayat, H., Dahi Taleghani, A., 2012. Drainage of poroelastic fractures and its implications on the performance of naturally fractured reservoirs, in: *46th US Rock Mechanics/Geomechanics Symposium*, Chicago, IL, USA.
- Bedayat, H., Dahi Taleghani, A., 2013. The equivalent inclusion method for poroelasticity problems, in: *Poromechanics V*, American Society of Civil Engineers, Reston, VA. pp. 1279–1288. doi:10.1061/9780784412992.153.
- Bedayat, H., Dahi Taleghani, A., 2014. Interacting double poroelastic inclusions. *Mechanics of Materials* 69, 204–212. doi:10.1016/j.mechmat.2013.10.006.

- Berryman, J.G., 1992. Effective stress for transport properties of inhomogeneous porous rock. *Journal of Geophysical Research* 97, 17409. doi:10.1029/92JB01593.
- Berryman, J.G., 1997. Generalization of Eshelby's formula for a single ellipsoidal elastic inclusion to poroelasticity and thermoelasticity. *Physical Review Letters* 79, 1142–1145. doi:10.1103/PhysRevLett.79.1142.
- Berryman, J.G., 2011. Mechanics of layered anisotropic poroelastic media with applications to effective stress for fluid permeability. *International Journal of Engineering Science* 49, 122–139. doi:10.1016/j.ijengsci.2010.06.027.
- Biot, M.A., 1941. General theory of three-dimensional consolidation. *Journal of Applied Physics* 12, 155. doi:10.1063/1.1712886.
- Biot, M.A., 1955. Theory of elasticity and consolidation for a porous anisotropic solid. *Journal of Applied Physics* 26, 182. doi:10.1063/1.1721956.
- Bower, A.F., 2011. *Applied mechanics of solids*. CRC Press.
- Bruschke, M.V., Advani, S.G., 1990. A finite element/control volume approach to mold filling in anisotropic porous media. *Polymer Composites* 11, 398–405. doi:10.1002/pc.750110613.
- Cederbaum, G., Li, L., Schulgasser, K., 2000. *Poroelastic structures*. Elsevier.
- Chen, Z.R., 2011. Poroelastic model for induced stresses and deformations in hydrocarbon and geothermal reservoirs. *Journal of Petroleum Science and Engineering* 80, 41–52. doi:10.1016/j.petrol.2011.10.004.
- Cheng, A.H.D., 1997. Material coefficients of anisotropic poroelasticity. *International Journal of Rock Mechanics and Mining Sciences* 34, 199–205. doi:10.1016/S0148-9062(96)00055-1.
- Cheng, A.H.D., Abousleiman, Y.N., Detournay, E., Cui, L., Roegiers, J.C., 1996. Mandel's problem revisited. *Géotechnique* 46, 187–195. doi:10.1680/geot.1996.46.2.187.

- Cowin, S.C., 1999. Bone poroelasticity. *Journal of Biomechanics* 32, 217–238. doi:10.1016/S0021-9290(98)00161-4.
- Cowin, S.C., Doty, S.B., 2007. *Tissue mechanics*. Springer New York, New York, NY. doi:10.1007/978-0-387-49985-7.
- Crampin, S., 1994. The fracture criticality of crustal rocks. *Geophysical Journal International* 118, 428–438. doi:10.1111/j.1365-246X.1994.tb03974.x.
- Cui, L., Cheng, A.H.D., Kaliakin, V.N., Abousleiman, Y.N., Roegiers, J.c., 1996. Finite element analysis of anisotropic poroelasticity: a generalized Mandel’s problem and an inclined borehole problem. *International Journal for Numerical and Analytical Methods in Geomechanics* 20, 381–401. doi:10.1002/(SICI)1096-9853(199606)20:6<381::AID-NAG826>3.0.CO;2-Y.
- Dahi Taleghani, A., Ahmadi, M., Olson, J.E., Wang, W., 2014. Thermal reactivation of microfractures and its potential impact on hydraulic fractures efficiency. Accepted for publication in *SPE Journal*.
- Dahi Taleghani, A., Olson, J.E., 2011. Numerical modeling of multistranded-hydraulic-fracture propagation: Accounting for the interaction between induced and natural fractures. *SPE Journal*, 575–581.
- Detournay, E., Cheng, A.H.D., 1991. Plane strain analysis of a stationary hydraulic fracture in a poroelastic medium. *International Journal of Solids and Structures* 27, 1645–1662. doi:10.1016/0020-7683(91)90067-P.
- Dormieux, L., Kondo, D., Ulm, F.J., 2006. *Microporomechanics*. John Wiley & Sons, Ltd, Chichester, UK. doi:10.1002/0470032006.
- Eshelby, J.D., 1957. The determination of the elastic field of an ellipsoidal inclusion, and related problems. *Proceedings of the Royal Society A: Mathematical, Physical and Engineering Sciences* 241, 376–396. doi:10.1098/rspa.1957.0133.
- Eshelby, J.D., 1959. The elastic field outside an ellipsoidal inclusion, in: *Proceedings of the Royal Society of London. Series A, Mathematical and Physical*, pp. 561–569.

- Eshelby, J.D., 1961. Elastic inclusions and inhomogeneities, in: Sneddon, I.N., Hill, R. (Eds.), *Progress in Solid Mechanics*, Vol.2. North-Holland, Amsterdam, pp. 89–140.
- Feng, Y., Okamoto, R.J., Namani, R., Genin, G.M., Bayly, P.V., 2013. Measurements of mechanical anisotropy in brain tissue and implications for transversely isotropic material models of white matter. *Journal of the mechanical behavior of biomedical materials* 23, 117–32. doi:10.1016/j.jmbbm.2013.04.007.
- Ferrari, M., 2000. Nanomechanics, and biomedical nanomechanics: Eshelby's inclusion and inhomogeneity problems at the discrete/continuum interface. *Biomedical Microdevices* , 273–281doi:10.1023/A:1009903205275.
- Ghabezloo, S., Hemmati, S., 2011. Poroelasticity of a micro-heterogeneous material saturated by two immiscible fluids. *International Journal of Rock Mechanics and Mining Sciences* 48, 1376–1379. doi:10.1016/j.ijrmms.2011.10.003.
- He, Z., Caratini, G., Dormieux, L., Kondo, D., 2013. Homogenization of anisotropic elastoplastic behaviors of a porous polycrystal with interface effects , 3213–3236doi:10.1002/nag.
- Hellmich, C., Ulm, F.j., 2002. Micromechanical model for ultrastructural stiffness of mineralized tissues. *Journal of Engineering Mechanics* 128, 898–908. doi:10.1061/(ASCE)0733-9399(2002)128:8(898).
- Hu, D.W., Zhou, H., Shao, J.F., 2013. An anisotropic damage-plasticity model for saturated quasi-brittle materials. *International Journal for Numerical and Analytical Methods in Geomechanics* 37, 1691–1710. doi:10.1002/nag.2103.
- Hudson, J.A., 1981. Wave speeds and attenuation of elastic waves in material containing cracks. *Geophysical Journal International* 64, 133–150. doi:10.1111/j.1365-246X.1981.tb02662.x.
- Kanj, M., Abousleiman, Y.N., Ghanem, R., 2003. Poromechanics of anisotropic hollow cylinders. *Journal of Engineering Mechanics* 129, 1277–1287. doi:10.1061/(ASCE)0733-9399(2003)129:11(1277).

- Khan, S., Ansari, S., Han, H., Khosravi, N., 2011. Importance of shale anisotropy in estimating in-situ stresses and wellbore stability analysis in Horn River Basin, in: Proceedings of Canadian Unconventional Resources Conference, Society of Petroleum Engineers. doi:10.2118/149433-MS.
- Khan, S., Williams, R., Ansari, S., Khosravi, N., 2012. Impact of mechanical anisotropy on design of hydraulic fracturing in shales, in: Proceedings of Abu Dhabi International Petroleum Conference and Exhibition, Society of Petroleum Engineers. doi:10.2118/162138-MS.
- Khoshgofta, M., Najarian, S., Farmanzad, F., Vahidi, B., Ghomshe, F.T., 2007. A biomechanical composite model to determine effective elastic moduli of the CNS Gray Matter. American Journal of Applied Sciences 4, 918–924. doi:10.3844/ajassp.2007.918.924.
- Levasseur, S., Collin, F., Charlier, R., Kondo, D., 2013. On micromechanical damage modeling in geomechanics: Influence of numerical integration scheme. Journal of Computational and Applied Mathematics 246, 215–224. doi:10.1016/j.cam.2012.05.022.
- Levin, V.M., Alvarez-Tostado, J.M., 2003. Eshelby’s formula for an ellipsoidal elastic inclusion in anisotropic poroelasticity and thermoelasticity. International Journal of Fracture 119/120, L77–L82. doi:10.1023/A:1024907500335.
- Li, L., Shirazi-Adl, A., Buschmann, M.D., 2003. Investigation of mechanical behavior of articular cartilage by fibril reinforced poroelastic models. Biorheology 40, 227–33.
- Li, S., Sauer, R.a., Wang, G., 2007. The Eshelby tensors in a finite ppherical domain-Part I: theoretical formulations. Journal of Applied Mechanics 74, 770. doi:10.1115/1.2711227.
- Li, S., Wang, G., 2008. Introduction to micromechanics and nanomechanics. World Scientific.
- Litewka, a., 2003. Load-induced oriented damage and anisotropy of rock-like materials. International Journal of Plasticity 19, 2171–2191. doi:10.1016/S0749-6419(03)00064-0.
- Malekmoitei, L., Farahmand, F., Shodja, H.M., Samadi-Dooki, A., 2013. An analytical approach to study the intraoperative fractures of femoral shaft during total hip arthroplasty. Journal of biomechanical engineering 135, 41004. doi:10.1115/1.4023699.

- Marquez, J.P., Genin, G.M., Zahalak, G.I., Elson, E.L., 2005. Thin bio-artificial tissues in plane stress: the relationship between cell and tissue strain, and an improved constitutive model. *Biophysical journal* 88, 765–77. doi:10.1529/biophysj.104.040808.
- Mehrabian, A., Abousleiman, Y.N., 2013. Generalized poroelastic wellbore problem. *International Journal for Numerical and Analytical Methods in Geomechanics* doi:10.1002/nag.2160.
- Moran, J.H., Gianzero, S., 1979. Effects of formation anisotropy on resistivitylogging measurements. *GEOPHYSICS* 44, 1266–1286. doi:10.1190/1.1441006.
- Mori, T., Tanaka, K., 1973. Average stress in matrix and average elastic energy of materials with misfitting inclusions. *Acta Metallurgica* 21, 571–574. doi:10.1016/0001-6160(73)90064-3.
- Morrow, D.A., Haut Donahue, T.L., Odegard, G.M., Kaufman, K.R., 2010. Transversely isotropic tensile material properties of skeletal muscle tissue. *Journal of the mechanical behavior of biomedical materials* 3, 124–9. doi:10.1016/j.jmbbm.2009.03.004.
- Mueller, M.C., 1991. Prediction of lateral variability in fracture intensity using multi-component shear-wave surface seismic as a precursor to horizontal drilling in the Austin Chalk. *Geophysical Journal International* 107, 409–415. doi:10.1111/j.1365-246X.1991.tb01402.x.
- Mura, T., 1987. *Micromechanics of defects in solids*. Martinus Nijhoff Publishers.
- Nemat-Nasser, S., Hori, M., 1999. *Micromechanics: overall properties of heterogeneous materials*. Elsevier, Amsterdam.
- Nowinski, J.L., Davis, C.F., 1970. A model of the human skull as a poroelastic spherical shell subjected to a quasistatic load. *Mathematical Biosciences* 8, 397–416. doi:10.1016/0025-5564(70)90120-3.
- Nur, A., Simmons, G., 1969. Stress-induced velocity anisotropy in rock: An experimental study. *Journal of Geophysical Research* 74, 6667–6674. doi:10.1029/JB074i027p06667.
- Pena, F.J.R., 1998. Elastic properties of sedimentary anisotropic rocks (measurments and applicatiosn). Ph.D. thesis. Massachusetts Institute of Technology.

- Pollard, D.D., Fletcher, R.C., 2005. Fundamentals of structural geology. Cambridge University Press.
- Rawal, C., Ghassemi, A., 2014. A reactive thermo-poroelastic analysis of water injection into an enhanced geothermal reservoir. *Geothermics* 50, 10–23. doi:10.1016/j.geothermics.2013.05.007.
- Rice, J.R., Cleary, M.P., 1976. Some basic stress diffusion solutions for fluid-saturated elastic porous media with compressible constituents. *Reviews of Geophysics* 14, 227. doi:10.1029/RG014i002p00227.
- Rickman, J.M., 2009. The role of elastic anisotropy in poroelastic transport. *Journal of Applied Physics* 106, 044911. doi:10.1063/1.3204649.
- Rudnicki, J.W., 2002a. Alteration of regional stress by reservoirs and other inhomogeneities: Stabilizing or destabilizing?, in: Vouille, G., Berest, P. (Eds.), *Proc. 9th Int. Congr. Rock Mechanics*, Vol. 3, Paris, Aug. 25–29, 1999, Paris, France. pp. 1629–1637.
- Rudnicki, J.W., 2002b. Eshelby transformations, pore pressure and fluid mass changes, and subsidence, in: *Poromechanics II, Proc. 2nd Biot Conference on Poromechanics*, Grenoble, France.
- Rutqvist, J., Wu, Y.S., Tsang, C.F., Bodvarsson, G., 2002. A modeling approach for analysis of coupled multiphase fluid flow, heat transfer, and deformation in fractured porous rock. *International Journal of Rock Mechanics and Mining Sciences* 39, 429–442. doi:10.1016/S1365-1609(02)00022-9.
- Sayers, C.M., 1994. The elastic anisotropy of shales. *Journal of Geophysical Research* 99, 767. doi:10.1029/93JB02579.
- Sayers, C.M., 2005. Seismic anisotropy of shales. *Geophysical Prospecting* 53, 667–676. doi:10.1111/j.1365-2478.2005.00495.x.
- Schoenberg, M., Sayers, C.M., 1995. Seismic anisotropy of fractured rock. *GEOPHYSICS* 60, 204–211. doi:10.1190/1.1443748.
- Shao, J.F., 1998. Poroelastic behaviour of brittle rock materials with anisotropic damage. *Mechanics of Materials* 30, 41–53. doi:10.1016/S0167-6636(98)00025-8.

- Shao, J.F., Chau, K., Feng, X., 2006. Modeling of anisotropic damage and creep deformation in brittle rocks. *International Journal of Rock Mechanics and Mining Sciences* 43, 582–592. doi:10.1016/j.ijrmms.2005.10.004.
- Shodja, H.M., Ojaghnezhad, F., 2007. A general unified treatment of lamellar inhomogeneities. *Engineering Fracture Mechanics* 74, 1499–1510. doi:10.1016/j.engfracmech.2006.08.016.
- Shodja, H.M., Rad, I., Soheilifard, R., 2003. Interacting cracks and ellipsoidal inhomogeneities by the equivalent inclusion method. *Journal of the Mechanics and Physics of Solids* 51, 945–960. doi:10.1016/S0022-5096(02)00106-0.
- Shojaei, A., Dahi Taleghani, A., Li, G., 2014. A continuum damage failure model for hydraulic fracturing of porous rocks. *International Journal of Plasticity* doi:10.1016/j.ijplas.2014.03.003.
- Soltanzadeh, H., Hawkes, C.D., 2012. Evaluation of caprock integrity during pore pressure change using a probabilistic implementation of a closed-form poroelastic model. *International Journal of Greenhouse Gas Control* 7, 30–38. doi:10.1016/j.ijggc.2011.10.006.
- Soltanzadeh, H., Hawkes, C.D., Sharma, J.S., 2007. poroelastic model for production- and injection-induced stresses in reservoirs with elastic properties different from the surrounding rock. *International Journal of Geomechanics* 7, 353–361. doi:10.1061/(ASCE)1532-3641(2007)7:5(353).
- Tan, X., Konietzky, H., 2014. Numerical study of variation in Biot’s coefficient with respect to microstructure of rocks. *Tectonophysics* 610, 159–171. doi:10.1016/j.tecto.2013.11.014.
- Tandon, G.P., Weng, G.J., 1984. The effect of aspect ratio of inclusions on the elastic properties of unidirectionally aligned composites. *Polymer Composites* 5, 327–333. doi:10.1002/pc.750050413.
- Teklu, T.W., Graves, R., Tutuncu, A.N., Kazemi, H., Alameri, W., Alsumaiti, A., 2012. Geomechanics considerations in enhanced oil recovery, in: *Proceedings of SPE Canadian Unconventional Resources Conference, Society of Petroleum Engineers*. doi:10.2118/162701-MS.

- Turner, C., Chandran, A., Pidaparti, R., 1995. The anisotropy of osteonal bone and its ultrastructural implications. *Bone* 17, 85–89. doi:10.1016/8756-3282(95)00148-7.
- Verruijt, A., 2014. Theory and problems of poroelasticity. Delf University of Technology.
- Voyiadjis, G.Z., Kattan, P.I., 2006. Advances in damage mechanics: metals and metal matrix composites with an introduction to fabric tensors, 2nd Edition, in: *Advances in Damage Mechanics: Metals and Metal Matrix Composites With an Introduction to Fabric Tensors*, 2nd Edition. second edi ed.. Elsevier Science Ltd, Oxford, p. 740.
- Wang, H., Towler, B., Soliman, M., 2007. Near wellbore stress analysis and wellbore strengthening for drilling depleted formations, in: *Proceedings of Rocky Mountain Oil & Gas Technology Symposium*, Society of Petroleum Engineers. pp. 1–12. doi:10.2118/102719-MS.
- Wang, H.F., 2000. Theory of linear poroelasticity with applications to geomechanics and hydrogeology. Princeton University Press.
- Wu, J., Herzog, W., Epstein, M., 1999. Modelling of location- and time-dependent deformation of chondrocytes during cartilage loading. *Journal of Biomechanics* 32, 563–572. doi:10.1016/S0021-9290(99)00034-2.
- Zhao, Y.H., Tandon, G.P., Weng, G.J., 1989. Elastic moduli for a class of porous materials. *Acta Mechanica* 76, 105–131. doi:10.1007/BF01175799.
- Zhou, K., Hoh, H.J., Wang, X., Keer, L.M., Pang, J.H., Song, B., Wang, Q.J., 2013. A review of recent works on inclusions. *Mechanics of Materials* 60, 144–158. doi:10.1016/j.mechmat.2013.01.005.
- Zhou, K., Keer, L.M., Jane Wang, Q., Ai, X., Sawamiphakdi, K., Glaws, P., Paire, M., Che, F., 2012. Interaction of multiple inhomogeneous inclusions beneath a surface. *Computer Methods in Applied Mechanics and Engineering* 217-220, 25–33. doi:10.1016/j.cma.2012.01.006.
- Zhou, X., Ghassemi, A., 2011. Three-dimensional poroelastic analysis of a pressurized natural fracture. *International Journal of Rock Mechanics and Mining Sciences* 48, 527–534. doi:10.1016/j.ijrmms.2011.02.002.

Zou, W., He, Q., Huang, M., Zheng, Q., 2010. Eshelby's problem of non-elliptical inclusions. *Journal of the Mechanics and Physics of Solids* 58, 346–372. doi:10.1016/j.jmps.2009.11.008.

Chapter 4

Eshelby Solution for Double Ellipsoidal Inhomogeneities: Applications in Geoscience

We developed a method and presented it as a *Mathematica* code to calculate the stress and strain fields inside and outside of two interacting ellipsoidal inhomogeneities with arbitrary orientation with respect to each other, using the Eshelby technique. The Eshelby technique can be used to determine the elastic fields in and around these inhomogeneities. Assuming same material properties for one of the inclusions and the surrounding matrix, this code can be also used for the single inhomogeneity problem. Different geological features like faults and aquifers can be modeled as inhomogeneous inclusions.

We start by reviewing Eshelby's solution for a single inclusion, a single inhomogeneity and double inhomogeneity problem with the required formulation to calculate Eshelby tensors. Then, we describe our code structure and validate it with existing solutions in the literature and present numerical solutions.

4.1 Introduction

Determining the elastic fields inside and outside of inhomogeneities has many applications in the geoscience, material science, and biomechanics. In geomechanics, the stress distribution in and around reservoirs, aquifers, intrusions, fault zones, caverns, dikes, compaction bands, and underground structures has been calculated using the Eshelby technique (Rudnicki,

2011). These geological structures may have different material properties and different strain conditions (e.g. different pressure, temperature, or inelastic deformations) rather than that of their surroundings. Rudnicki (2002a,b); Walsh (2002); Soltanzadeh et al. (2007); Chen (2011); Soltanzadeh and Hawkes (2012); Bedayat and Dahi Taleghani (2013, 2014a,b) are some examples of using Eshelby technique to calculate stress changes due to fluid injection or withdrawal.

An inhomogeneity is defined as a sub-volume of the medium, that has different material properties from those of its surroundings, whereas an inclusion is a finite sub-volume of a medium, which may undergo different strain status from that of the surrounding environment. If a finite sub-volume of a medium experiences both of the above conditions at the same time, it would be considered as an inhomogeneous inclusion. Hereafter, we use the term inhomogeneity instead of inhomogeneous inclusion.

Eshelby (1957, 1959) formulated the elastic fields generated by an ellipsoidal inhomogeneity in an isotropic elastic infinite medium, which undergoes a uniform strain. This solution implies that the stress and strain distribution inside an ellipsoidal inhomogeneity is uniform, if the applied strains in the absence of the surrounding material, i.e. eigenstrain, is uniform. Elastic and plastic strains, pressure changes, and thermal expansions are examples of different types of strains, which could be referred to as eigenstrains (Mura, 1987).

Existence of inhomogeneities in a material, changes the overall response and the elastic field in the material. The problem of interacting inhomogeneities have been studied extensively in the past decades. For example, Horii and Nemat-Nasser (1985) used the method of pseudotractions to calculate the stress and strain fields in a linearly elastic homogeneous solid which contains 2D inhomogeneities; Honein et al. (1992) solved analytically the interaction of two 2D inclusions under anti-plane shear. For 3D interacting inhomogeneities, Moschovidis and Mura (1975) used the Equivalent Inclusion Method (EIM) and the superposition principal along Taylor series expansion to solve the two ellipsoidal inhomogeneities problem; Kachanov and Laures (1989) solved the problem of closely spaced, strongly inter-

acting penny shape cracks. Later, the computational efficiency of Moschovidis and Mura (1975) solution for interactive inclusions was improved by Shodja et al. (2003); and the solution was further modified to solve poroelastic isotropic (Bedayat and Dahi Taleghani, 2014a, 2013) and poroelastic anisotropic (Bedayat and Dahi Taleghani, 2014b) inhomogeneities. The Eshelby's method has been also utilized to solve more complex problems like lamellar inhomogeneities (Shodja and Ojaghnezhad, 2007), inclusions in finite media (Li et al., 2007), non-ellipsoidal inclusions (Zou et al., 2010), , inclusions in half-space (Zhou et al., 2012), or analysis to simulate elasto-plastic large deformations of composites (Shojaei and Li, 2013). See Zhou et al. (2013) for an extensive review on the subject.

Healy (2009) published a code for calculation and visualisation of the internal and external elastic fields for spheroidal inclusions. Later, Meng et al. (2012) published a code for elastic fields generated by an ellipsoidal inhomogeneity under remote in-situ stresses. We developed a *Mathematica* code that calculates the stress and strain fields inside and outside a general double ellipsoidal inhomogeneity problem. Assuming same material properties for one of the inclusions and the surrounding matrix, this code can be also used for a single inhomogeneity problem (see Section 4.7).

The outline of this paper is as follows: Section 4.2 reviews the Eshelby's solution for the single inclusion, the single inhomogeneity and the double inhomogeneity problem. Then in Section 4.3, the formulation required to calculate the Eshelby tensor is provided for a single ellipsoidal inclusion. In Section 4.4, we described the code structure. Finally, we verified our code with existing solutions and presented a numerical example in Section 4.5.

4.2 Theory

4.2.1 Single inclusion

Consider an ellipsoidal inclusion in an infinite elastic solid, which undergoes a uniform eigen-strain ε_{ij}^T (see Fig. 4.1). Eshelby (1957, 1959) showed that the actual strain and stress inside

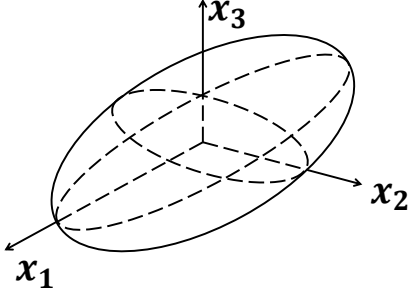


Figure 4.1: An ellipsoidal inclusion with principal axis parallel to Cartesian coordinate system (x_1, x_2, x_3)

the inclusion are uniform and given by

$$\varepsilon_{ij} = S_{ijkl} \varepsilon_{kl}^T, \quad (4.1)$$

$$\sigma_{ij} = C_{ijkl}^0 [\varepsilon_{kl} - \varepsilon_{kl}^T], \quad (4.2)$$

where ε_{ij} and σ_{ij} are the components of strain and stress tensors in the matrix, respectively; C_{ijkl}^0 is the elastic moduli of the matrix; Eshelby tensor S_{ijkl} , is a fourth rank tensor which is a function of geometry and Poisson's ratio of the ellipsoidal inclusion.

We provided the details to calculate the Eshelby tensor in Section 4.9 (see Mura (1987) for more details).

4.2.2 Single inhomogeneity

Considering a fictitious uniform homogenizing eigenstrain ε^* , EIM can be used to determine the stress and strain in inhomogeneities. EIM solves the inhomogeneity problem by modeling a homogenous inclusion which undergoes fictitious uniform homogenizing eigenstrain ε^* , plus

an external transformation strain ε^T , which is the transformation strain. Defining ε^{**} to be

$$\varepsilon^{**} = \varepsilon^T + \varepsilon^*, \quad (4.3)$$

the actual strain and stress inside of the inhomogeneity are

$$\varepsilon_{ij} = S_{ijkl}\varepsilon_{kl}^{**}, \quad (4.4)$$

$$\sigma_{ij} = C_{ijkl}^1[\varepsilon_{kl} - \varepsilon_{kl}^T], \quad (4.5)$$

where C_{ijkl}^1 is the elasticity tensor of the inhomogeneity; and ε^* can be calculated from solving the following equation

$$C_{ijkl}^0[S_{klmn}\varepsilon_{mn}^{**} - \varepsilon_{kl}^{**}] = C_{ijkl}^1[S_{klmn}\varepsilon_{mn}^{**} - \varepsilon_{kl}^T]. \quad (4.6)$$

For the exterior points, stress and strain fields can be calculated by substituting the fourth rank tensor D_{ijkl} for S_{ijkl} in Eq. (4.4). $D_{ijkl}(x)$ is similar to Eshelby's tensor, but for the exterior points. If $x \in \Omega$, then $D_{ijkl}(x) = S_{ijkl}$ (Mura, 1987, p. 87). See Section 4.3 for more details.

4.2.3 Double interacting inclusions

Moschovidis and Mura (1975) solved the stress field caused by two interacting inhomogeneities (Ω_1 and Ω_2) embedded in an infinite elastic medium (see Fig. 4.2) by writing EIM equations for each inhomogeneity individually. Hence, the system of consistency equations for two inhomogeneities under the applied stress σ_{ij}^0 (similar to equation Eq. (4.6) for a single inclusion), will be

$$C_{ijkl}^1[\varepsilon_{kl}^0 + \varepsilon_{kl}^1 + \varepsilon_{kl}^2] = C_{ijkl}^0[\varepsilon_{kl}^0 + \varepsilon_{kl}^1 + \varepsilon_{kl}^2 - \varepsilon_{kl}^{1*}] \quad \text{in } \Omega_1, \quad (4.7)$$

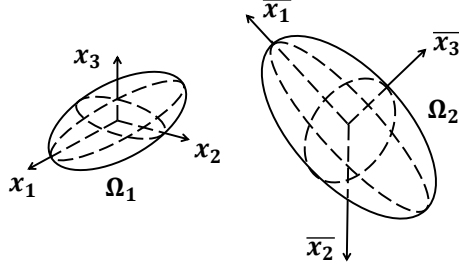


Figure 4.2: Two ellipsoidal inhomogeneities

$$C_{ijkl}^2[\varepsilon_{kl}^0 + \varepsilon_{kl}^1 + \varepsilon_{kl}^2] = C_{ijkl}^0[\varepsilon_{kl}^0 + \varepsilon_{kl}^1 + \varepsilon_{kl}^2 - \varepsilon_{kl}^{2*}] \quad \text{in } \Omega_2, \quad (4.8)$$

where C_{ijkl}^1 is the elastic moduli of Ω_1 ; C_{ijkl}^2 is the elastic moduli of Ω_2 ; ε_{kl}^{1*} is the equivalent eigenstrain for Ω_1 ; ε_{kl}^{2*} is the equivalent eigenstrain for Ω_2 ; and ε_{kl}^1 and ε_{kl}^2 are the corresponding strains caused by ε_{kl}^{1*} and ε_{kl}^{2*} .

Let's assume that all the strains in Eqs. (4.7) and (4.8) can be represented in the form of polynomials with respect to the local Cartesian coordinate system and approximating $D_{ijkl}(x)$ by its Taylor expansion around the geometric center of the inhomogeneity, the stress field inside and outside of double inhomogeneity system can be calculated (see Section 4.8 for more details).

4.3 Formulation

Here, we provide the formulation required to calculate Eshelby tensor for an ellipsoidal inclusion Ω , embedded in the infinite medium M . Suppose Ω is given by

$$\frac{x_1^2}{a_1^2} + \frac{x_2^2}{a_2^2} + \frac{x_3^2}{a_3^2} \leq 1, \quad (4.9)$$

where a_i ($i = 1, 2$, and 3) are size of the principal half axis of the ellipsoidal inclusion. According to Mura (1987) strain fields can be expanded as

$$\varepsilon_{ij}^1(x) = D_{ijkl}^1(x)B_{kl}^1 + D_{ijklq}^1(x)B_{klq}^1 + D_{ijklqr}^1(x)B_{klqr}^1 + \dots, \quad (4.10)$$

$$\varepsilon_{ij}^2(x) = D_{ijkl}^2(\bar{x})B_{kl}^2 + D_{ijklq}^2(\bar{x})B_{klq}^2 + D_{ijklqr}^2(\bar{x})B_{klqr}^2 + \dots, \quad (4.11)$$

where $B_{ij\dots}$ are coefficients in the eigenstrain polynomial expansion (see Section 4.8) and $D_{ij\dots}$ can be calculated as

$$\begin{aligned} D_{ijkl}(x) = & \frac{1}{8\pi(1-\nu)} \left[\psi_{,kl ij} - 2\nu\delta_{kl}\phi_{,ij} \right. \\ & \left. - (1-\nu)[\phi_{,kj}\delta_{il} + \phi_{,ki}\delta_{jl} + \phi_{,lj}\delta_{ik} + \phi_{,li}\delta_{jk}] \right], \end{aligned} \quad (4.12)$$

$$\begin{aligned} D_{ijklq}(x) = & \frac{1}{8\pi(1-\nu)} \left[\psi_{q,kl ij} - 2\nu\delta_{kl}\phi_{q,ij} \right. \\ & \left. - (1-\nu)[\phi_{q,kj}\delta_{il} + \phi_{q,ki}\delta_{jl} + \phi_{q,lj}\delta_{ik} + \phi_{q,li}\delta_{jk}] \right], \end{aligned} \quad (4.13)$$

etc.,

where

$$\psi(x) = \int_{\Omega} |x - x'| dx', \quad (4.14)$$

$$\phi(x) = \int_{\Omega} \frac{dx'}{|x - x'|}. \quad (4.15)$$

$\psi(x)$, $\phi(x)$ and their derivatives can be calculated in terms of I , V and their derivatives (Ferrers, 1877; Dyson, 1891; Moschovidis, 1975; Mura, 1987)

$$I(\lambda) = 2\pi a_1 a_2 a_3 \int_{\lambda}^{\infty} \frac{ds}{\Delta(s)}, \quad (4.16)$$

$$I_i(\lambda) = 2\pi a_1 a_2 a_3 \int_{\lambda}^{\infty} \frac{ds}{(a_i^2 + s)\Delta(s)}, \quad (4.17)$$

$$I_{ij}(\lambda) = 2\pi a_1 a_2 a_3 \int_{\lambda}^{\infty} \frac{ds}{(a_i^2 + s)(a_j^2 + s)\Delta(s)}, \quad (4.18)$$

etc.,

and

$$V(x) = \pi a_1 a_2 a_3 \int_{\lambda}^{\infty} \frac{U(s)}{\Delta(s)} ds, \quad (4.19)$$

$$V_i(x) = \pi a_1 a_2 a_3 \int_{\lambda}^{\infty} \frac{U(s)}{(a_i^2 + s)\Delta(s)} ds, \quad (4.20)$$

$$V_{ij}(x) = \pi a_1 a_2 a_3 \int_{\lambda}^{\infty} \frac{U(s)}{(a_i^2 + s)(a_j^2 + s)\Delta(s)} ds, \quad (4.21)$$

etc.,

where

$$\Delta(s) = \sqrt{(a_1^2 + s)(a_2^2 + s)(a_3^2 + s)}, \quad (4.22)$$

$$U(s) = 1 - \left[\frac{x_1^2}{(a_1^2 + s)} + \frac{x_2^2}{(a_2^2 + s)} + \frac{x_3^2}{(a_3^2 + s)} \right], \quad (4.23)$$

In Eqs. (4.16) to (4.21), λ is equal to zero for points located inside Ω . If x is located outside Ω , then λ would be the largest positive root of

$$\frac{x_1^2}{a_1^2 + \lambda} + \frac{x_2^2}{a_2^2 + \lambda} + \frac{x_3^2}{a_3^2 + \lambda} = 1. \quad (4.24)$$

For more detailed formulation see Section 4.9.

4.4 Description of the Mathematica code

We structured the code with multiple files, so changing the input data and following the calculation procedures would be easier for the user. This code is designed to calculate the stress tensor along a defined path line segment in 3D space.

input_report.nb retrieves the properties of this line segment. Geometrical specifications of the inhomogeneities including size, location and direction of their principal axes should be entered in **input_geometry.nb**. **input_material_properties.nb** retrieves the material properties of the inhomogeneities and the matrix, i.e. shear moduli and Poisson's ratios. The initial stresses in the medium should be modified in **input_stress.nb**.

Users can get the stress values at different points with **run.nb**. All the results will be saved in **project.mx** and can be plotted by **plot.nb**, which exports the results to a graph in the *pdf* format.

The rest of files perform the calculations and solve for stresses. **constants.nb** contains some general definitions; **elastic_moduli.nb** calculates the elastic moduli of the inhomogeneities and matrix; **check_point** checks if the target point is inside or outside of the inhomogeneity and **check_lambda** calculates λ (see Eq. (4.24)); **lambda_0.nb** calculates D tensors for the case of $\lambda = 0$, whereas **lambda.nb** calculates D tensors for the case of $\lambda \neq 0$; **Dtensor1.nb** and **Dtensor2.nb** assign proper values to the tensor D for the two inclu-

sions; **system.nb** generates the system of equations required to calculate the homogenizing eigenstrains and solves it for the proper homogenizing eigenstrains; Finally, **single_points** calculates the stress and strain in the target location.

Detailed description of the duties for each file can be found in the comments written in the files.

4.5 Verification and Numerical results

This code has been verified with three different cases. These cases covers stress values for single and double inclusion problems with different shapes, elastic moduli and eigenstrain. First, we verified our code for stress calculations of the single inhomogeneity problem. The results were calculated assuming same material properties for the surrounding matrix and the secondary fictitious inclusion. We validated the results with the stress (σ_{11}) distribution solution provided by Healy (2009) and Meng et al. (2012) for a single void inhomogeneity (cavity) under far-field loading, assuming various inhomogeneity aspect ratios (see Fig. 4.3(a)). σ_{33} values for the same cavity are shown in Fig. 4.3(b), which implies that we may face compressive or tensile stresses near the cavities depending on their aspect ratios. Then, we reproduced the results reported by Mura (1987) for the stress values at a particular point of a single ellipsoidal inhomogeneity and its surroundings, for different inhomogeneity aspect ratios and various elastic modulus ratios of the inhomogeneity and the matrix (see Fig. 4.3(c)). Finally, we verified the code for the case of two interacting inclusions with the solution provided by Moschovidis (1975) for stress distribution along axis of symmetry (x_3) for the case of two ellipsoidal cavities with uniform unit internal pressure (see Fig. 4.4). These solutions were in exact agreement with the previous published solutions.

The presented computer code could be used to calculate stress changes in formations with different lithologies (material properties) and varying pore pressure (eigenstrain). For example producing hydrocarbon from reservoirs result in pore pressure decrease inside the reservoir. This alteration of pore pressure and subsequent stress changes above and below

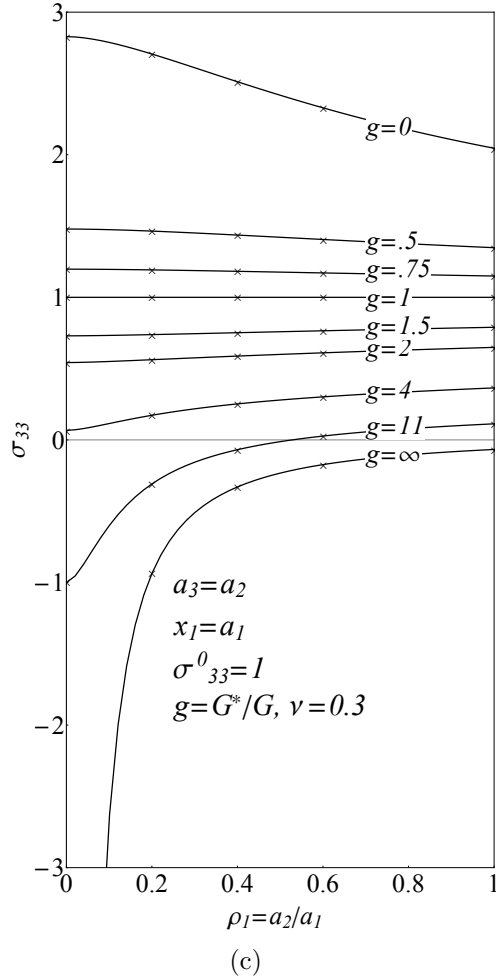
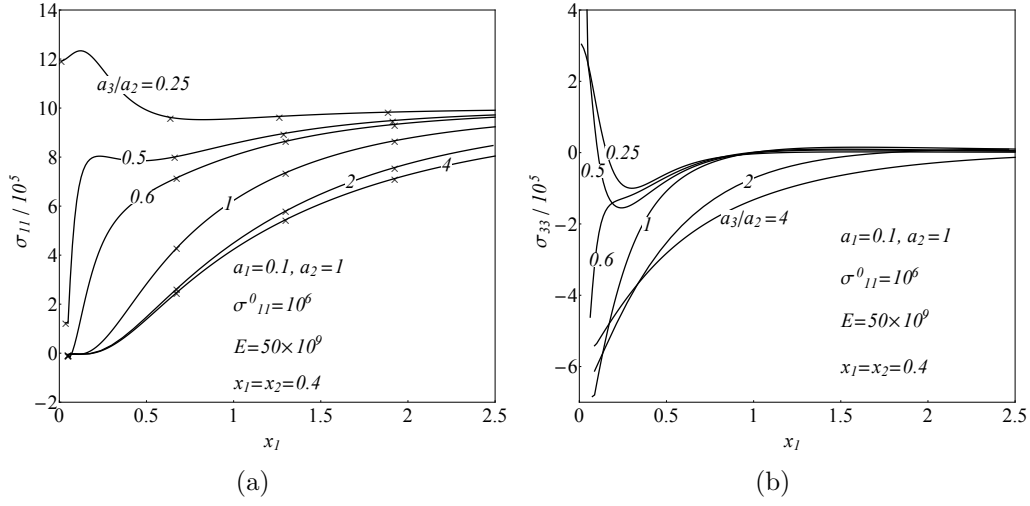


Figure 4.3: (a, b) σ_{11} and σ_{33} vs x_1 , for a single void inhomogeneity for various values of a_3/a_2 , compare with Meng et al. (2012) and Healy (2009); (c) σ_{33} vs a_2/a_1 for an ellipsoidal inhomogeneity for various values of $g = \frac{G^*}{G^0}$, compare with Mura (1987).

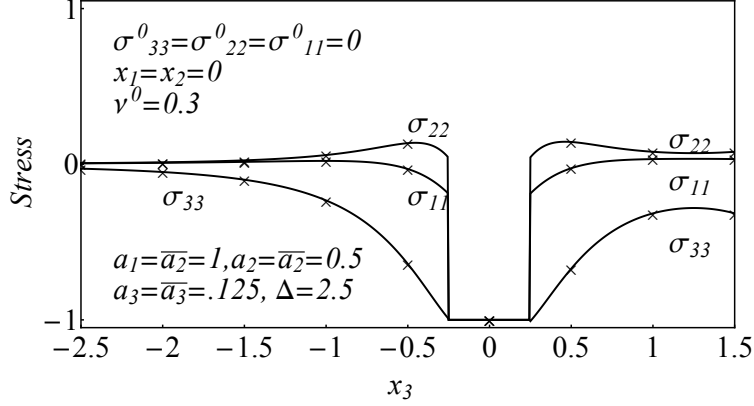


Figure 4.4: Stress vs x_3 for two interacting ellipsoidal cavities with uniform unit internal pressure, compare with Moschovidis (1975).

the reservoir may cause faulting or seismic activities inside and outside of the reservoir. Assuming uniform distribution of pore pressure inside the reservoir, the Eshelby's solution is used to calculate the stress regime inside and outside of the reservoir. In the case of closely located reservoirs, using double inhomogeneity model incorporates the interaction effect. Changes in pore pressure can be calculated with choosing the proper transformation strain ε^T

$$\varepsilon_{mn}^T = L_{mnij} \alpha_{ij} p, \quad (4.25)$$

where L_{mnij} is the tensor of elastic compliances, inverse of C_{mnij} , p is change in pore pressure and α_{ij} is the Biot coefficient (Bedayat and Dahi Taleghani, 2014a,b).

Figure 4.5 shows the amount of changes in horizontal and vertical stresses due to unit pressure drop inside an isolated reservoir, whereas Figure 4.6 shows that of two closely located reservoirs, using double interacting inhomogeneity model. It can be seen in the case of using double interacting model, stresses inside the reservoirs wont be uniform. For example, considering existence of two reservoirs and their interaction effect, the magnitude of σ_{33} at point $x = (0, 0, -1)$ is 8% larger (more compressive) than that of the prediction of the single inhomogeneity model (compare Fig. 4.5(c) with Fig. 4.6(c)).

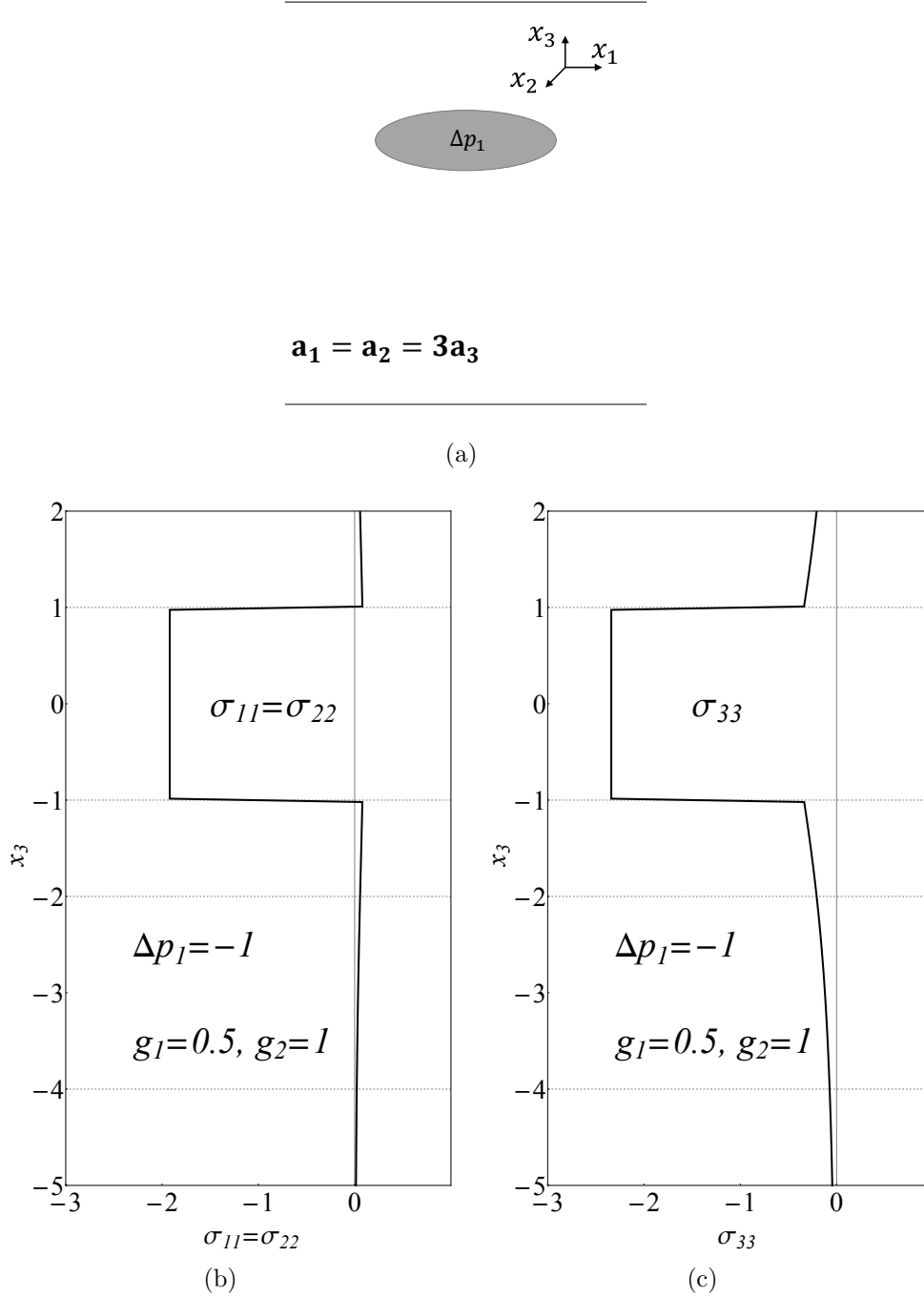


Figure 4.5: (a) Schematic of an ellipsoidal inhomogeneity which models pore pressure changes in a reservoir. This model calculates stress distribution inside and outside of the reservoir, due to pore pressure changes inside the reservoirs. (b) Changes in $\sigma_{11} = \sigma_{22}$ vs x_3 (c) changes in σ_{33} vs x_3 due to unit pressure drop inside the reservoir. It is assumed $g_1 = \frac{G^*}{G^0} = 0.5$ and $a_2/a_1 = 1, a_1/a_3 = 3$. $x_3 = 0$ is center of the inhomogeneity.

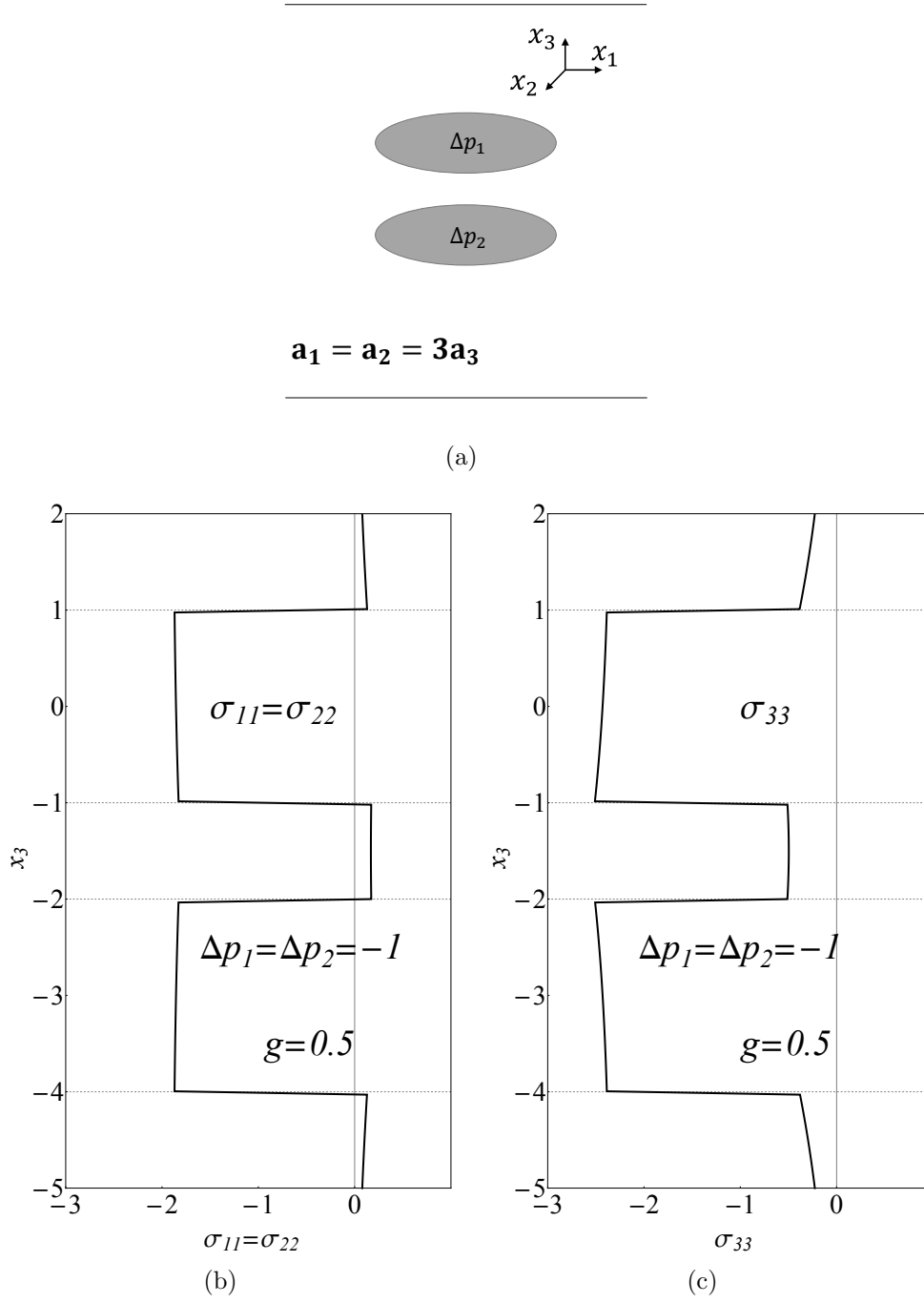


Figure 4.6: (a) Schematic of two ellipsoidal inhomogeneities which models pore pressure changes in two adjacent reservoirs. This model calculates stress distribution inside and outside of two adjacent reservoir, due to pore pressure changes inside the reservoirs. (b) Changes in $\sigma_{11} = \sigma_{22}$ vs x_3 (c) changes in σ_{33} vs x_3 due to unit pressure drop inside two adjacent reservoirs. It is assumed $g_1 = g_2 = \frac{G^*}{G^0} = 0.5$ and $a_2/a_1 = 1$, $a_1/a_3 = 3$. $x_3 = 0$ and $x_3 = -3$ are centers of the two ellipsoidal inhomogeneities.

4.6 Conclusion

Determining the elastic fields inside and outside of inhomogeneities have many applications in the geoscience, material science, and biomechanics. For example, many geological phenomena and structures like reservoirs, aquifers, intrusions, fault zones, caverns, dikes, compaction bands, and other underground structures can be modeled as inhomogeneous inclusions, i.e. have different loading conditions and material properties rather than those of the their surroundings.

We developed a *Mathematica* code to calculate the stress and strain fields inside and outside of two interacting ellipsoidal inhomogeneities with arbitrary orientation with respect to each other. This model can be used to predict pore pressure inside and outside of depleting reservoirs. The results shows neglecting the interaction effect between the reservoirs, predicts lower compressive stresses in depleted formations. Assuming same material properties for one of the inclusions and the surrounding matrix, this code can be also used for a single inhomogeneity problem. This code is based on the solution provided by Moschovidis and Mura (1975) for elastic and Bedayat and Dahi Taleghani (2014a) for poroelastic inhomogeneities. Considering interaction of the inhomogeneities, stress distribution inside the inhomogeneities wont be uniform.

4.7 Supplementary data

Supplementary data associated with this article can be found in the author’s website.

4.8 Double inhomogeneity problem

In this section, we present a short review of the solution developed by Moschovidis and Mura (1975) to solve for double interacting inhomogeneities. Consider x_i and \bar{x}_i are the local coordinate systems taken at the center of Ω_1 and Ω_2 , respectively. These coordinate systems

$$+ \frac{1}{2} \sum_{m=1}^3 \frac{1}{(a_m^2 + \lambda)^n}, \quad (4.41)$$

and the derivatives of λ are

$$\lambda_{,q} = \frac{1}{C_1} F_q, \quad (4.42)$$

$$\lambda_{,qp} = \frac{1}{C_1} [F_{q,p} - \lambda_{,q} C_{1,p}], \quad (4.43)$$

$$\lambda_{,qpr} = -\frac{1}{C_1} [\lambda_{,qp} C_{1,r} - F_{q,pr} + \lambda_{,qr} C_{1,p} + \lambda_{,q} C_{1,pr}], \quad (4.44)$$

$$\begin{aligned} \lambda_{,qp rt} = & -\frac{1}{C_1} [\lambda_{,qpr} C_{1,t} + \lambda_{,qpt} C_{1,r} + \lambda_{,qp} C_{1,rt} - F_{q,prt} \\ & + \lambda_{,qrt} C_{1,p} + \lambda_{,qr} C_{1,pt} + \lambda_{,qt} C_{1,pr} + \lambda_{,q} C_{1,prt}], \end{aligned} \quad (4.45)$$

etc.,

where

$$F_q = \frac{2x_q}{(a_Q^2 + \lambda)}, \quad (4.46)$$

$$F_{q,p} = \frac{1}{(a_Q^2 + \lambda)} [2\delta_{qp} - F_q \lambda_{,p}], \quad (4.47)$$

$$F_{q,pr} = -\frac{1}{(a_Q^2 + \lambda)} [F_{q,p} \lambda_{,r} + F_{q,r} \lambda_{,p} + F_q \lambda_{,pr}], \quad (4.48)$$

$$F_{q,prt} = -\frac{1}{(a_Q^2 + \lambda)} [F_{q,pr} \lambda_{,t} + F_{q,pt} \lambda_{,r} + F_{q,p} \lambda_{,rt} + F_{q,rt} \lambda_{,p}$$

$$+ F_{q,rt}\lambda_{,p} + F_{q,r}\lambda_{,pt} + F_{q,t}\lambda_{,pr} + F_q\lambda_{,prt}], \quad (4.49)$$

$$C_n = \frac{x_i^2}{(a_I^2 + \lambda)^{n+1}}, \quad (4.50)$$

$$C_{1,q} = \frac{F_q}{a_Q^2 + \lambda} - 2C_2\lambda_{,q}, \quad (4.51)$$

$$C_{2,q} = \frac{F_q}{(a_Q^2 + \lambda)^2} - 3C_3\lambda_{,q}, \quad (4.52)$$

$$C_{1,qp} = \frac{1}{a_Q^2 + \lambda} \left[F_{q,p} - \frac{F_q}{a_Q^2 + \lambda} \lambda_{,p} \right] - 2[C_{2,p}\lambda_{,q} + C_2\lambda_{,qp}], \quad (4.53)$$

$$\begin{aligned} C_{2,qp} &= \frac{2\delta_{qp}}{(a_Q^2 + \lambda)^3} - \frac{6x_q}{(a_Q^2 + \lambda)^4} \lambda_{,p} - \frac{6x_p}{(a_P^2 + \lambda)^4} \lambda_{,q} \\ &\quad + 12C_4\lambda_{,q}\lambda_{,p} - 3C_3\lambda_{,qp}, \end{aligned} \quad (4.54)$$

$$\begin{aligned} C_{1,qpt} &= -\frac{1}{(a_Q^2 + \lambda)^2} \left[F_{q,p} - \frac{F_q}{a_Q^2 + \lambda} \lambda_{,p} \right] \lambda_{,t} \\ &\quad + \frac{1}{a_Q^2 + \lambda} \left[F_{q,pt} - \frac{F_{q,t}}{a_Q^2 + \lambda} \lambda_{,p} - \frac{F_q}{a_Q^2 + \lambda} \lambda_{,pt} + \frac{F_q}{(a_Q^2 + \lambda)^2} \lambda_{,p}\lambda_{,t} \right] \\ &\quad - 2[C_{2,pt}\lambda_{,q} + C_{2,p}\lambda_{,qt} + C_{2,t}\lambda_{,qp} + C_2\lambda_{,qpt}], \end{aligned} \quad (4.55)$$

etc.

Similarly, V integrals and their derivative can be written as

$$V = \frac{1}{2}[I - x_r x_r I_R], \quad (4.56)$$

$$V_i = \frac{1}{2}[I_i - x_r x_r I_{Ri}], \quad (4.57)$$

$$V_{ij} = \frac{1}{2}[I_{ij} - x_r x_r I_{Rij}], \quad (4.58)$$

etc.,

and

$$V_{ij\dots k,p} = -x_p I_{Pij\dots k}, \quad (4.59)$$

$$V_{ij\dots k,pq} = -[\delta_{pq} I_{Pij\dots k} + x_p I_{Pij\dots k,q}], \quad (4.60)$$

$$V_{ij\dots k,pqr} = -[\delta_{pq} I_{Pij\dots k,r} + \delta_{pr} I_{Pij\dots k,q} + x_p I_{Pij\dots k,qr}], \quad (4.61)$$

etc.,

So that we get the equations for ϕ , ψ and their derivatives as

$$\phi = V, \quad (4.62)$$

$$\phi_n = a_N^2 x_n V_N, \quad (4.63)$$

$$\begin{aligned} \phi_{mn} = a_M^2 & \left[x_m x_n a_N^2 V_{MN} \right. \\ & \left. + \frac{1}{4} \delta_{mn} [V - x_r x_r V_R - a_M^2 (V_M - x_r x_r V_{RM})] \right], \end{aligned} \quad (4.64)$$

$$\phi_{,ij} = -\delta_{ij}I_I - x_i I_{I,J} \quad (4.65)$$

$$\phi_{n,i} = a_N^2(\delta_{in}V_N + x_n V_{N,i}), \quad (4.66)$$

$$\phi_{n,ij} = a_N^2(\delta_{in}V_{N,j} + \delta_{jn}V_{N,i} + x_n V_{N,ij}), \quad (4.67)$$

and

$$\begin{aligned} \psi_{,ijkl} = & -\delta_{ij}\delta_{kl}[I_K(\lambda) - a_I^2 I_{IK}(\lambda)] - (\delta_{ik}\delta_{jl} + \delta_{jk}\delta_{il})[I_J(\lambda) - a_I^2 I_{IJ}(\lambda)] \\ & - \delta_{ij}x_k[I_K(\lambda) - a_I^2 I_{IK}(\lambda)]_{,l} - (\delta_{ik}x_j + \delta_{jk}x_i)[I_J(\lambda) - a_I^2 I_{IJ}(\lambda)]_{,l} \\ & - (\delta_{il}x_j + \delta_{jl}x_i)[I_J(\lambda) - a_I^2 I_{IJ}(\lambda)]_{,k} - x_i x_j [I_J(\lambda) - a_I^2 I_{IJ}(\lambda)]_{,kl} \end{aligned} \quad (4.68)$$

4.10 References

- Bedayat, H., Dahi Taleghani, A., 2013. The equivalent inclusion method for poroelasticity problems, in: *Poromechanics V*, American Society of Civil Engineers, Reston, VA. pp. 1279–1288. doi:10.1061/9780784412992.153.
- Bedayat, H., Dahi Taleghani, A., 2014a. Interacting double poroelastic inclusions. *Mechanics of Materials* 69, 204–212. doi:10.1016/j.mechmat.2013.10.006.
- Bedayat, H., Dahi Taleghani, A., 2014b. On the inhomogeneous anisotropic poroelastic inclusions. *Mechanics of Materials* (Under Review) .
- Chen, Z.R., 2011. Poroelastic model for induced stresses and deformations in hydrocarbon and geothermal reservoirs. *Journal of Petroleum Science and Engineering* 80, 41–52. doi:10.1016/j.petrol.2011.10.004.

- Dyson, F., 1891. The potentials of ellipsoids of variable densities. *Quart. J. Pure Appl. Math* 25, 259–288.
- Eshelby, J.D., 1957. The determination of the elastic field of an ellipsoidal inclusion, and related problems. *Proceedings of the Royal Society A: Mathematical, Physical and Engineering Sciences* 241, 376–396. doi:10.1098/rspa.1957.0133.
- Eshelby, J.D., 1959. The elastic field outside an ellipsoidal inclusion, in: *Proceedings of the Royal Society of London. Series A, Mathematical and Physical*, pp. 561–569.
- Ferrers, N., 1877. On the potentials of ellipsoids, ellipsoidal shells, elliptic laminae and elliptic rings of variable densities. *QJ Pure Appl. Math* 14, 1–22.
- Healy, D., 2009. Elastic field in 3D due to a spheroidal inclusion MATLAB code for Eshelby's solution. *Computers & Geosciences* 35, 2170–2173. doi:10.1016/j.cageo.2008.11.012.
- Honein, E., Honein, T., Herrmann, G., 1992. On two circular inclusions in harmonic problems. *Quarterly of applied mathematics* 50, 479–499.
- Horii, H., Nemat-Nasser, S., 1985. Elastic fields of interacting inhomogeneities. *International Journal of Solids and Structures* 21, 731–745. doi:10.1016/0020-7683(85)90076-9.
- Kachanov, M.L., Laures, J.P., 1989. Three-dimensional problems of strongly interacting arbitrarily located penny-shaped cracks. *International Journal of Fracture* 41, 289–313. doi:10.1007/BF00018861.
- Li, S., Sauer, R.a., Wang, G., 2007. The Eshelby tensors in a finite pherical domain-Part I: theoretical formulations. *Journal of Applied Mechanics* 74, 770. doi:10.1115/1.2711227.
- Meng, C., Heltsley, W., Pollard, D.D., 2012. Evaluation of the Eshelby solution for the ellipsoidal inclusion and heterogeneity. *Computers & Geosciences* 40, 40–48. doi:10.1016/j.cageo.2011.07.008.
- Moschovidis, Z.A., 1975. Two ellipsoidal inhomogeneities and related problems treated by the equivalent inclusion method. Ph.D. thesis. Northwestern University, Evanston.

- Moschovidis, Z.A., Mura, T., 1975. Two-ellipsoidal inhomogeneities by the Equivalent Inclusion Method. *Journal of Applied Mechanics* 42, 847. doi:10.1115/1.3423718.
- Mura, T., 1987. *Micromechanics of defects in solids*. Martinus Nijhoff Publishers.
- Rudnicki, J.W., 2002a. Alteration of regional stress by reservoirs and other inhomogeneities: Stabilizing or destabilizing?, in: Vouille, G., Berest, P. (Eds.), *Proc. 9th Int. Congr. Rock Mechanics*, Vol. 3, Paris, Aug. 25-29, 1999, Paris, France. pp. 1629– 1637.
- Rudnicki, J.W., 2002b. Eshelby transformations, pore pressure and fluid mass changes, and subsidence, in: *Poromechanics II*, *Proc. 2nd Biot Conference on Poromechanics*, Grenoble, France.
- Rudnicki, J.W., 2011. Eshelbys technique for analyzing inhomogeneities in geomechanics, in: Leroy, Y.M., Lehner, F.K. (Eds.), *Mechanics of Crustal Rocks*. Springer Vienna, pp. 43–72. doi:10.1007/978-3-7091-0939-7.
- Shodja, H.M., Ojaghnezhad, F., 2007. A general unified treatment of lamellar inhomogeneities. *Engineering Fracture Mechanics* 74, 1499–1510. doi:10.1016/j.engfracmech.2006.08.016.
- Shodja, H.M., Rad, I., Soheilifard, R., 2003. Interacting cracks and ellipsoidal inhomogeneities by the equivalent inclusion method. *Journal of the Mechanics and Physics of Solids* 51, 945–960. doi:10.1016/S0022-5096(02)00106-0.
- Shojaei, A., Li, G., 2013. Viscoplasticity analysis of semicrystalline polymers: A multiscale approach within micromechanics framework. *International Journal of Plasticity* 42, 31–49. doi:10.1016/j.ijplas.2012.09.014.
- Soltanzadeh, H., Hawkes, C.D., 2012. Evaluation of caprock integrity during pore pressure change using a probabilistic implementation of a closed-form poroelastic model. *International Journal of Greenhouse Gas Control* 7, 30–38. doi:10.1016/j.ijggc.2011.10.006.
- Soltanzadeh, H., Hawkes, C.D., Sharma, J.S., 2007. poroelastic model for production- and injection-induced stresses in reservoirs with elastic properties different from the surrounding rock. *International Journal of Geomechanics* 7, 353–361. doi:10.1061/(ASCE)1532-3641(2007)7:5(353).

- Walsh, J.B., 2002. Subsidence above a planar reservoir. *Journal of Geophysical Research* 107, 2202. doi:10.1029/2001JB000606.
- Zhou, K., Hoh, H.J., Wang, X., Keer, L.M., Pang, J.H., Song, B., Wang, Q.J., 2013. A review of recent works on inclusions. *Mechanics of Materials* 60, 144–158. doi:10.1016/j.mechmat.2013.01.005.
- Zhou, K., Keer, L.M., Jane Wang, Q., Ai, X., Sawamiphakdi, K., Glaws, P., Paire, M., Che, F., 2012. Interaction of multiple inhomogeneous inclusions beneath a surface. *Computer Methods in Applied Mechanics and Engineering* 217-220, 25–33. doi:10.1016/j.cma.2012.01.006.
- Zou, W., He, Q., Huang, M., Zheng, Q., 2010. Eshelby’s problem of non-elliptical inclusions. *Journal of the Mechanics and Physics of Solids* 58, 346–372. doi:10.1016/j.jmps.2009.11.008.

Chapter 5

Drainage of Poroelastic Fractures and Its Implications on the Performance of Naturally Fractured Reservoirs ¹

Large volumes of natural gas and oil are stored in low-permeability fractured reservoirs around the world. Extensive field and lab measurements have revealed presence of natural fracture in different scales and their fractal distributions. The log normal distribution of fractures length and width and their consistency throughout the formation is well documented for different basins in the literature; but the mechanical implications and the potential roles of these distributions on the fluid flow behavior in the rock is not yet studied. This paper provides poroelastic analysis for a single micro-fracture subject to fluid withdrawal (production) through the fracture. Formation is assumed to be a low permeable poroelastic medium. The main drive behind studying this problem was the fact that core flooding measurements in laboratory studies indicate that permeability of tight formations rock samples is in the order of nanodarcy, however the rate of production from the stimulated and even non-stimulated wells are leading us to average values for shale permeability, which are orders of magnitudes higher than the permeability measured in the lab. In this paper, we are trying to verify the role of natural fractures and their poroelastic properties to explain discrepancy in the measured permeability using different methods. To achieve this goal, we provide an

¹Bedayat, H., & Dahi Taleghani, A., 2012. Drainage of Poroelastic Fractures and Its Implications on the Performance of Naturally Fractured Reservoirs. In 46th US Rock Mechanics/Geomechanics Symposium. Chicago, IL, USA. ARMA-2012-562.

analytical solution for fracture volume changes due to fluid withdrawal (production). The roles of differential in-situ stress and formation pressure in determining the crack volume changes were found to be significant. The results could be used to relate the significant reduction in production from some of the shale gas wells to the closure of microfractures or even larger non-propped fractures. In general having the knowledge of mechanical and hydraulic behavior of natural micro-fractures in low permeability reservoirs could be a key to predict the production decline in these formations and provide insight to more sophisticated stimulation techniques in future.

5.1 Introduction

The scarce amount of conventional hydrocarbon reservoirs and the increase of fuel consumption all over the world have made production from unconventional hydrocarbon resources inevitable. Large volumes of natural gas and oil are stored in low-permeability fractured reservoirs around the world. Tight gas sandstones are part of what is known as unconventional gas, which also includes coal bed methane, shale gas and natural gas hydrates. Based on the U.S. Gas Policy Act of 1978, if the in-situ gas permeability of a reservoir is equal to or less than 0.1 md, it is designated as a tight gas formation (Kazemi, 1982). Independent of this definition, natural fractures are extremely important to unconventional gas reservoirs (Aguilera, 2008), because without fractures, it is not possible to recover hydrocarbons from these reservoirs.

Because of the low permeability of these formations and the low conductivity of the natural fracture networks, stimulation techniques such as hydraulic fracturing are necessary to make economic production possible. The low conductivity of the natural fracture system could be caused by occluding cements that precipitated during the diagenesis process (Laubach, 2003; Gale et al., 2007; Dahi Taleghani, 2011). For instance, almost all the cores recovered from the Forth Worth basin in the Barnett Shale contain cemented natural

fractures (Gale et al., 2007). In the Delaware basin, few partially cemented fractures are identified in the cores, and the rest of the fractures are sealed by cements (Ali, 2009).

The fact that natural fractures might be sealed by cements does not mean that they can be ignored while designing well completion processes. Cemented natural fractures can still act as weak paths for fracture growth (Dahi Taleghani and Olson, 2011). One common observation during hydraulic fracturing in naturally fractured reservoirs is a high leakoff rate during the treatment. In some cases, fluid leakoff in these reservoirs are reported to be as high as fifty times larger than the fluid leakoff in non-fractured reservoirs. This issue becomes more interesting with the knowledge that in non-fractured reservoirs, the leakoff rate depends on formation permeability, net treatment pressure and fracture fluid parameters (Valkó and Economides, 1995); however field observation during hydraulic fracturing in fractured reservoirs shows that, surprisingly, leakoff in these reservoirs primarily depends on net treatment pressure and fracture fluid parameters but not formation permeability (Britt et al., 1994; Barree, 1998). All these observations confirms the opening of natural fractures during hydraulic fracturing treatments.

Fractures are discrete discontinuity in a rock mass that developed as a response to stress, i.e., brittle failure. They are a universal element in sedimentary rocks. Furthermore, except some extremely ductile rocks such as salt or certain shale, all rocks in all depths can be considered as fractured media. In fractured rocks, fractures are responsible for the main part of the permeability and they affect the overall mechanical behavior of the rock mass (Britt et al., 1994; Gillespie et al., 1993). Fractures exist on a wide range of scales from microns to hundreds of kilometers, and it is known that throughout this scale range they have a significant effect on processes in the Earth's crust including fluid flow and rock strength. Early work was spread though a wide range of scales from core through outcrop to aerial photographs and satellite image scales. More recently, the manner in which fracture system properties at different scales relate to each other, i.e., their scaling attributes, has received increasing attention motivated by the promise of statistical prediction that scaling laws offer

(Bonnet et al., 2001). Furthermore, several independent field studies revealed (Marrett et al., 1999) extension fractures exhibit simple power-law scaling across 3.4-4.9 orders of magnitude, regardless of rock type or movement mode. The data show no evidence of natural gaps or scaling changes. Each data set consists of independent measurements made at different observational scales; a power-law regression to the subset of smaller fractures in each case provides an extrapolation that accurately predicts associated larger fractures. Consequently, data representing a limited range of fracture sizes may be used to characterize a much broader spectrum of fracture sizes.

Log normal distribution of microfractures provides some insights into our problem; for instance although aperture of microfractures is too small that no proppants can be placed inside these fractures (less than couple of millimeters), but due to their presence in large numbers, they can increase wellbore/reservoir contact area for manifolds (see Fig. 5.1). As mentioned earlier, since these microfractures are not propped, they will be open if fluid pressure inside the fracture and the surrounding rock stresses allow them to stay open. In other words, the total length of the microfractures or contact area between the well and the reservoir is a function of net pressure, and this function based on fractures attributes and reservoir properties could be different . Transport properties of the cracked rocks depend

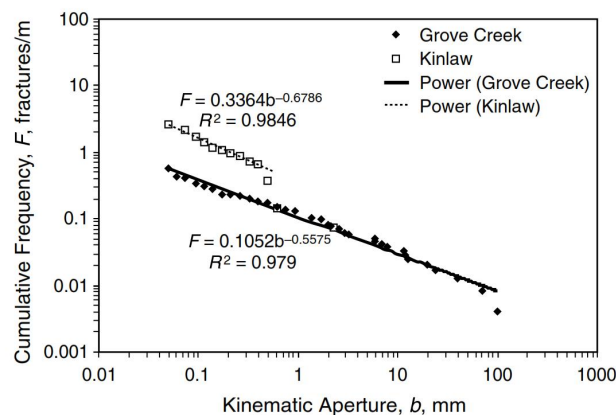


Figure 5.1: Aperture size distribution in Groove Creek and Kinlaw formations follow power-law relations. Micro-fractures occur much more frequently than large size fractures (Gale, 2002).

on fractures attributes, including aperture, which is usually assumed to be a function of confining pressure and pore-fluid pressure only, although counter arguments exist in the literature (Laubach et al., 2004). Based on this assumption, fractures will be closed when pore pressure is less than the confining pressure. In reality, although fluid pressure in the hydrocarbon reservoirs is usually less than the minimum horizontal stress, fractures are still open. Some authors explained this effect by fracture surfaces asperity (Gangi and Carlson, 1996); however we know that natural fracture's profile is not so rough that their asperity makes considerable opening for permeability. Increasing the elastic modulus of rock caused by diagenesis can cause residual opening for fractures. To implement this scenario, we apply variable elastic properties through time and then by using superposition model, we predict residual crack opening. Following this argument, in our fluid flow calculations in this paper, we always assumed that fractures are initially open, but their width depending on reservoir pressure and insitu stresses is subject to change.

By putting the above-mentioned facts together, ignoring the role of microfractures and their pressure sensitivity could lead to quite different predictions for fluid flow behavior. Fluid flow in naturally fractured reservoirs is typically simulated with dual-porosity or dual-permeability models (Gilman and Kazemi, 1988). These techniques are very useful in understanding the physics of matrix-fracture fluid interaction. However they often represent an unrealistic assumption about fracture pattern geometry, where the reservoir is idealized as a stack of sugar-cubes. An alternative to this approach is to discretely represent the fractures as high permeability cells in a fine-girded finite difference model (such as the commercial reservoir simulator Eclipse-100). Philip et al. (2005), used discrete fracture networks analysis to show that equivalent permeability strongly depends on fracture intensity as measured by cumulative length, average fracture length and fracture connectivity. Though, both of these methods are incapable of considering pressure-dependent fracture length changes and fracture openings.

Besides the above-discussed field observations, core measurements in laboratory indicate that permeability of rock samples recovered from NFRs (for example shale reservoirs) is in the order of nanodarcy, however the rate of production from the stimulated and even non-stimulated wells are leading us to average values of much higher probabilities. Some researchers have tried to relate this phenomenon to the presence of micro-scale natural fractures in the formation David and Ravalec-Dupin (2007). Hence in this paper, we try to verify the role of natural fractures and their poroelastic properties on production. Some recovered cores from the hydraulic fractures have confirmed the presence of large number of small size natural fractures on the surface of induced hydraulic fractures. However they are too small to contain proppants, but they can increase reservoir/fracture contact surface tremendously. On the other hand since these fractures are not propped, their opening and consequently their permeability will be a function of pressure and poroelastic properties of the rock. In this paper, we provide analytical solution for fracture volume changes due to fluid withdrawal (production) and similarly fluid injection. Producing and injecting fluids change pore pressure and rock stresses. The fluid flow induced stresses causes deformations in the rock that changes fracture apertures (Heffer et al., 1995). Thus change in the hydraulic conductivity of fractures and consequently overall permeability could directly affect production (Koutsabeloulis et al., 1994; Heffer et al., 1995). Therefore, having knowledge of mechanical as well as hydraulic behavior of natural microfractures in low permeability reservoirs is a key for understanding and predicting the reservoir behavior during production.

As the first step to tackle this problem, we try to demonstrate the behavior of a single microfractures to pressure and stress changes in the formation due to the production. This work provides poroelastic analysis of a stationary micro-fracture due to fluid production through the fracture. Atkinson and Craster (1991); Craster and Atkinson (1994) solved this problem analytically for a semi-infinite growing hydraulic fracture using Wiener-Hopf and integral transform method. However, these methods are not applicable for finite size stationary fractures, and their asymptotic solution could not predict fracture behavior between

long-term and short-term. Almost at the same time, Detournay and Cheng (1991) tried to solve poroelasticity equations to calculate leak-off volume in a stationary finite-size hydraulic fracture.

5.2 Statement of the Problem & Assumptions

In this paper, we are trying to investigate the poroelastic behavior of a single microfracture. Rather than considering a population of microfractures, we start with poroelastic analysis for a single fracture with the length of $2L$ in an infinite homogeneous and isotropic poroelastic medium and show how fracture length and its depth or more precisely the magnitude of in-situ stress normal to the fracture plane may affect fracture volume (see Fig. 5.2). Hence, fracture is assumed to keep its constant length, fracture volume changes imply fracture width, i.e., permeability changes. The formation rock is assumed to be fully saturated with a Newtonian fluid with viscosity, μ . The mechanical behavior of the rock is assumed to be linear elastic, so we can limit our analysis to linear fracture mechanics (Detournay and Cheng, 1991). The fracture is assumed to be drained into a connected borehole or through a network of fractures. Thus, the initial fracture pressure is presumed to be equal to the formation pressure, i.e. $p_f = p_r = p_0$. Since, the borehole fluid has lower pressure than formation fluid and fracture has higher permeability than the formation matrix, formation fluid begins to flow into the borehole. Due to production, we expect instantaneous fluid pressure drop inside the fracture. Thus the fractures pore pressure at time $t = t^{0+}$ is equal to $p_b h$ and it will remain constant for a long time, $t > 0$. To avoid further complications, we assume that fracture remains in the plane, so we can use plain strain condition for stress analysis. Figure 3 demonstrates the schematic view of the problem.

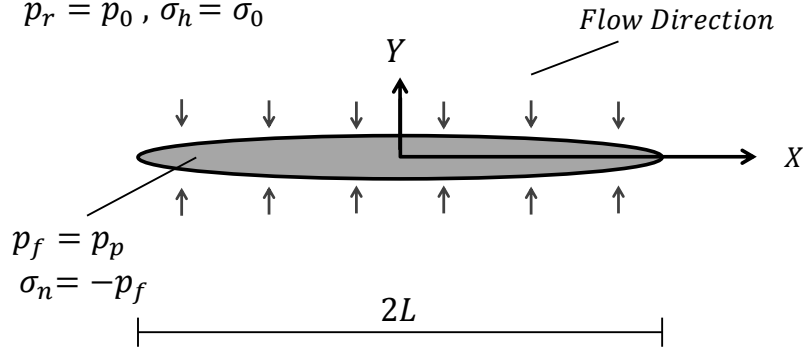


Figure 5.2: The schematic picture for a single crack in an infinite poroelastic medium.

5.3 Governing Equations

The governing equations for drainage from the single fracture are poroelasticity equations, which can be categorized into four different groups: force equilibrium equations, Darcy's law, mass balance and Biot's constitutive equations (Biot, 1941)

- Force equilibrium equations

$$\sigma_{ij,j} = 0. \quad (5.1)$$

- Darcy's law, which describes the fluid transport in the rock. By neglecting the gravity effect, Darcy's law can be written as

$$q_i = -\frac{k_{ij}}{\mu} \frac{\partial p}{\partial x_j} = -\kappa p_{,i}, \quad (5.2)$$

where κ is mobility ratio.

- Continuity equation or mass balance for the fluid phase

$$\frac{\partial \zeta}{\partial t} + q_{i,i} = 0, \quad (5.3)$$

where ζ is incremental fluid content and it is defined as

$$\zeta = \frac{\partial m_f}{\rho_{f0}}. \quad (5.4)$$

- Biot's poroelastic constitutive equations, which describe the constitutive equations for a fluid-filled porous media. It assumes linear and reversible relationship between stresses (σ_{ij}, p) on one side and kinematics i.e. strains and fluid content $(\varepsilon_{ij}, \zeta)$ on the other side,

$$2G\varepsilon_{ij} = \sigma_{ij} - \nu\sigma_{kk}\delta_{ij} + \alpha(1 - 2\nu)p\delta_{ij}, \quad (5.5)$$

$$2G\zeta = \alpha(1 - 2\nu)\sigma_{kk} + \frac{\alpha^2(1 - 2\nu)^2}{\nu_u - \nu}p, \quad (5.6)$$

where δ_{ij} is the Kronecker delta ($\delta_{ij} = 1$ for $i = j$, and $\delta_{ij} = 0$ for $i \neq j$) and index notation convention has been used; so i and j indices take values 1 and 2.

Our approach for solving this problem is essentially inspired by modal decomposition and superposition method previously developed and used to solve several poroelasticity problems like sudden pressurization of a borehole. Detournay and Cheng (1991) solved the stress and pressure distribution for a stationary hydraulic fracture using this method too. In hydraulic fracturing, fluid is injected into the fracture to induce further tensile stresses and consequently cracking the formation rock. Injection increases fluid pressure inside the fracture as well as pore pressure in the fracture vicinity. Pressure difference between inside and outside of the crack, pushes fluid to move from the fracture into the formation ($p_f - p_r > 0$). However, the situation for producing fluids from the fracture is almost vice versa. Fluid moves from the formation rock with higher pore pressure to fractures with lower pressure ($p_f - p_r < 0$). The same governing equations still applies to this problem but with different boundary conditions and initial conditions due to the change of the fluid flow direction. We assume the stress intensity factor at the tip of the receding fracture is equal to zero.

Following discussions in the previous section, we assume that at the initial time ($t = 0$), fractures are open. Pre-existing fractures might be open due to existence of driving pore pressure larger than minimum effective horizontal stress, thermal stress, residual in-situ stress or the effect of a near major fault (Engelder and Lacazette, 1990; Olson et al., 2009; Gale et al., 2010). At the initial time, the condition is undrained and fracture volume in undrained condition can be calculated using linear elastic fracture mechanics solution Sneddon (1946). For a unit uniform stress applied on the fracture wall, the initial fracture opening is given by

$$D_n(x) = -\frac{2(1 - \nu_u)}{G}\sqrt{L^2 - x^2} \quad (5.7)$$

and initial fracture volume may also be derived by integration of Eq. (5.7).

Multiplying the magnitude of the net fluid pressure inside the fracture by the initial fracture volume for unit pressure gives the volume of the fracture for a given reservoir pressure, i.e.

$$V_f^{initial} = \frac{\pi L^2(1 - \nu_u)}{G}p_d, \quad (5.8)$$

where, p_d is the net pressure, and it is defined as the difference between fluid pressure inside the fracture and in-situ minimum stress.

5.3.1 Mode decomposition

The normal traction and pore pressure along the fracture surface is equal to the fluid pressure inside the fracture ($\sigma_n = -p_f, p_p = p_f$). Therefore, the response of the crack can be decomposed into two fundamental problems: (1) a step change in stress while maintaining constant pore pressure, (2) a step change in pore pressure while maintaining constant stress. The fracture response in general condition is the linear combination of each of these modes. In the calculations of the fundamental solutions, it has been assumed that the pore pressure

inside the fracture drops immediately and it will not change by time. However for the problems with time varying pressure, Duhamels theorem can be simply utilized generate solution for arbitrary pressure changes in time.

The boundary conditions for two fundamental loading modes are provided below:

- Mode *I*

$$\begin{aligned}\sigma_n(x, t) &= -1 \\ p(x, t) &= 0\end{aligned}\tag{5.9}$$

- Mode *II*

$$\begin{aligned}\sigma_n(x, t) &= 0 \\ p(x, t) &= -1\end{aligned}\tag{5.10}$$

Let F_1 and F_2 be the fundamental solutions for mode *I* and mode *II*, respectively. In the presence of compressive in-situ stresses (σ_0), and reservoir initial pore pressure ($p_r = p_0$), the solution for fracture volume or fracture width may be given as

$$F_p = (p_f - \sigma_0)F_1 + (p_f - p_0)F_2.\tag{5.11}$$

The reader may notice that to simplify the problem, mode *I* and mode *II* are representing the unit excess fluid pressure inside the fracture. However the fluid pressure inside the fracture is less than fluid pressure inside the medium. Hence, $p_p - p_f$ would be less than zero for a fluid producing fracture. We always assumed that the formation pore pressure is greater than or equal to the wellbore/fracture pressure. This difference in pressure causes the fluid to migrate from the reservoir to the micro-fracture. Note micro-fractures are assumed to have hydraulic connectivity with the wellbore, directly or by means of other fractures.

5.3.2 Fundamental solutions

Initial response for mode I loading is mainly due to the instantaneous change of fracture traction, so the solution is similar to elasticity solution except the Poissons ratio which is undrained, i.e.

$$V_c^1(t = 0^+) = \frac{\pi L^2(1 - \nu_u)}{G}. \quad (5.12)$$

This increase in volume causes generation of pore pressure near the fracture wall. Hence, liquid flows to the fracture after generation of excessive pore pressure. The amount of liquid exchange volume may be calculated by integrating one dimensional flow flux perpendicular to fracture length over the time, multiplying by circumference of fracture and the amount of generated pore pressure. One dimensional flow perpendicular to fracture opening is a valid assumption for a short time after pressure generation in the vicinity of the fracture. Therefore the amount of liquid exchange volume for mode I is

$$V_{ex}^1(t) = -\frac{8\alpha L^2(1 - 2\nu)(1 - \nu_u)}{G\sqrt{\pi}(1 - \nu)}\sqrt{\frac{ct}{L^2}} \quad for \quad \frac{ct}{L^2} \ll 1, \quad (5.13)$$

where c is the diffusivity coefficient given by

$$c = \frac{2\kappa G(1 - \nu)(\nu_u - \nu)}{\alpha^2(1 - 2\nu)^2(1 - \nu_u)}. \quad (5.14)$$

The amount of fluid which flows inside the fracture plus its initial volume is equal to total fracture volume change. Therefore, the short-term response will be mainly driven by summation of instantaneous volume change and product of the amount of instantaneous generated pore pressure field by volume change due to existence of unit pure pore pressure inside the fracture.

$$V_c^1(t) = \frac{\pi L^2(1 - \nu_u)}{G} + \left(\frac{16L^2\nu_u - \nu)(1 - \nu_u)}{G\sqrt{\pi}(1 - \nu)}\sqrt{\frac{ct}{L^2}} \quad for \quad \frac{ct}{L^2} \ll 1. \quad (5.15)$$

As time evolves to infinity, the fracture volume reaches to the elasticity solution

$$V_c^1(\infty) = \frac{\pi L^2(1 - \nu)}{G}, \quad (5.16)$$

which is exactly same as Eq. (5.13), unless the undrained Poisson's ratio is substituted with the drained Poisson's ratio.

Also as time goes to infinity, fluid exchange volume for mode *I* reaches to

$$V_{ex}^1(\infty) = -\frac{\alpha\pi L^2(1 - 2\nu)}{2G}. \quad (5.17)$$

For mode *II*, using the principal of virtual work (Cleary, 1977), and calculated fluid exchange volume for mode *I* (which is equal to fracture volume change in mode *II*), the volume of the fracture right after application of mode *II* loading is given by

$$V_c^2(t) = -\frac{8\alpha L^2(1 - 2\nu)(1 - \nu_u)}{G\sqrt{\pi}(1 - \nu)}\sqrt{\frac{ct}{L^2}} \quad for \quad \frac{ct}{L^2} \ll 1, \quad (5.18)$$

which at times equal to infinity reaches to

$$V_c^2(\infty) = -\frac{\alpha\pi L^2(1 - 2\nu)}{2G}. \quad (5.19)$$

For a short time and unit excess pore pressure, similar to Eq. (5.14), fluid exchange volume is equal to integral of one dimensional flow flux perpendicular to fracture opening over the time multiplied by fracture circumference. Thus, fluid exchange for mode *II* will be

$$V_c^2(t) = \frac{8\kappa L^2}{c\sqrt{\pi}}\sqrt{\frac{ct}{L^2}} \quad for \quad \frac{ct}{L^2} \ll 1. \quad (5.20)$$

As times evolves to infinity, the fluid exchange volume may be estimated with leak off volume from a circular hole with the same circumference, with unit rise constant pressure loading

on its diameter (Carslaw and Jaeger, 1959)

$$V_{ex}^2(t) = \frac{8\kappa}{\pi} \int_{\varepsilon}^{\infty} \frac{1 - e^{-cu^2t}}{cu^3[J_0^2(\frac{2L}{\pi}u) + Y_0^2(\frac{2L}{\pi}u)]} du \quad \text{for} \quad \frac{ct}{L^2} \gg 1, \quad (5.21)$$

where J_0 and Y_0 are zero order Bessel functions of first and second kinds, respectively. Finally, using the superposition principle and substituting Eqs. (5.15) to (5.19) in Eq. (5.11), the final volume change of the fracture under the both modes loading is given by

$$V_c(t) = (p_p - \sigma_0)V_c^1(t) + (p_p - p_0)V_c^2(t). \quad (5.22)$$

The transitional response of the fracture between these two asymptotic conditions ($t = 0, t = \infty$), should be calculated numerically with boundary element methods or finite element methods (Vandamme et al., 1989; Ghassemi and Zhang, 2006). The volume of the fracture at any time is equal to sum of initial volume and change of the volume.

5.4 Results and Discussions

Through some examples, we investigate micro-fractures volume changes versus time due to formation pressure changes. Using Eq. (5.22) long-term and short-term solutions for fracture volume changes are calculated and for the transition between mentioned asymptotic conditions, exponential regression has been used which agrees with approximate displacement discontinuity solutions used in other references (Detournay and Cheng, 1991; Vandamme et al., 1989).

Fractures are assumed to be open during production. The term $(p_p - \sigma_0)$ might be positive or negative depending on the magnitude of in-situ stresses. Thus, the resultant changes in the fracture volume caused by mode I might be positive or negative. Therefore, one might expect that in different tectonic regimes and wellbore pressure condition, effective stresses may increase or decrease the total fracture volume i.e. overall permeability.

According to Eqs. (5.18) and (5.19), fracture volume in mode two (V_c^2) is a negative value. Moreover, the term $(p_p - p_0)$ is always negative means fluid migration from reservoir to the wellbore. As a result the resultant change in the fracture volume generated by mode II is always positive. As a consequence, the impact of pure fluid drainage loading (production) is the expansion of the fracture volume. Therefore, mode I and mode II compete against each other and may generally decrease or increase the fracture volume. This value should be added to initial fracture volume, Eq. (5.8), to calculate the final fracture volume. Since, the total volume of the fracture can never be a negative value, in the case of negative value for the fracture volume, the fracture should be considered already closed ($V_f = 0$) with no contribution to production.

In low pressure (depleted) reservoir conditions or reservoirs with high horizontal stress, which $p_p < \sigma_0$, decrease in fracture volume caused by mode I , may counterbalance the increase of volume generated by mode II .

5.4.1 Numerical results

Table 5.1: Different example descriptions for numerical analysis

Example description		$s = p_f/p_0$	$r = \sigma_0/p_0$
Ex 1	Reservoirs with low confining stress	0.5	0.8, 1.0, 1.2
Ex 2	Reservoirs with large confining stress	0.5	1.5, 2.0
Ex 3	Bottomhole pressure effect	0.5, 0.8	1.2
Ex 4	Post Hydraulic fracturing treatment	1.2	0.8, 1.0, 1.2

To confirm the findings in the previous section, we try to demonstrate the importance of the reservoir pressure, tectonic environments, wellbore pressure, and rock elastic properties on fracture volume through some numerical examples with realistic parameter values (see Table 5.1 for example descriptions). To follow with dimensionless variables in presenting results, change in the fracture volume is normalized by dividing the fracture volume change

to the instant volume change of fracture. This normalized value is a good indicator to show the change in the volume of the fracture versus time. This normalized value is plotted versus dimensionless time which is given by

$$t^* = \frac{ct}{L^2}. \quad (5.23)$$

t^* is essentially the poroelastic diffusion time-scale. Time in this problem is a multi-scale problem, in general. These time scales are (1) fracture closure time, (2) diffusion time for fluid to reach fracture, which is a function of rock permeability, and (3) poroelastic diffusivity time, which is the amount of time required for pore-pressure to interact with stress changes. So here, we limit our analyses to the third time-scale.

In Eq. (5.23), $t^* = 100$ could be a representative of the long term behaviour. The actual time may be calculated by inserting the proper value of L and c into Eq. (5.24)

$$t = \frac{100L^2}{c}. \quad (5.24)$$

Thus for different diffusivity coefficient, c , and different fracture length, L , results in different time-scale periods for the problem.

- Reservoirs with low confining stress

Now let's consider a reservoir with low fluid pressure gradient. The input geomechanical parameters are shown in Table 5.2.

Table 5.2: Input parameters			
Permeability	k	1×10^{-9}	darcy
Shear Modulus	G	5.00	GPa
Undrained Poisson's Ratio	ν_u	0.20	
Poisson's Ratio	ν	0.33	
Biot's Coefficient	α	0.78	
Fluid Viscosity	μ	1.00	cpoise
Diffusivity Coefficient	c	7×10^{-9}	m^2/s

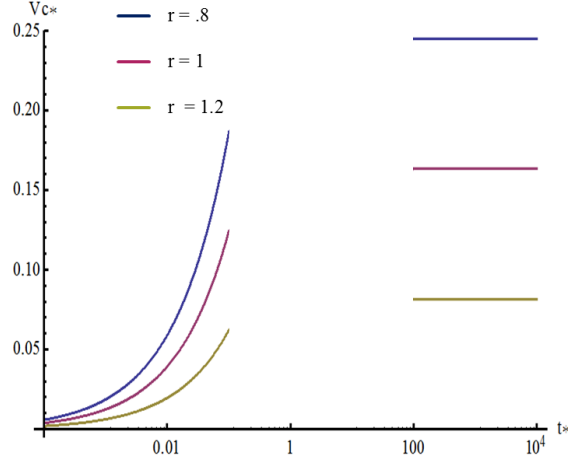


Figure 5.3: Volume changes of a single fracture due to production in a low confining stress versus dimensionless time.

The bottomhole pressure is assumed to be equal to half of the reservoir pressure and confining stress varies from the fracture volume change is calculated for possible ranges, i.e. Figure 5.3 shows how fracture volume changes in reservoirs with low confining stresses (for instance shallow reservoirs). The combination of mode *I* and mode *II* leads to overall increase in fracture volume. In reservoirs with low confining stress, right after pressure reduction in the fractures (when fracture pressure is equal to wellbore pressure), fracture volume decreases. However as time evolves fracture volume increases with time.

- Reservoirs with large confining stress

Now, we calculate the volume change trend for reservoirs with large confining stress which results in different fracture behavior. This case resembles reservoirs located in large depths. Figure 5.4 shows how fractures close in this type of reservoirs. Combination of mode *I* and mode *II* of loading leads to overall decrease in fracture volume in this type of reservoirs. In highly confined reservoirs, due to impact of mode *I*, the amount of decrease in fracture volume is more than reservoirs with low horizontal stress

- Bottomhole pressure effect

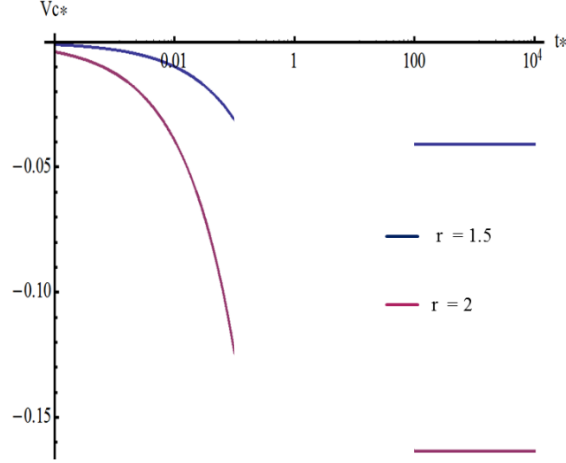


Figure 5.4: Volume changes of a fracture due to production under large confining stresses versus dimensionless time.

Combination of p_f , p_0 and σ_0 may lead to different outcome for changes in fractures volume. Figure 5.5 shows two reservoirs with different bottomhole pressure but with the same confining stresses ($r = 1.2$). Dimensionless volume, for large difference between wellbore pressure and reservoir pressure increases as time passes. However in the case of larger wellbore pressure, fracture volume is decreasing. In the latter case decrease in fracture volume caused by mode I offsets the increase of volume caused by mode II .

- Post Hydraulic fracturing treatment There is a potential application of these calculations to study the behavior of microfracture induced on hydraulic fractures walls due to induced tensile thermal stresses. For a period of time after termination of hydraulic fracturing treatments, fluid pressure is not still in equilibrium with the formation so fluid pressure inside the fracture is slightly higher than formation pressure, but it doesn't mean that formation fluid may not be released to the fracture (Gidley et al., 1990) This excessive pore pressure guarantee initial opening of these fractures. However as time evolves and fluid leaks off to the formation, we expect the fractures experience less volume. Nevertheless, Fig. 5.6 shows in reservoirs with low confining stress, fracture volume increases.

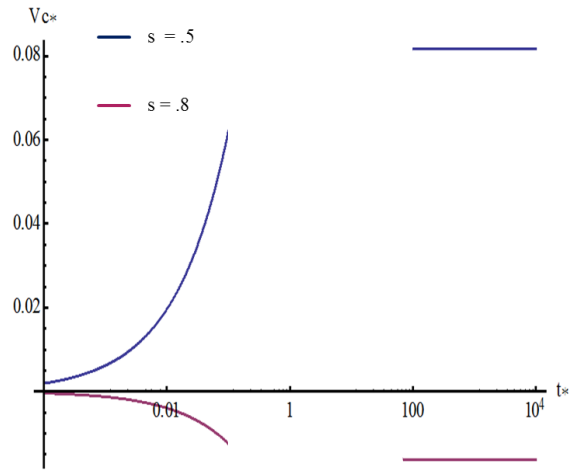


Figure 5.5: Volume changes of a fracture due to production under large confining stresses versus dimensionless time.

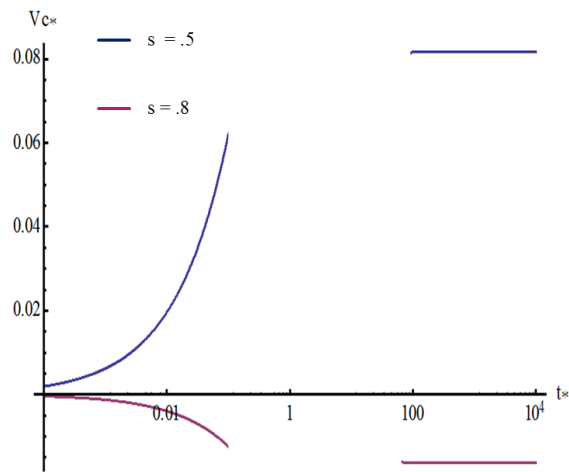


Figure 5.6: Volume changes of a fracture due to production under large confining stresses versus dimensionless time.

5.5 Conclusion

We presented poroelastic solution for the drainage of a single microfracture. Moreover we investigated the effects of formation pressure, rock mechanical properties, insitu stress and bottomhole pressure on the volume of the fractures. Since, fractures width changes affect their hydraulic conductivity and subsequently overall permeability of reservoirs, therefore production could be affected by the change of fractures volume.

It has been shown that the difference between bottomhole pressure and reservoir pressure results in the augmentation of the fracture volume. This increase may be counterbalanced by large horizontal stresses in the reservoir. In case of reservoirs with low confining stresses, fracture volume increases with time. However, in reservoirs with large confining stress, the fracture volume is decreasing. Additionally, we showed bottomhole pressure changes under certain condition could change reverse behavior of the poroelastic fractures in the reservoir.

The poroelastic response of the fractures is not the only factor which influences the reservoir productivity. Other aspects such as the presence of multiphase fluids should also be considered in further analyses in future. Here, we considered plane strain geometry for natural fractures. It might be more realistic to consider penny shaped fractures with axisymmetric geometry for this problem as well. The next step will be the investigation of the effect of numerous micro-fractures on the major macro-size fracture and its productivity.

5.6 References

- Aguilera, R., 2008. Role of natural fractures and slot porosity on tight gas sands, in: Proceedings of SPE Unconventional Reservoirs Conference, Society of Petroleum Engineers. pp. 10–12. doi:10.2118/114174-MS.
- Ali, W.A., 2009. Lithofacies, depositional environment, burial history and calculation of organic richness from the wireline logs: a study of Barnett Shale in the Delaware Basin, Pecos Co., West Texas, and comparison with the Barnett Shale in the Fort Worth Basin. Ph.D. thesis. University of Texas at Austin.

- Atkinson, C., Craster, R.V., 1991. Plane strain fracture in poroelastic media. *Proceedings of the Royal Society A: Mathematical, Physical and Engineering Sciences* 434, 605–633. doi:10.1098/rspa.1991.0116.
- Barree, R.D., 1998. Applications of pre-frac injection/falloff tests in fissured reservoirs - field examples, in: *Proceedings of SPE Rocky Mountain Regional/Low-Permeability Reservoirs Symposium*, Society of Petroleum Engineers. doi:10.2118/39932-MS.
- Biot, M.A., 1941. General theory of three-dimensional consolidation. *Journal of Applied Physics* 12, 155. doi:10.1063/1.1712886.
- Bonnet, E., Bour, O., Odling, N.E., Davy, P., Main, I., Cowie, P., Berkowitz, B., 2001. Scaling of fracture systems in geological media. *Reviews of Geophysics* 39, 347. doi:10.1029/1999RG000074.
- Britt, L.K., Hager, C.J., Thompson, J.W., 1994. Hydraulic fracturing in a naturally fractured reservoir, in: *Proceedings of International Petroleum Conference and Exhibition of Mexico*, Society of Petroleum Engineers. doi:10.2118/28717-MS.
- Carslaw, H.S., Jaeger, J.C., 1959. *Conduction of heat in solids*. Second edi ed., Oxford University Press, London.
- Cleary, M.P., 1977. Fundamental solutions for a fluid-saturated porous solid. *International Journal of Solids and Structures* 13, 785–806. doi:10.1016/0020-7683(77)90065-8.
- Craster, R.V., Atkinson, C., 1994. Crack problems in a poroelastic medium: an asymptotic approach. *Philosophical Transactions of the Royal Society A: Mathematical, Physical and Engineering Sciences* 346, 387–428. doi:10.1098/rsta.1994.0026.
- Dahi Taleghani, A., 2011. Modeling simultaneous growth of multi-branch hydraulic fractures, in: *45th US Rock Mechanics/Geomechanics Symposium*, San Francisco, CA.
- Dahi Taleghani, A., Olson, J.E., 2011. Numerical modeling of multistranded-hydraulic-fracture propagation: Accounting for the interaction between induced and natural fractures. *SPE Journal* , 575–581.
- David, C., Ravalec-Dupin, M.L., 2007. *Rock physics and geomechanics in the study of reservoirs and repositories*. Geological Society, London, Special Publications 284, 1–14.

- Detournay, E., Cheng, A.H.D., 1991. Plane strain analysis of a stationary hydraulic fracture in a poroelastic medium. *International Journal of Solids and Structures* 27, 1645–1662. doi:10.1016/0020-7683(91)90067-P.
- Engelder, T., Lacazette, A., 1990. Natural hydraulic fracturing, in: Barton, N., Stephansson, O. (Eds.), *International Symposium on Rock Joints*.
- Gale, J.F.W., 2002. Specifying lengths of horizontal wells in fractured reservoirs. *SPE Reservoir Evaluation & Engineering* 5. doi:10.2118/78600-PA.
- Gale, J.F.W., Lander, R.H., Reed, R.M., Laubach, S.E., 2010. Modeling fracture porosity evolution in dolostone. *Journal of Structural Geology* 32, 1201–1211. doi:10.1016/j.jsg.2009.04.018.
- Gale, J.F.W., Reed, R.M., Holder, J., 2007. Natural fractures in the Barnett Shale and their importance for hydraulic fracture treatments. *AAPG Bulletin* 91, 603–622. doi:10.1306/11010606061.
- Gangi, A.F., Carlson, R.L., 1996. An asperity-deformation model for effective pressure. *Tectonophysics* 256, 241–251. doi:10.1016/0040-1951(95)00167-0.
- Ghassemi, A., Zhang, Q., 2006. Poroelastostatic analysis of the response of a stationary crack using the displacement discontinuity method. *Journal of Engineering Mechanics* 132, 26–33. doi:10.1061/(ASCE)0733-9399(2006)132:1(26).
- Gidley, J.L., Holditch, S.A., Nierode, D.E., Jr., R.W.V. (Eds.), 1990. *Recent advances in hydraulic fracturing*. Society of Petroleum Engineers.
- Gillespie, P.A., Howard, C.B., Walsh, J.J., Watterson, J., 1993. Measurement and characterisation of spatial distributions of fractures. *Tectonophysics* 226, 113–141. doi:10.1016/0040-1951(93)90114-Y.
- Gilman, J., Kazemi, H., 1988. Improved calculations for viscous and gravity displacement in matrix blocks in dual-porosity simulators (includes associated papers 17851, 17921, 18017, 18018, 18939, 19038, 19361 and 20174). *Journal of Petroleum Technology* 40. doi:10.2118/16010-PA.

- Heffer, K.J., Last, N.C., Koutsabeloulis, N.C., Gutierrez, M., Makurat, A., 1995. Site-response models from high-resolution seismic reflection and refraction data recorded in Santa Cruz, California. *International Journal of Rock Mechanics and Mining Sciences & Geomechanics Abstracts* 32.
- Kazemi, H., 1982. Low-permeability gas sands. *Journal of Petroleum Technology* 34, 2229–2232. doi:10.2118/11330-PA.
- Koutsabeloulis, N.C., Heffer, K.J., Wong, S., 1994. Numerical geomechanics in reservoir engineering. *Computer Methods and Advances in Geomechanics* 92.
- Laubach, S.E., 2003. Practical approaches to identifying sealed and open fractures. *AAPG bulletin* 4, 561–579.
- Laubach, S.E., Olson, J.E., Gale, J.F.W., 2004. Are open fractures necessarily aligned with maximum horizontal stress? *Earth and Planetary Science Letters* 222, 191–195. doi:10.1016/j.epsl.2004.02.019.
- Marrett, R., Ortega, O.J., Kelsey, C.M., 1999. Extent of power-law scaling for natural fractures in rock. *Geology* 27, 799. doi:10.1130/0091-7613(1999)027<0799:EOPLSF>2.3.CO;2.
- Olson, J.E., Laubach, S.E., Lander, R.H., 2009. Natural fracture characterization in tight gas sandstones: Integrating mechanics and diagenesis. *AAPG Bulletin* 93, 1535–1549. doi:10.1306/08110909100.
- Philip, Z., Jennings, J., Olson, J.E., Laubach, S.E., Holder, J., 2005. Modeling coupled fracture-matrix fluid flow in geomechanically simulated fracture networks. *SPE Reservoir Evaluation & Engineering* 8. doi:10.2118/77340-PA.
- Sneddon, I.N., 1946. The distribution of stress in the neighbourhood of a crack in an elastic solid. *Proceedings of the Royal Society A: Mathematical, Physical and Engineering Sciences* 187, 229–260. doi:10.1098/rspa.1946.0077.
- Valkó, P., Economides, M.J., 1995. *Hydraulic fracture mechanics*. UK: Wiley.

Vandamme, L., Detournay, E., Cheng, A.H.D., 1989. A two-dimensional poroelastic displacement discontinuity method for hydraulic fracture simulation. *International Journal for Numerical and Analytical Methods in Geomechanics* 13, 215–224. doi:10.1002/nag.1610130209.

Chapter 6

Pressurized Poroelastic Inclusions: Short-term and Long-term Asymptotic Solutions

This paper provides a semi-analytical asymptotic short-term and long-term solutions for the volume change and the corresponding leak-off volume for a fluid saturated three-dimensional poroelastic inclusion considering fluid exchange with the surrounding poroelastic medium. Considering possibly different material properties and different fluid pressure of hydrocarbon bearing formations or proppant filled fractures in comparison to those of the surrounding geological structures, fractures or the whole reservoirs can be considered as inclusions. The approach used for solving this problem is inspired by the theory of inclusions and modal decomposition technique previously developed and used to solve several poroelasticity problems. Previous studies on the topic have not incorporated the hydraulic communication between the inclusion and the surrounding medium; therefore, fluid pressure changes in the surrounding rock due fluid pressure changes in the inclusion was ignored. An example of this problem would be a pressurized stationary fracture, which depending on pressure might have fluid exchange with the surroundings. Some numerical examples considering inclusions with different aspect ratios and material properties are provided to better describe the significance of fluid exchange.

6.1 Introduction

This paper provides a semi-analytical asymptotic short-term and long-term solutions for the volume change and the corresponding leak-off volume for a fluid saturated three-dimensional poroelastic inclusion considering fluid exchange with the surrounding poroelastic medium (see Fig. 6.1).

Inclusions are defined as finite sub-volumes of the medium, which may possess a different strain status from that of the surrounding environment. If the inclusion has different material properties, it is considered to be an inhomogeneous inclusion. Considering possibly different material properties and different fluid pressure of hydrocarbon bearing formations or proppant filled fractures in comparison to those of the surrounding geological structures, fractures or the whole reservoirs can be considered as inclusions. For example Rudnicki (2002a,b); Chen (2011); Soltanzadeh and Hawkes (2012); Bedayat and Dahi Taleghani (2014) modeled stress alterations in the poroelastic inclusions due to pore fluid pressure changes using the theory of the inclusions. All these studies assumed that there is no hydraulic communication between the inclusion and the surrounding medium. Therefore, the fluid pressure in the surrounding rock will not change due to fluid pressure changes in the inclusion and there is no fluid exchange with the matrix. However, these assumptions are reasonable for modeling situations like rock compaction-drive and gas expansion-drive hydrocarbon reservoirs, as well as for geological carbon sequestration. The lack of hydraulic communication could be the result of a cap rock or an impermeable fault. For example, high permeability sandstone formations could be contained by extremely less permeable shale layers.

Here, we solved for the volume change of an ellipsoidal poroelastic inclusion and its corresponding leak-off volume, assuming hydraulic communication between the inclusion and the matrix. An example of this problem would be a pressurized stationary fracture, which depending on pressure might have fluid exchange with the surroundings. It is notable that, pressurized elliptical fractures can be considered as a special case of ellipsoidal inclusions

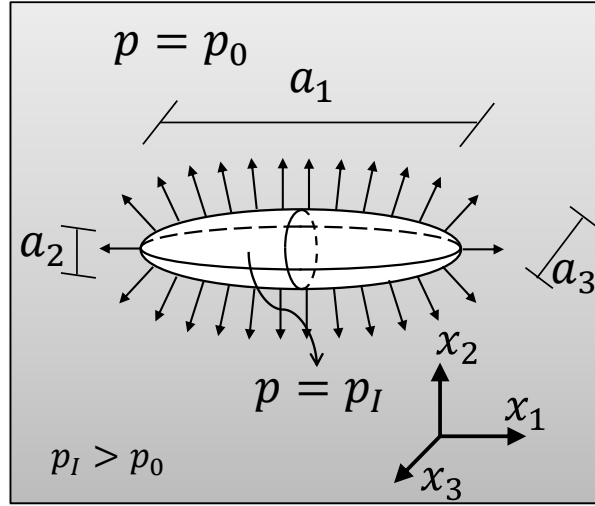


Figure 6.1: An ellipsoidal poroelastic inclusion with principal axes (a_1, a_2, a_3) along major Cartesian coordinate system axis. The fluid pore pressure inside the inclusion and the matrix are p_I and p_0 , respectively ($p_I > p_0$).

where one of the principal axes of the ellipsoid becomes infinitely small (Mura, 1987). Detournay and Cheng (1991) have solved the asymptotic response of the similar problem for a stationary plane strain fracture embedded in an infinite poroelastic medium. They used the modal decomposition concept and used the solution of the internally-loaded Griffith fracture (which assumes elliptic profile for the fracture) to address the problem.

Let's assume a poroelastic inclusion embedded in a poroelastic medium. Initially, at time $t = 0$, the fluid pressure inside the inclusion and the surrounding medium (hereafter, matrix) are assumed to be p_0 . However, for $t > 0$ the fluid pressure inside the inclusion increases to p_I and is kept constant. Here we provide an asymptotic solution based on the following assumptions :

- (1) The matrix is homogenous, isotropic and behaves according to linear poroelasticity theory (Biot, 1941) and poroelastic constitutive equations (Rice and Cleary, 1976);
- (2) Both fluid in the inclusion and the matrix behave as Newtonian fluids and have the same rheological properties;

(3) The matrix is subjected to uniform far-field stresses $\sigma_x = \sigma_y = \sigma_z = \sigma_0$;

The outline of this paper is as follows: Section 6.2 describes the approach used for solving this problem. In Section 6.2.1 we review the governing equations used to solve the asymptotic volume change of the poroelastic inhomogeneity, and in Section 6.2.3 we describe the Eshelby solution for poroelastic inclusions. Then in Section 6.3, we describe our approach to solve the volume change of the inclusion for short term and long term responses. Finally, Some numerical examples considering inclusions with different aspect ratios and material properties are provided to better describe the significance of fluid exchange toward the end of the paper.

6.2 Solution Methods

6.2.1 General approach

The approach used for solving this problem is inspired by modal decomposition and superposition method previously developed and used to solve several poroelasticity problems such as sudden pressurization of a borehole (Detournay and Cheng, 1988) and plain strain stationary fracture (Detournay and Cheng, 1991). Considering that the normal traction and pore pressure along the inclusion surface is equal to the fluid pressure inside the inclusion ($\sigma_n = -p_I, p = p_I$), the response of the inclusion can be decomposed into two fundamental problems: (1) a step change in stress while there is no pore pressure change inside the inclusion ($\sigma_n = -1_{(0,\infty]}, p = 0$); (2) a step change in pore pressure while there is no stress change inside the inclusion ($\sigma_n = 0, p = 1_{(0,\infty]}$). Therefore, the inclusion response in the general condition can be considered as a linear combination of each of these modes. Here, we assume that there is no initial pore pressure difference between the inclusion and the surrounding matrix, and pore pressure inside the inclusion increases immediately to p_I and it will not change by time. However, in cases when pressure varies with time, Duhamel's theorem can be applied (see Section 6.7). Thus, the boundary conditions for the two fundamental loading

modes are

$$\text{Mode (1)} = \begin{cases} \sigma_n(x, t) = -1 \\ p(x, t) = 0, \end{cases} \quad (6.1)$$

and

$$\text{Mode (2)} = \begin{cases} \sigma_n(x, t) = 0 \\ p(x, t) = 1, \end{cases} \quad (6.2)$$

Let $\Delta V_I^{(1)}$ and $\Delta V_I^{(2)}$ be the volume change of the inclusion for mode (1) and mode (2), respectively. Therefore, in the presence of compressive in-situ stresses (σ_0), and the matrix initial pore pressure (p_0), the solution for change in the inclusion volume may be given as

$$\Delta V_I(p_I) = p_I \Delta V_I^{(1)} + (p_I - p_0) \Delta V_I^{(2)}. \quad (6.3)$$

The asymptotic values of $\Delta V_I^{(1)}$ and $\Delta V_I^{(2)}$ are calculated in Section 6.3, which can be substituted in to find the final volume of the inclusion.

6.2.2 Governing equations of poroelastic medium

The governing equations for solving this problem can be categorized into four different groups: force equilibrium equations, fluid flow (Darcy's law), mass balance and Biots constitutive equations (Biot, 1941) :

(1) Force equilibrium equations

$$\sigma_{ij,j} = 0, \quad (6.4)$$

where σ_{ij} is the total stress.

(2) Darcy's law, is used to describe the fluid transport in the rock. By neglecting the gravity effect, Darcy's law can be written as

$$q_i = -\frac{k_{ij}}{\mu} \frac{\partial p}{\partial x_j} = -\kappa p_{,i}, \quad (6.5)$$

where p is the fluid pressure; q is the specific discharge vector; x_i indicates the flow direction; k_{ij} is the permeability tensor; μ is the dynamic viscosity of the fluid; and κ is the mobility ratio.

(3) Continuity equation or mass balance for the fluid phase can be written as

$$\frac{\partial \zeta}{\partial t} + q_{i,i} = 0, \quad (6.6)$$

where t is time; and ζ is incremental fluid content and is defined as

$$\zeta = \frac{\delta m_f}{\rho_{f0}}, \quad (6.7)$$

where δm_f is the mass change of pore fluid; and ρ_{f0} is the density of the fluid in the reference state.

(4) Biot's poroelastic constitutive equations, is used to describe the constitutive equations for a fluid-filled porous media. Linear and reversible relationship between stresses (σ_{ij}, p) on one side and kinematics i.e. strains and fluid content (ε_{ij}, ζ) on the other side are implied in Biot theory. The Biot's constitutive equations for isotropic poroelastic materials can be written as

$$\varepsilon_{ij} = \frac{1}{2G} \left[\sigma_{ij} - \left(\frac{3K - 2G}{9K} \right) \sigma_{kk} \delta_{ij} + \frac{2G}{3K} \alpha p \delta_{ij} \right], \quad (6.8)$$

$$\zeta = \frac{\alpha}{K} \left(\frac{\sigma_{kk}}{3} + \frac{p}{B} \right), \quad (6.9)$$

where δ_{ij} is the Kronecker delta ($\delta_{ij} = 1$ for $i = j$, and $\delta_{ij} = 0$ for $i \neq j$), ε_{ij} and σ_{ij} are the components of strain and stress tensor in the solid matrix, respectively; and p is the pore fluid pressure. There are four material constants in the poroelastic constitutive equations: the Biot coefficient α ; drained bulk modulus K ; shear modulus G ; and B the Skempton's coefficient

$$B = \frac{3(\nu_u - \nu)}{\alpha(1 - 2\nu)(1 + \nu_u)}, \quad (6.10)$$

where ν and ν_u are drained and undrained Poisson's ratio, respectively.

The combination of all these equations to solve the time-dependent interaction of rock deformation and fluid flow for the case of no fluid source, is given by the inhomogeneous diffusion equation for pore pressure

$$\frac{B}{3} \frac{\partial \sigma_{kk}}{\partial t} + \frac{\partial p}{\partial t} = c \nabla^2 p, \quad (6.11)$$

where c is the diffusivity coefficient

$$c = \frac{2(1 - \nu)(1 + \nu_u)^2}{9(1 - \nu_u)(\nu_u - \nu)} \kappa G B^2. \quad (6.12)$$

6.2.3 Poroelastic inclusions

Consider an ellipsoidal inclusion in an infinite elastic solid, which undergoes a uniform eigen-strain ε_{ij}^T , the applied strains in the absence of the surrounding material. Eshelby (1957, 1959) showed that the actual strain and stress inside the inclusion are uniform and given by

$$\varepsilon_{ij} = S_{ijkl} \varepsilon_{kl}^T, \quad (6.13)$$

$$\sigma_{ij} = C_{ijkl}^0 [\varepsilon_{kl} - \varepsilon_{kl}^T], \quad (6.14)$$

where ε_{ij} and σ_{ij} are the components of strain and stress tensors in the matrix, respectively; C_{ijkl}^0 is the elastic moduli of the matrix; and Eshelby tensor S_{ijkl} , is a fourth rank tensor which is a function of geometry and Poisson's ratio of the ellipsoidal inclusion (see Mura (1987) for more details). Rudnicki (2002a) combined the Eshelby formulation and constitutive equations of poroelastic medium Eq. (6.8) and (6.14) to solve the pressurized poroelastic inclusion problem. Considering a poroelastic pressurized inclusion, the eigenstrain ε^T (which is the stress-free transformation strain) can be obtained by setting $\sigma_{ij} = 0$ in Eq. (6.8)

$$\varepsilon_{mn}^T = C_{mnij}^{-1} \alpha_{ij} p = L_{mnij} \alpha_{ij} p, \quad (6.15)$$

where L_{mnij} is the tensor of elastic compliances, inverse of C_{mnij} . Therefore the corresponding strain field can be calculated from Eq. (6.13). Obtaining strain field inside the inclusion, the inclusion volume change may be calculated using volumetric strain times the initial volume as

$$\Delta V_I = \varepsilon_{kk}^T V_0. \quad (6.16)$$

The volume change calculated in Eq. (6.16) does not consider fluid leak-off from the inclusion. The effect of fluid diffusion from the inclusion to the matrix is considered in calculating the asymptotic inclusion volume analysis.

6.3 Asymptotic Analysis

6.3.1 Mode (1) loading

Short term response for the inclusion volume. Let's assume an ellipsoidal inhomogeneity is embedded in an infinite medium and it is pressurized with unit uniform pressure. According to Eq. (6.16), the volume change of the inhomogeneity ΔV_I right after the change

of the fluid pressure on the inhomogeneity surface (at $t = 0^+$) can be calculated from

$$\Delta V_I^{(1)}(0^+) = \varepsilon_{kk} V_I^0, \text{ assuming undrained material conditions.} \quad (6.17)$$

Subsequently, at $t = 0^+$ due to the application of the unit normal stress $\sigma_n = -1$ on the inclusion wall, an area with excessive pore pressure generates near the inhomogeneity surface. The magnitude of the pore pressure in this area can be calculated considering the undrained elastic response of the inhomogeneity ($\zeta = 0$ in Eq. (6.9)). Hence the excessive pore pressure value in the inhomogeneity vicinity is

$$\lim_{t \rightarrow 0^+} p = -\frac{B}{3} \sigma_{kk} = B, \quad (6.18)$$

which causes fluid flow from the inhomogeneity surface to the matrix and it can be modeled similar to mode (2) loading behavior (see Section 6.3.1) and Eq. (6.21)). Thus the final volume change of the inhomogeneity is

$$\Delta V_I^{(1)}(t) = \Delta V_I^{(1)}(0^+) + (-B) \Delta V_I^{(2)}(t). \quad (6.19)$$

Long term response for the inclusion volume. Consider the condition for long enough time, i.e. time evolves to infinity. The pore pressure generated by the mode (1) loading near the inhomogeneity surface (see Eq. (6.18)) should dissipate, therefore the second term in Eq. (6.19) vanishes. Hence, the long-term volume change can be calculated similar to Eq. (6.17) but using drained material properties

$$\Delta V_I^{(1)}(\infty) = \varepsilon_{kk} V_0. \quad (6.20)$$

Short term response for the leak-off volume. As mentioned before, the pore pressure field generated in Eq. (6.18) should dissipate, due to pressure gradient in the matrix.

According to Section 6.6, the fluid flux $Q_{\sqrt{A}}$ for a unit pressure difference between an ellipsoidal surface with surface area equal to A (here, the inhomogeneity) and the matrix can be approximate as

$$Q_{\sqrt{A}} = \kappa \sqrt{A} \frac{1}{\sqrt{\pi} \sqrt{\frac{ct}{A}}} \left(\left(S_{\sqrt{A}}^* \sqrt{\pi} \sqrt{\frac{ct}{A}} \right)^n + 1 \right)^{\frac{1}{n}}, \quad (6.21)$$

where t is the actual time; $S_{\sqrt{A}}^*$ is the dimensionless conduction shape factor; and n is the blending coefficient (see Table 6.2). Consequently by integrating the flux over time on the inclusion surface, and multiplying the pore pressure drop calculated in Eq. (6.18) ($\Delta p = -B$), the fluid leak-off volume for short time scale ($\frac{ct}{A} \ll 1$) will be

$$\begin{aligned} V_l^{(1)}(t) &= -B \int_0^t Q_{\sqrt{A}} dt \\ &= \frac{2B\kappa A \sqrt{t}}{\sqrt{c} \sqrt{\pi}} {}_2F_1 \left(-\frac{1}{n}, \frac{1}{n}; 1 + \frac{1}{n}; - \left(S_{\sqrt{A}}^* \sqrt{\pi} \right)^n \left(\frac{ct}{A} \right)^{\frac{n}{2}} \right), \end{aligned} \quad (6.22)$$

where ${}_2F_1(a, b; c; z)$ is the Gauss's hypergeometric function. The negative sign in Eq. (6.22) indicates fluid flow toward the inclusion.

Long term response for the leak-off volume. Considering that no fluid exchange between the matrix and its boundary after prolonged time, the long term leak-off volume can be calculated as the integration of increment of fluid content $\zeta|_{t=\infty}$ over the isopressure surface and has the form

$$V_l^{(1)}(\infty) = \int_t Q_{\sqrt{A}} = \int_V \zeta|_{t=\infty} dV. \quad (6.23)$$

On the other hand, as time evolves to infinity the excess pore pressure in the matrix will dissipate ($p = 0$). Therefore from Eq. (6.8) and (6.9) and solving for ζ we get

$$\lim_{t \rightarrow +\infty} \zeta = \alpha \lim_{t \rightarrow +\infty} \varepsilon_{kk}. \quad (6.24)$$

which is equal to the magnitude of the volumetric strain times the Biot coefficient. As a result, the long term response of the leak-off volume will be

$$V_l^{(1)}(\infty) = \alpha \varepsilon_{kk} V_I^0. \quad (6.25)$$

6.3.2 Mode (2) loading

Response for the inclusion volume. Using the reciprocal theorem of poroelasticity (Cheng and Predeleanu, 1987), it is possible to show that the mode (2) inclusion volume is equal to the mode (1) fluid leak-off volume at all times, therefore

$$V_I^{(2)} = V_l^{(1)}. \quad (6.26)$$

Thus, from the mode (1) results ($p = 1$), we have

$$V_I^{(2)}(t) = \frac{2B\kappa A\sqrt{t}}{\sqrt{c}\sqrt{\pi}} {}_2F_1\left(-\frac{1}{n}, \frac{1}{n}; 1 + \frac{1}{n}; -\left(S_{\sqrt{A}}^* \sqrt{\pi}\right)^n \left(\frac{ct}{A}\right)^{\frac{n}{2}}\right) \text{ for } \sqrt{\frac{ct}{A}} \ll 1. \quad (6.27)$$

The mode (2) inclusion volume is equal to the mode (1) fluid leak-off volume at all times.

Therefore

$$V_I^{(2)}(\infty) = \alpha \varepsilon_{kk} V_I^0. \quad (6.28)$$

The leak-off volume. The early time behavior of the fluid leak-off volume can be calculated from the Eq. (6.22). Thus, for mode (2) loading conditions, the short term leak-off volume is given by

$$\begin{aligned} V_l^{(2)}(t) &= \int_0^t Q_{\sqrt{A}} dt \\ &= \frac{2\kappa A\sqrt{t}}{\sqrt{c}\sqrt{\pi}} {}_2F_1\left(-\frac{1}{n}, \frac{1}{n}; 1 + \frac{1}{n}; -\left(S_{\sqrt{A}}^* \sqrt{\pi}\right)^n \left(\frac{ct}{A}\right)^{\frac{n}{2}}\right). \end{aligned} \quad (6.29)$$

As time evolves to infinity, Eq. (6.11) uncouples to become a homogenous diffusion equation. Thus similar to the short term response of the leak-off volume, the long term response of the leak-off volume is given by

$$V_l^{(2)}(t) = \frac{2\kappa A \sqrt{t}}{\sqrt{c} \sqrt{\pi}} {}_2F_1 \left(-\frac{1}{n}, \frac{1}{n}; 1 + \frac{1}{n}; - \left(S_{\sqrt{A}}^* \sqrt{\pi} \right)^n \left(\frac{ct}{A} \right)^{\frac{n}{2}} \right). \quad (6.30)$$

6.4 Numerical Results

We provide some numerical examples, considering inclusions with different aspect ratios AR , and material properties. Inclusions are assumed to be ellipsoidal with principal half axes a_i , where $a_1 = AR \times a_2 = AR \times a_3$. All results are plotted for $AR = 10, 1.0$, and 0.001 which represent prolate spheroid, sphere, and circular disk shape inclusions, respectively. Here, we defined non-dimensionalized volume of the inclusion V_I^* , as the ratio of the volume change of the inclusion to its initial volume. Similarly, V_l^* is defined to be the ratio of the fluid leak-off volume from the inclusion to the inclusion initial volume. The superscripts indicate the corresponding loading mode behavior. These non-dimensionalized volume changes have been plotted versus the dimensionless time $t^* = ct/l^2$, where $l = a_1$.

Figure 6.2 shows the inclusion volume change ratio and leak-off volume ratio for different inclusion aspect ratios. The material properties used to generate these numerical examples are $\nu = 0.2$, $\nu_u = 0.4$, $\alpha = 0.89$ and $B = 0.8$. The dimensionless mode 2 leak-off volume $V_l^{(2)*}$ versus t^* has been plotted in Fig. 6.2(a). It can be seen that higher inclusion aspect ratio results in larger values of $V_l^{(2)*}$. As the inclusion aspect ratio increases, the ratio of the inclusion surface area A to its volume V_0 increases too. Therefore, leak-off volume which is strong function of the surface area of the inclusion increases.

Figure 6.2(b) shows the volume change ratio of the inclusion for mode 1 loading. As can be seen, the long term solution is the same for all inclusion aspect ratios, which happens due to the same volumetric strain for uniform pressure distribution in the inclusion.

Figure 6.2(c) plots the negative of the volume change ratio of the inclusion for mode 2 loading and the dimensionless mode 1 leak-off volume. Comparing values in Figs. 6.2(b) and 6.2(c), indicates higher values for the inclusion volume change regarding mode 1 loading than mode 2 loading.

Having the asymptotic solution for the different modes, we can calculate the total volume change of the inclusion. For example, the final variation of the inclusion volume, combining both modes 1 and 2 is

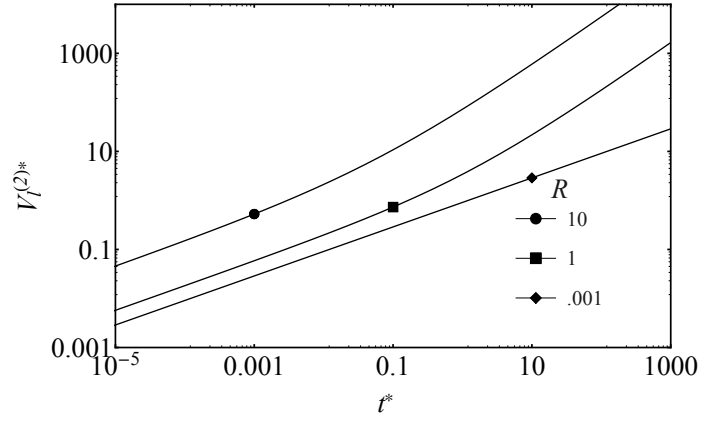
$$\Delta V_I = V_I^0 [p_I(\varepsilon_{kk}) - (p_I - p_0)(\alpha \varepsilon_{kk})]. \quad (6.31)$$

Fig. 6.3 shows how changes of poroelastic material properties of the inclusions affects the results. The poroelastic material properties used to generate numerical examples in Fig. 6.3 are $\nu = 0.2$, $\alpha = 1$, and varying ν_u . Figures 6.3(a) and 6.3(c) show that the Mode 2 inclusion and leak-off volume ratios are weak function of Poisson's ratio. However, Mode 1 inclusion volume change ratio varies significantly by changes of Poisson's ratio. Figure 6.3(b) indicates higher volume change ratios for less difference in drained and undrained Poisson's ratio.

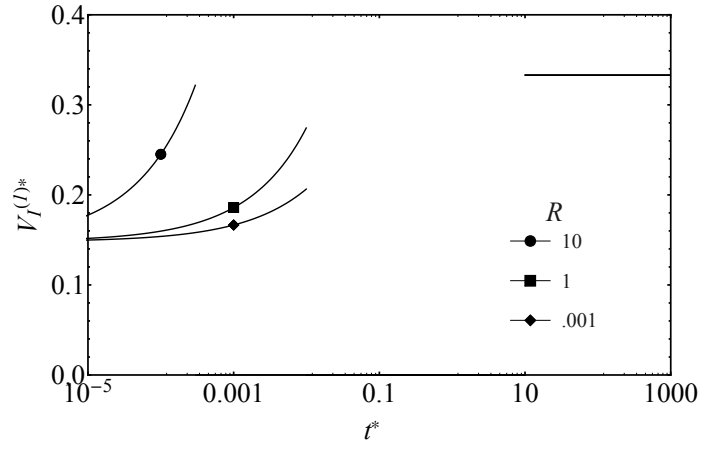
6.5 Summary and Conclusion

In this paper we provided semi-analytical asymptotic (short-term and long-term) solutions for the volume change of a pressurized poroelastic inclusion embedded in an infinite three-dimensional poroelastic medium. Previous studies on the topic have not incorporated the hydraulic communication between the inclusion and the surrounding medium; therefore, fluid pressure changes in the surrounding rock due fluid pressure changes in the inclusion was ignored.

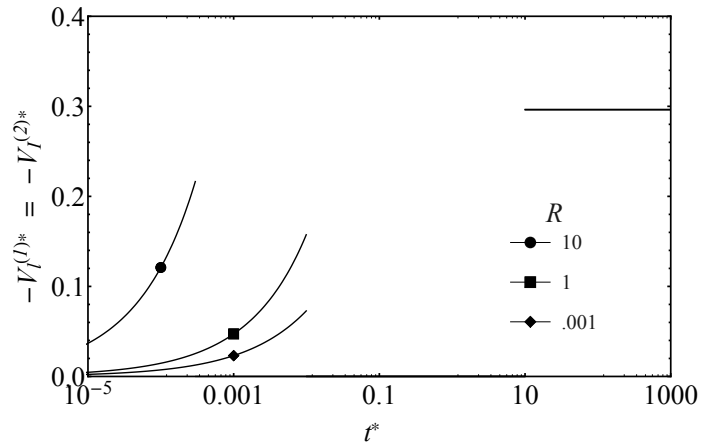
Furthermore, we provided numerical examples of inclusion volume change scenarios, considering inclusions with different aspect ratios. The results show the same long term non-dimensionalized volume change for inhomogeneities with different aspect ratios. Comparing



(a)

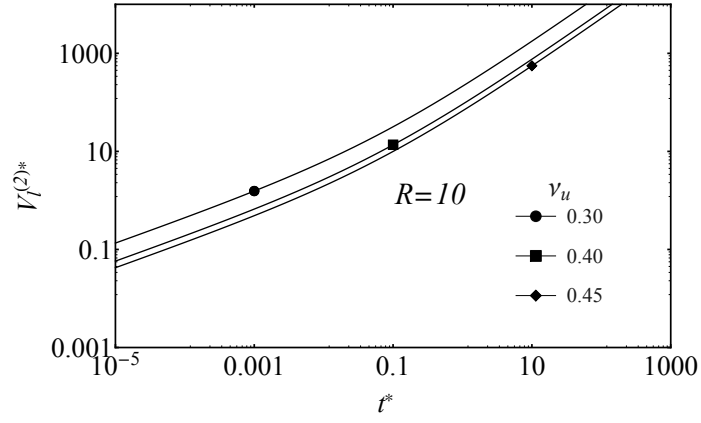


(b)

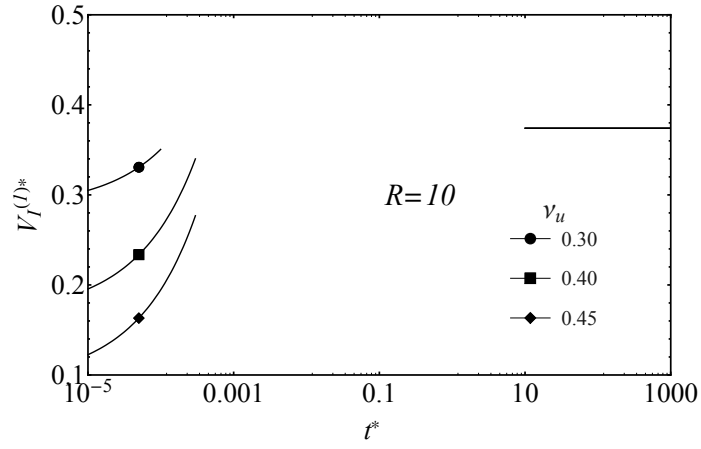


(c)

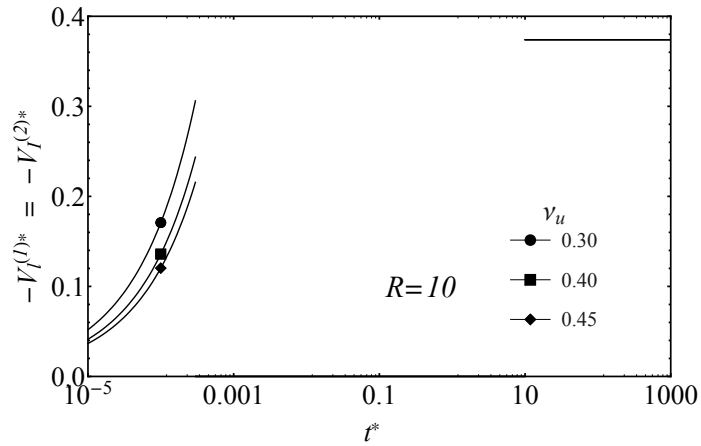
Figure 6.2: (a) Mode 2 leak-off volume ratio (b) Mode 1 volume change ratio (c) Mode 2 volume change ratio; for different inclusion ratios. The material properties are assumed to be $\nu = 0.2$, $\nu_u = 0.4$, $\alpha = 0.89$ and $B = 0.8$.



(a)



(b)



(c)

Figure 6.3: (a) Mode 2 leak-off volume ratio (b) Mode 1 volume change ratio (c) Mode 2 volume change ratio; assuming $R = 10$, and for different undrained Poisson's ratios . The material properties are assumed to be $\nu = 0.2$, $\alpha = 1$.

non-dimensionalized volume change values of mode 1 and mode 2 loadings, indicates higher values for mode 1 loading condition.

Results show that the Mode 2 inclusion and leak-off volume ratios are weak function of Poisson's ratio. However, Mode 1 inclusion volume change ratio varies significantly by changes of Poisson's ratio.

6.6 Diffusion equation solution on an ellipsoidal surface

Considering the complete analogy between the heat conduction and the fluid pressure diffusion equations (for example, the Fourier's law in heat transport is equivalent to the Darcy's law in fluid flow, see Table 6.1), the problem of transient fluid diffusion from an isopressure body into the medium can be solved using the available solutions in the literature for heat conduction from isothermal bodies into an infinite homogenous medium. The non-

Table 6.1: The analogy between heat conduction and fluid diffusion equations

Parameter	Heat Conduction	Fluid Diffusion
Material property	Thermal conductivity (k)	Mobility (κ)
Material property	Thermal diffusivity (α)	Fluid diffusivity (c)
Potential Function	Temperature	Pressure
Flux	Heat transfer rate	Flow rate

dimensional heat diffusion equation in the media can be written as (Yovanovich et al., 1995)

$$\nabla^2 \phi(r, \tau) = \frac{\partial \phi(r, \tau)}{\partial \tau}, \quad (6.32)$$

where

$$\phi(r, \tau) = \frac{T(r, \tau) - T_\infty}{T_0 - T_\infty},$$

$$\phi(r, \tau = 0) = 0,$$

$$\phi(r = r_0, \tau > 0) = 1,$$

$$\phi(r \rightarrow \infty, \tau > 0) \rightarrow 0, \quad (6.33)$$

and T is temperature; t is the actual time; r defines the surface of isothermal body; T_0 is the surface area temperature, T_∞ is the matrix temperature at the initial time $t = 0$. The non-dimensional time τ can be expressed as

$$\tau = \frac{\alpha t}{\ell^2}. \quad (6.34)$$

Here, $\ell = \sqrt{A}$ is the characteristic length of the isotherm surface; A is the total surface of the body; α is thermal diffusivity. Using linear superposition technique and adding a blending coefficient n (n is a coefficient to improve the model for all body shapes regardless of their aspect ratio, see Churchill and Usagi (1972) for more details), Yovanovich et al. (1995) showed that explicit solution for the dimensionless flux Q^* , of instantaneous heat flow is

$$Q_{\sqrt{A}}^* = \frac{1}{\sqrt{\pi} \sqrt{Fo_{\sqrt{A}}}} \left(\left(S_{\sqrt{A}}^* \sqrt{\pi} \sqrt{Fo_{\sqrt{A}}} \right)^n + 1 \right)^{\frac{1}{n}}, \quad (6.35)$$

where

$$Fo_{\sqrt{A}} = \frac{\alpha t}{A}, \quad (6.36)$$

$$Q = \frac{k A Q^* \theta_0}{\ell}, \quad (6.37)$$

$$\theta_0 = T_0 - T_\infty, \quad (6.38)$$

and k is thermal conductivity; $S_{\sqrt{A}}^*$ is the dimensionless conduction shape factor; and Q is the actual flux. $S_{\sqrt{A}}^*$ and n , for different shapes are provided in Table 6.2.

Table 6.2: Dimensionless conduction shape factors and blending coefficients for different geometries (from Yovanovich et al. (1995))

Inclusion shape	$S_{\sqrt{A}}^*$	n
Circular disk ($AR = 0$)	3.192	1.10
Oblate spheroid ($AR = 0.5$)	3.529	0.99
Prolate spheroid ($AR = 1.93$)	3.564	0.99
Prolate spheroid ($AR = 10$)	4.195	0.87

Considering the existed analogy between heat conduction and fluid diffusion equations, for the problem of transient fluid diffusion from an isopressure body we will have

$$Q'_{\sqrt{A}} = \frac{1}{\sqrt{\pi} \sqrt{Fo'_{\sqrt{A}}}} \left(\left(S'_{\sqrt{A}} \sqrt{\pi} \sqrt{Fo'_{\sqrt{A}}} \right)^n + 1 \right)^{\frac{1}{n}}, \quad (6.39)$$

where

$$Fo'_{\sqrt{A}} = \frac{ct}{A}, \quad (6.40)$$

$$Q = \frac{\kappa A Q'_{\sqrt{A}} \theta'_0}{\ell}, \quad (6.41)$$

$$\theta'_0 = p_0 - p_{\infty}, \quad (6.42)$$

and c is fluid diffusivity; κ is mobility.

6.7 Duhamel's theorem

The transitional time dependent behavior can be calculated by using Duhamel's theorem. In order to apply Duhamel's theorem, it is necessary to have a problem with a zero initial condition and a single non-homogeneous term that varies in time. According to this theorem, if $F(t)$ is the response of a linear system with a zero initial condition to a single, constant non homogeneous term with magnitude of unity (referred to as the fundamental solution), then the response of the same system to a single, time-varying non-homogeneous with magnitude

$p(t)$ can be obtained from the fundamental solution according to :

$$F(t) = \int_{\tau=0}^t T_f(t-\tau) \frac{dp(\tau)}{d\tau} d\tau + p(0)T_f(t). \quad (6.43)$$

where $p(0)$ is the value of p at $t = 0$ and $p(t)$ must be continuous in time (Nellis and Klein, 2008).

6.8 References

- Bedayat, H., Dahi Taleghani, A., 2014. Interacting double poroelastic inclusions. *Mechanics of Materials* 69, 204–212. doi:10.1016/j.mechmat.2013.10.006.
- Biot, M.A., 1941. General theory of three-dimensional consolidation. *Journal of Applied Physics* 12, 155. doi:10.1063/1.1712886.
- Chen, Z.R., 2011. Poroelastic model for induced stresses and deformations in hydrocarbon and geothermal reservoirs. *Journal of Petroleum Science and Engineering* 80, 41–52. doi:10.1016/j.petrol.2011.10.004.
- Cheng, A.H.D., Predeleanu, M., 1987. Transient boundary element formulation for linear poroelasticity. *Applied Mathematical Modelling* 11, 285–290. doi:10.1016/0307-904X(87)90144-2.
- Churchill, S.W., Usagi, R., 1972. A general expression for the correlation of rates of transfer and other phenomena. *AIChE Journal* 18, 1121–1128. doi:10.1002/aic.690180606.
- Detournay, E., Cheng, A.H.D., 1988. Poroelastic response of a borehole in a non-hydrostatic stress field. *International Journal of Rock Mechanics and Mining Sciences & Geomechanics Abstracts* 25, 171–182. doi:10.1016/0148-9062(88)92299-1.
- Detournay, E., Cheng, A.H.D., 1991. Plane strain analysis of a stationary hydraulic fracture in a poroelastic medium. *International Journal of Solids and Structures* 27, 1645–1662. doi:10.1016/0020-7683(91)90067-P.

- Eshelby, J.D., 1957. The determination of the elastic field of an ellipsoidal inclusion, and related problems. *Proceedings of the Royal Society A: Mathematical, Physical and Engineering Sciences* 241, 376–396. doi:10.1098/rspa.1957.0133.
- Eshelby, J.D., 1959. The elastic field outside an ellipsoidal inclusion, in: *Proceedings of the Royal Society of London. Series A, Mathematical and Physical*, pp. 561–569.
- Mura, T., 1987. *Micromechanics of defects in solids*. Martinus Nijhoff Publishers.
- Nellis, G., Klein, S., 2008. *Heat transfer*. Cambridge University Press.
- Rice, J.R., Cleary, M.P., 1976. Some basic stress diffusion solutions for fluid-saturated elastic porous media with compressible constituents. *Reviews of Geophysics* 14, 227. doi:10.1029/RG014i002p00227.
- Rudnicki, J.W., 2002a. Alteration of regional stress by reservoirs and other inhomogeneities: Stabilizing or destabilizing?, in: Vouille, G., Berest, P. (Eds.), *Proc. 9th Int. Congr. Rock Mechanics*, Vol. 3, Paris, Aug. 25–29, 1999, Paris, France. pp. 1629–1637.
- Rudnicki, J.W., 2002b. Eshelby transformations, pore pressure and fluid mass changes, and subsidence, in: *Poromechanics II, Proc. 2nd Biot Conference on Poromechanics*, Grenoble, France.
- Soltanzadeh, H., Hawkes, C.D., 2012. Evaluation of caprock integrity during pore pressure change using a probabilistic implementation of a closed-form poroelastic model. *International Journal of Greenhouse Gas Control* 7, 30–38. doi:10.1016/j.ijggc.2011.10.006.
- Yovanovich, M., Teertstra, P., Culham, J.R., 1995. Modeling transient conduction from isothermal convex bodies of arbitrary shape. *Journal of Thermophysics and Heat Transfer* 9, 385–390. doi:10.2514/3.678.

Chapter 7

Summary and Future Works

7.1 Summary

Poroelastic inclusions could have a wide range of applications from rock mechanics problems to tissue mechanics. For example, many geological phenomena and structures like reservoirs, aquifers, intrusions, fault zones, caverns, dikes, compaction bands, and other underground structures can be modeled as inhomogeneous inclusions. Considering different material properties and different pressure/temperature of hydrocarbon bearing formations in comparison to those of the surrounding geological structures, hydrocarbon reservoirs and subsurface fractures can be considered as inhomogeneities embedded inside an infinite poroelastic medium. Moreover, elliptic fractures are special cases of ellipsoidal inhomogeneities when their elastic moduli are zero, and one of the principal axes of the ellipsoid approaches zero.

This dissertation is comprised of two major interrelated topics. The first focus is to investigate stress distribution inside and outside of poroelastic inclusions due to alteration of fluid pressure inside the inclusion (no hydraulic communication between the inclusion and the surrounding matrix) and its application in reservoir geomechanics (Chapters 2 to 4). The second objective involves calculating the volume changes of a poroelastic plain strain fracture/ellipsoidal inclusion due to change of fluid pressure inside the fracture/inclusion, considering fluid exchange between the inclusion and the matrix (Chapters 5 and 6). The results obtained from the first topic are directly utilized to investigate the latter subject. The summary and conclusions of the main results is as follows:

An analytical approach for determining stress distribution around two interacting elastic inhomogeneities, was derived for double poroelastic interacting inhomogeneous inclusions. These inclusions are assumed to be embedded in an infinite elastic medium and under nonuniform far-field loading. This method is applicable to three-dimensional problems, and inclusions may be oriented arbitrarily with respect to each other. Using the Equivalent Inclusion Method (EIM) and polynomial expansion of strain fields in the local coordinate systems, the solution for two ellipsoidal poroelastic inhomogeneities are derived. To solve this problem eigenstrains were expanded, and higher order Eshelby's tensors and their derivatives were calculated at the center of each inhomogeneity. I found that to get more accurate results, it is necessary to use more polynomial terms for eigenstrains and higher rank Eshelby's tensors, especially when dealing with very close inclusions.

The results show that the distance of centers of the inhomogeneities and their relative stiffness to the medium affect the associated stress field. Considering same distance for inhomogeneities, the interaction effect is more significant on stiffer inclusions.

A source code (in Mathematica) to calculate the stress and strain fields inside and outside of two interacting ellipsoidal inhomogeneities with arbitrary orientation with respect to each other is developed.

The Equivalent Inclusion Method (EIM) is used to solve for stress and strain distribution inside and outside of an anisotropic poroelastic inhomogeneity. Finding the equivalent eigenstrain, graphical results for strain and stress ratio are presented, and further explored the sensitivity of parameters of different elastic and poroelastic parameters on results assuming transverse isotropic condition for both poroelastic and elastic parameters of the inhomogeneity.

The results show how neglecting the effect of both anisotropic poroelastic and elastic properties may result in large differences in stress calculations. The stress ratio changes are much larger in the direction parallel to the axis of symmetry than the directions in the plain of symmetry.

The poroelastic solution for the drainage of a single microfracture considering the effects of formation pressure, rock mechanical properties, in-situ stress and bottomhole pressure on the volume of the fractures is derived. Since, fractures width changes affect their hydraulic conductivity and subsequently overall permeability of reservoirs, therefore production could be affected by the change of fractures volume.

It has been shown that the difference between bottomhole pressure and reservoir pressure results in the augmentation of the fracture volume. This increase may be counterbalanced by large horizontal stresses in the reservoir. In case of reservoirs with low confining stresses, fracture volume increases with time. However, in reservoirs with large confining stress, the fracture volume is decreasing. Additionally, it has been shown how the bottomhole pressure changes under certain condition could change reverse behavior of the poroelastic fractures in the reservoir.

A semi-analytical asymptotic (short-term and long-term) solutions for the volume change of a pressurized poroelastic inclusion embedded in an infinite three-dimensional poroelastic medium are derived. Most previous studies assumed no hydraulic communication between the inclusion and the surrounding medium; therefore, the fluid pressure in the surrounding rock will not change due to fluid pressure changes in the inclusion, and there will be no fluid leak-off from the inclusion.

Numerical examples of inclusion volume change scenarios, considering inclusions with different aspect ratios are provided. The results show the same long term non-dimensionalized volume change for inhomogeneities with different aspect ratios. The approach used for solving this problem is inspired by modal decomposition and superposition method previously developed and used to solve several poroelasticity problems such as sudden pressurization of a borehole and plain strain stationary fracture. Considering that the normal traction and pore pressure along the inclusion surface is equal to the fluid pressure inside the inclusion ($\sigma_n = -p_I, p = p_I$), the response of the inclusion can be decomposed into two fundamental problems: (1) a step change in stress while there is no pore pressure change inside the inclu-

sion ($\sigma_n = -1_{(0,\infty]}$, $p = 0$); (2) a step change in pore pressure while there is no stress change inside the inclusion ($\sigma_n = 0$, $p = 1_{(0,\infty]}$). Therefore, the inclusion response in the general condition can be considered as a linear combination of each of these modes.

Comparing non-dimensional volume change for mode 1 and mode 2 loadings, indicates higher values for the mode 1 loading condition. Results show that the Mode 2 inclusion and leak-off volume ratios are weak functions of the Poisson's ratio. However, Mode 1 inclusion volume change ratio varies significantly with changes of Poisson's ratio.

7.2 Recommendations for Future Works

The following recommendations are made for possible future research:

- The mechanical modeling of the ellipsoidal poroelastic inhomogeneities can be extended to non ellipsoidal inhomogeneities using semi analytical methods exist in the damage mechanics literature.
- Here the surrounding matrix is assumed to be an infinite elastic/poroelastic full space. The solution of mechanical behavior of the same type of problems in a semi infinite half space can be used to model some geological structures such as shallow reservoirs or aquifers.

Appendix: Letters of Permission to Use Published Material

The Permissions from Elsevier publishing company are presented in the following pages:



RightsLink®

Home

Account
Info

Help



Conference Proceeding: Poromechanics V: Proceedings of the Fifth Biot Conference on Poromechanics

Conference Proceeding Paper: The Equivalent Inclusion Method for Poroelectricity Problems

Author: H. Bedayat, A. Dahi Taleghani

Publisher: American Society of Civil Engineers

Date: 06/18/2013

Copyright © 2013, ASCE. All rights reserved.

Logged in as:
Houman Bedayat

LOGOUT

Permissions Request

As an ASCE author, you are permitted to reuse your own content for another ASCE or non-ASCE publication.

Please add the full credit line "With permission from ASCE" to your source citation. Please print this page for your records.

Type of use: Dissertation/Thesis

Portion: full article

Format: print and electronic

Use of this content will make up more than 25% of the new work: no

Author of this ASCE work or ASCE will publish the new work: yes

BACK

CLOSE WINDOW

Copyright © 2014 [Copyright Clearance Center, Inc.](#) All Rights Reserved. [Privacy statement.](#)
Comments? We would like to hear from you. E-mail us at customercare@copyright.com

Vita

Houman Bedayat was born in Tehran, Iran in 1984. He joined Craft and Hawkins Department of Petroleum Engineering geomechanics research group at LSU as a Ph.D. student in Fall 2010 where he started his research under the supervision of Dr. Arash Dahi Taleghani. During his PhD program he worked as research assistant and teaching assistant.

Before joining LSU, Houman was a master's student in geotechnical engineering at Sharif University of Technology, where he worked on lateral displacement of piles in saturated soils. He has also perused his undergrad degree from civil engineering department at Sharif University of Technology.

He has received the Paper Contest Award from Petroleum Engineering Department at LSU (2014), the American Association of Drilling Engineers (AADE) Award (2013), AADE Scholarship (2013) and GDL Foundation Research Scholarship for two consecutive years (2011-2012) during his PhD program. Houman is currently a member of Society of Petroleum Engineers (SPE), American Association of Petroleum Geologists (AAPG), American Rock Mechanics Association (ARMA), American Association of Drilling Engineers (AADE), Society of Exploration Geophysicists (SEG), American Society of Civil Engineers (ASCE) and the Honor Society of Petroleum Engineers (Pi Epsilon Tau). He has also founded the ARMA and SEG student chapters at LSU and served as president and vice president of these chapters while he was a student.

Houman Bedayat is expected to receive his Doctor of Philosophy degree at the 2014 Fall Commencement. Houman may be reached at Houman.Bedayat@gmail.com in future.